


MULTI-SCALE DYNAMICS OF MIXED SAND AND GRAVEL DELTAIC COASTS

Doctoral Thesis

Rafael Jesús Bergillos Meca

Supervisors:

Miguel Ortega Sánchez and Gerd Masselink

Andalusian Institute for Earth System Research

University of Granada

Environmental Fluid Dynamics Group

Doctoral Programme: Dynamics of Biogeochemical Flows and its Applications

September 2017

Editor: Universidad de Granada. Tesis Doctorales
Autor: Rafael Jesús Bergillos Meca
ISBN: 978-84-9163-732-5
URI: http://hdl.handle.net/10481/48946

To my uncle José María

To see what is in front of one's nose needs a constant struggle.

George Orwell

Acknowledgements

This thesis has been supervised by Profs. Miguel Ortega-Sánchez and Gerd Masselink. I am indebted to them not only for their scientific guidelines, instructive revisions and helpful tips, but also for their motivating comments, empathy and mutual respect. Thank you Migue for your trust, continuous assistance, productive training and funny talks since the fist day. Thank you Gerd for your hospitality as well as for our enjoyable research discussions and non-working meetings.

I would like to thank Prof. Miguel A. Losada for his patience, valuable time, scientific suggestions and other useful pieces of advice. I really think he is the father of up-to-date coastal engineering in Spain and one of the leading scientists worldwide in this field. He is going to receive this month a deserved tribute to acknowledge his educational and research trajectory; this thesis is an additional little tribute to his cutting-edge knowledge and professional career.

I also acknowledge the rest of co-authors (Cristóbal Rodríguez-Delgado, Agustín Millares and Alejandro López-Ruiz), Editors-in-Chief and Associate Editors (Gunter Bloschl, Francesco Comiti, Edward Anthony, Wei-Ning Xiang, Alberto Piola, Iñigo Losada and Peter Nielsen) and anonymous reviewers of my thesis papers for their improvements to this work.

I am grateful to the members of the Environmental Fluid Dynamics Group of the University of Granada, Fluvial Dynamic and Hydrology Group of the University of Córdoba, and Coastal Processes Research Group of Plymouth University. Apart from the aforementioned members, I am particularly indebted to Miguel A. Reyes-Merlo and Manuel Cobos for their support with the field surveys, Francisca Martínez Ruiz for sieving analysis, Javier Herrero and Robert McCall for their assistance with the WiMMed and XBeach-G models, respectively, and Pedro Magaña for his help with the thesis template and other computer issues.

The thesis would have not been possible without the funding provided by the Spanish Ministry Economy and Competitiveness (Project CTM2012-32439, Research Contract BES-2013-062617 and Mobility Grants EEBB-I-15-10002, EEBB-I-16-11009 and EEBB-I-17-12498). I also thank Andalusian Regional Government, Demarcación Hidrográfica de las Cuencas Mediterráneas Andaluzas, Puertos del Estado, Servicio Provincial de Costas de Granada, Instituto de Estadística y Cartografía de Andalucía, and Plan Nacional de Ortofotografía Aérea for providing information.

It would be unfair to forget the long academic path before this thesis, so that I have to acknowledge the academic staff of my primary school, secondary school, Degree Programme in Civil Engineering and Master Programme in Environmental Hydraulics (Specialities in Integral Management of Ports and Coastal Zones, and Integral Management of River Basins). Among them, I am specially grateful to the members of my research group (Profs. Losada, Baquerizo, Ortega-Sánchez, Santiago, Moñino and Díez-Minguito).

I have not walked alone along this path, but my relatives, friends and couple have been faithful travelling companions. I thank my parents for bringing me up during my childhood, my sisters and cousins for their constant and unconditional support, and my friends for being the best adoptive family I could have ever chosen. The last words of this section are dedicated to Isabel: this thesis is only a small step of my life, it is just a single step of our lives.

Abstract

Deltaic systems are located at the transition between fluvial and maritime environments. They all have high environmental, economic and social importance, and respond rapidly to both natural and human-driven changes. On the other hand, mixed sand and gravel (MSG) beaches are common in previously para-glaciated coastal regions and coasts with steep hinterlands, and are widespread in the UK, Denmark, Canada, New Zealand and Mediterranean countries. They are also found when nourishment projects use gravel to protect eroded sandy beaches. Despite their societal importance, the research advances on gravel and MSG beaches are limited compared to those on sandy beaches. The main objective of this thesis is to analyse, characterize and model the dynamics of MSG deltaic coasts based on a multi-scale investigation carried out in the Guadalfeo delta, a Mediterranean delta in a semi-arid and high-mountain basin of southern Spain. To meet this overall objective, five specific goals were proposed, which were addressed in five different chapters.

First, the effects of the construction of a reservoir 19 km from the mouth on the dynamics of the delta are analysed in Chapter 3. The sediment volume transported as bedload and accumulated in the delta was estimated under two scenarios by means of a calibrated hydrological model: a managed scenario, considering the flows drained by the dam, and an unmanaged scenario, considering the absence of such infrastructure. Bathymetric and topographic measurements were analysed and correlated with the fluvial and maritime forcing agents. Results indicated that the reservoir has significantly modified the dynamics downstream: the coast has lost almost 0.3 hm^3 of sediments since the entry into operation of the dam, generating a 1.4-km coastline retreat around the mouth, with a maximum retreat of 87 m (92% of the initial). Under unmanaged conditions, more than 2 hm^3 of bedload would have reached the coast. Based on the results, three new management scenarios of flows drained by the dam, in combination with bypassed sediment from the reservoir, were proposed to prevent more severe consequences in the delta and the silting of the reservoir. The proposed methodology for new management scenarios can be extended to other worldwide deltas and represents an advanced tool for decision making.

Secondly, Chapter 4 details the spatial and temporal variability of the river mouth, focusing on the influence of submerged morphological changes on wave propagation and longshore sediment transport (LST). Bathymetric measurements were carried out over a 15-year period (1999 - 2014), a wave propagation model (Delft3D-Wave) was calibrated and applied, and the complete littoral drift time series were obtained using statistical downscaling techniques. Results showed that the river damming led to coastline retreat and bed-level erosion up to 3 m along a 1-km section around the river mouth, with maximum erosion rates in excess of 760 m^3/m. These subtidal morphological changes reduced wave refraction and led to higher breaking wave energy. Variations in wave climate during the study period also played a role in influencing the coastline dynamics. Although the erosion around the river mouth has decreased since 2008, partly due to a sediment pulse in 2010, eastward LST rates under westerly storm wave conditions have significantly increased since then. This has led to the propagation of the sediment deficit towards the east of the mouth, endangering urban developments at this location. This chapter provides insights into the shift from wave-river dominated deltas towards deltaic coasts increasingly controlled by wave directionality and LST, and represents an advance on the understanding of the dynamics of many worldwide deltas where the river sediment supply has decreased due to human activities.

The changes in the morphology and sedimentology of the MSG beach forced by wave and water-level variations as well as human intervention through nourishment are studied in Chapter 5. Monthly and storm event-driven field surveys, consisting of topographical measurements and sediment sampling, were carried out over a one-year period (October 2013 - September 2014). Three prevailing sediment fractions (sand, fine gravel and coarse gravel) and two end-member morphological states of the upper beach profile (convex with multiple berms and concave with a single storm berm) were identified. Between them, several transitional profiles were formed, characterized by developing berms that progressively overlapped, generating sediment variability both across the beach profile and with depth. Results indicated that the total run-up (including water-level) reached during an event represents a more accurate threshold than wave height for differentiating between erosional and depositional conditions. They also suggested that MSG coasts recover faster from storm erosion than sandy beaches. The long-term benefit of the artificial nourishment was limited and this was attributed to the too fine nourished sediment used and its placement too high on the beach profile. This chapter deepens into the knowledge of the morpho-sedimentary dynamics of MSG beaches under varying wave and water-level conditions.

Chapter 6 addresses the evolution of the coast forced by an artificial nourishment project ended in December 2014 through the analysis of field observations and the modelling of hydro- and morphodynamics. The beach profile and coastline were periodically surveyed over a six-month period; the Delft3D-Wave model was applied; four LST equations were tested through comparisons with bathymetric data; and the one-line model was applied between topographic surveys. Results indicated that severe coastline retreat (dry beach area loss > 208 m^2/day) occurred during the 45 days following the intervention. This was mainly attributable to the morphology of the nourished coastline, the different characteristics of the nourished sediment compared to natural sizes, and the occurrence of an intense westerly storm. The Van Rijn formulation provided the best fits to the observed volumetric changes, obtaining modelled/measured ratios of 93.1% and 77.4% for the two study beach profiles. The outputs of the one-line model based on the Van Rijn approach were also the best, with RMSEs decreasing during the study period and lower than 4.6 m over the last 3 months. These results show that the applied methodology constitutes a management tool for modelling the evolution of MSG coasts.

Finally, the beach profile response forced by storm waves from varying directions is investigated in Chapter 7. Beach morphology was monitored over a 36-day period between January and February 2015, and profile response was compared to model predictions using the XBeach-G model and a LST formulation. XBeach-G was applied over 2-day periods of low energy, south-westerly (SW) storm and south-easterly (SE) storm conditions, and was coupled to LST using a parametric approach which distributes the LST across the swash, surf and nearshore zones. The Delft3D-Wave model was used to obtain the inshore conditions required to drive XBeach-G and the LST formulation. The storm response was clearly influenced by the free-board (difference between the height of the berm and the total run-up) and was strongly dependent on storm-wave direction, with the SW and SE storms eroding and building up the surveyed area, respectively. Model results indicated that XBeach-G on its own is capable of reproducing the beach response under SW storm conditions (BSS > 0.95), but not under SE storms due to the higher LST gradients. The combination of XBeach-G and LST improved the fits to measured profiles under both SW (BSS > 0.96) and SE (BSS > 0.88) storms. This coupled approach represents an extension of XBeach-G to make it more suitable for coasts highly influenced by both cross-shore and LST, such as beaches with different coastline orientations and/or forced by varying wave directions.

Resumen

Los sistemas deltaicos se localizan en la transición entre ambientes fluviales y marítimos. Presentan un alto valor ambiental, económico y social, y responden rápidamente tanto a cambios naturales como a aquéllos inducidos por el hombre. Por su parte, las playas heterogéneas (PHs) son costas comunes en países de todo el mundo como, tales como Reino Unido, Dinamarca, Canadá, Nueva Zelanda, Canadá, Reino Unido, Dinamarca o los Mediterráneos. Además, la utilización de gravas en la regeneración de playas de arena hace que sean cada vez más frecuentes. A pesar de su importancia, los avances científicos en playas de grava y PHs han sido limitados en comparación con los de playas de arena. El objetivo principal de esta tesis es analizar, caracterizar y modelar la dinámica de playas deltaicas heterogéneas con base en una investigación a distintas escalas llevada a cabo en el delta del Guadalfeo, un delta Mediterráneo en una cuenca semi-árida y montañosa del sur de España. Para la consecución de este objetivo global se propusieron y abordaron cinco objetivos específicos, que fueron abordados en cinco capítulos distintos.

En primer lugar, los efectos de la construcción de un embalse a 19 km de la desembocadura en la dinámica del delta son analizados en el Capítulo 3. El volumen de sedimento transportado por fondo y acumulado en el delta fue estimado mediante un modelo hidrológico en dos escenarios: un escenario regulado, considerando los caudales desaguados por la presa, y un escenario no regulado, suponiendo que no existiera dicha infraestructura. Medidas batimétricas y topográficas fueron analizadas y relacionadas con los forzamientos fluvial y marítimo. Los resultados indicaron que el embalse ha modificado significativamente la dinámica aguas abajo: la costa ha perdido casi 0.3 hm^3 de sedimento desde la puesta en funcionamiento del embalse, generando un retroceso de la línea de costa a lo largo de 1.4 km en torno a la desembocadura de hasta 87 m (92% del inicial). En condiciones no reguladas, más de 2 hm^3 de sedimento habrían alcanzado la costa. Con base en estos resultados, tres nuevos escenarios de gestión de caudales desaguados por la presa y volúmenes de sedimentos extraídos del embalse fueron propuestos para evitar consecuencias más severas en la costa y la colmatación del embalse. Esta metodología para definir los escenarios de gestión es extensible a otros deltas, sirviendo como herramienta de apoyo a la toma de decisiones.

En segundo lugar, el Capítulo 4 detalla la variabilidad espacio-temporal de la desembocadura, centrado en la influencia de los cambios de la morfología sumergida en la propagación de oleaje y el transporte longitudinal de sedimentos (TLS). Medidas batimétricas fueron llevadas a cabo durante un periodo de 15 años (1999 - 2014), un modelo de propagación de oleaje (Delft3D-Wave) fue calibrado y aplicado, y las series completas de TLS fueron calculadas mediante técnicas de downscaling estadístico. Los resultados mostraron que la regulación fluvial indujo retroceso de la línea de costa y erosión del fondo de hasta 3 m a lo largo de un 1 km en torno a la desembocadura, con máximas tasas de erosión mayores a 760 m^3/m. Estos cambios morfológicos redujeron la refracción del oleaje, incrementando la energía del oleaje en rotura. Las variaciones del clima marítimo durante el periodo de estudio también influyeron en la dinámica costera. Aunque la erosión en torno a la desembocadura ha disminuido desde 2008, parcialmente debido a un pulso de sedimento en 2010, las tasas de TLS en tormentas procedentes del oeste se han incrementado significativamente desde entonces. Esto ha contribuido a la propagación de la erosión hacia el este de la desembocadura, poniendo en peligro desarrollos urbanísticos en ese tramo. Este capítulo proporciona información sobre el cambio de deltas dominados por oleaje y caudal hacia deltas principalmente dominados por oleaje y TLS, representando un avance en el conocimiento de la dinámica de deltas en los que el aporte fluvial ha disminuido debido a acciones humanas.

Los cambios morfológicos y sedimentarios de la PH en función del oleaje y nivel del mar así como tras una regeneración son estudiados en el Capítulo 5. Se realizaron campañas de campo mensuales y antes/después de tormentas durante un año (octubre 2013 - septiembre 2014) para medir la topografía del perfil de playa y tomar muestras de sedimentos. Fueron identificados tres fracciones de sedimento predominantes (arena, grava fina y grava gruesa) y dos estados límites del perfil emergido (convexo con múltiple bermas y cóncavo con una berma de tormenta). Entre dichos estados, se formaron varios perfiles de transición, caracterizados por la creación de bermas que progresivamente se solaparon, generando variabilidad de sedimento a lo largo del perfil y en profundidad. Los resultados indicaron que el run-up total (incluyendo el nivel del mar) es un umbral más preciso que la altura de ola para diferenciar entre condiciones de erosión y sedimentación. Además, sugieren que las PHs se recuperan más rápidamente que las playas de arena. El beneficio a largo plazo de la regeneración fue limitado, siendo atribuido al demasiado fino sedimento empleado en comparación con el natural y la demasiado alta localización del sedimento aportado en el perfil de playa. Este capítulo profundiza en el conocimiento de la dinámica morfo-sedimentaria de PHs en condiciones variables de oleaje y nivel del mar.

El Capítulo 6 aborda la evolución de la costa tras una regeneración finalizada en diciembre de 2014 mediante el análisis de medidas de campo y el modelado de la hidro- y morfodinámica. El perfil de playa y la línea de costa fueron medidos periódicamente durante seis meses, el modelo Delft3D-Wave fue aplicado; cuatro ecuaciones de TLS fueron testadas comparando con datos batimétricos; y el modelo de una línea fue aplicado entre campañas topográficas. Los resultados indicaron que un severo retroceso de la línea de costa (pérdida de playa seca > 208 m^2/día) tuvo lugar en los 45 días después de la intervención. Esto fue atribuido a la morfología de la línea de costa regenerada, las diferentes características del sedimento aportado con respecto al natural y la ocurrencia de una intensa tormenta del oeste. La formulación de Van Rijn proporcionó los mejores ajustes a los cambios morfológicos, obteniendo relaciones modelados/medidos del 93.1% y el 77.4% en los dos perfiles estudiados. Los resultados del modelo de una línea con las tasas de Van Rijn fueron también los mejores, con RMSEs disminuyendo durante el periodo de estudio y menores a 4.6 m en los últimos tres meses. Por tanto, la metodología aplicada constituye una herramienta de gestión para el modelado de la respuesta de PHs.

Por último, la respuesta del perfil de playa ante tormentas de direcciones cambiantes es investigada en el Capítulo 7. La morfología del perfil fue medida en un periodo de 36 días entre enero y febrero de 2015, y fue comparada con resultados del modelo XBeach-G y de una formulación de TLS. EL XBeach-G fue aplicado durante periodos de 2 días de bajo contenido energético (BCE), tormenta del suroeste (TSO) y tormenta del sureste (TSE), y fue acoplado con TLS mediante un enfoque paramétrico que distribuye el TLS a lo largo del perfil. El modelo Delft3D-Wave fue utilizado para obtener las condiciones de olaje requeridas para aplicar el XBeach-G y la fórmula de TLS. La respuesta de la playa fue claramente influenciada por la diferencia entre la altura de la berma y el run-up total, y dependiente de la dirección del oleaje, con la TSO y la TSE erosionando y recuperando el perfil, respectivamente. Los resultados indicaron que el XBeach-G es capaz de reproducir la respuesta de la playa ante TO (BSS > 0.95), pero no ante TSE debido a los mayores gradientes de TLS. La combinación del XBeach-G con TLS mejoró los ajustes a los perfiles medidos tras la TSE (BSS > 0.96) y la TSE (BSS > 0.88). Este enfoque acoplado representa una extensión del XBeach-G para hacerlo más apropiado en costas muy influenciadas por el transporte transversal de sedimentos y el TLS, tales como playas con diferentes orientaciones de la línea de costa y/o forzadas por direcciones del oleaje cambiantes.

CONTENTS

List of Figures

List of Tables

CHAPTER 1

INTRODUCTION

1.1 Context

1.1.1 Deltaic systems

Deltaic systems are located at the transition between fluvial and maritime environments; therefore, climatic, sedimentary and tectonic processes interact in a complex way on these systems (Coleman and Wright, 1975; Orton and Reading, 1993; Overeem, 2005; Syvitski and Saito, 2007). Their study is of great interest, as they represent a crucial link for understanding the interaction between fluvio-deltaic and marine sedimentation processes (Trincardi and Syvitski, 2005). These systems are particularly vulnerable to coastline variations (Overeem, 2005; Syvitski and Saito, 2007), because numerous activities take place along deltaic shorelines and these all have high ecological, economic, and social importance.

They respond rapidly to both natural and human-driven changes (Coleman and Wright, 1975; Orton and Reading, 1993). Their response to natural changes is mainly controlled by the supply of sediment reaching the coastal domain (Mateo and Siringan, 2007). In recent centuries, anthropogenic activities, such as channelization, channel deviation, dredging, deforestation or damming, have significantly altered natural processes and modified the morphology of deltaic environments (Yang et al., 2006; Syvitski et al., 2009; Hood, 2010; Kondolf et al., 2014; Anthony, 2015). In addition, (relative) sea-level rise is probably one of the most severe effects causing the retreat of worldwide deltas (Syvitski et al., 2009), with the micro-tidal Mediterranean deltas being particularly vulnerable (Jeftic et al., 1996; Nicholls and Hoozemans, 1996). In the present context of natural and artificial decline of river sediment transport, the assessment of the input of sediments and their redistribution toward the adjacent coastal areas is crucial for sustainable management (Pont et al., 2002; Walling and Fang, 2003).

During the last few decades, many examples of Mediterranean deltas being strongly modified by human activities have been studied. In the Ebro River (northeastern Spain), a very intense reshaping of the deltaic area occurred after the construction of dams in the upper course (Jiménez

and Sánchez-Arcilla, 1993; Jiménez et al., 1997). Simeoni et al. (2007) and Simeoni and Corbau (2009) reviewed how natural and human factors have controlled the Po delta (Italy) over time, whereas human-induced changes in the geomorphology of the Nile delta (Egypt) were studied by means of the Landsat Enhanced Thematic Mapper combined with published charts and field observations (Frihy and Komar, 1993; Frihy et al., 2003; El Banna and Frihy, 2009). Sabatier et al. (2006) and Sabatier et al. (2009) connected the large scale coastal behaviour of the Rhône delta with the impact and efficiency of hard engineering projects. The recent evolution of the Adra River delta (southeastern Spain) was reconstructed through historical maps, aerial photographs and bathymetric data (Jabaloy-Sánchez et al., 2010). Petropoulos et al. (2015) explored the changes in the Axios and Aliakmonas deltas (Greece) over a 25-year period (1984-2009) using photo-interpretation of Landsat TM images and a classification method based on support vector machines. Other numerous works have also focused on the influence of both natural and human-induced changes on the evolution of worldwide deltas, such as the Yangtze (Yang et al., 2011), Huanghe (Fan et al., 2006), Mekong (Le et al., 2007), Niger (Abam, 1999), Volta (Anthony et al., 2016), Danube (Vespremeanu-Stroe et al., 2007; Tatui et al., 2014), Arno (Pranzini, 2001) or Ombrone (Pranzini, 1994).

These works generally analysed the dynamics of the subaerial part of the delta, including the coastline, attributing the observed coastal retreat to reductions in the fluvial (and sediment) inputs to the coastal system due to human interventions, such as water extraction for irrigation and dam building (Syvitski et al., 2005; Syvitski et al., 2009). However, detailed comparisons and quantifications of how the deltaic systems would have evolved with and without the anthropic influence, and proposals of management methodologies to reduce coastal erosion are still lacking. In addition, the alterations in the submerged morphology due to these interventions, and the resulting modification of predominant coastal processes on a yearly-decadal scale have also received very limited attention. Wave refraction and longshore sediment transport (LST) are among the coastal processes affected by changes to the submerged bathymetry, whilst at the same time main drivers of coastal morphological changes over these temporal scales (De Vriend et al., 1993; Almar et al., 2015). This fact, in combination with the environmental, social and economic value of these systems (Stanley and Warne, 1993; Sánchez-Arcilla and Jiménez, 1997; Trincardi et al., 2004), reveals the importance of this thesis.

1.1.2 Mixed sand and gravel coasts

Gravel and mixed sand-gravel beaches are common in previously para-glaciated coastal regions and coasts with steep hinterlands, and are widespread in the UK (Carter and Orford, 1984; Poate et al., 2016), Denmark (Clemmensen and Nielsen, 2010; Clemmensen et al., 2016), Canada (Engels and Roberts, 2005; Dashtgard et al., 2006), Mediterranean (Bramato et al., 2012; Bergillos et al., 2016d) and New Zealand (Shulmeister and Kirk, 1993; Soons et al., 1997). They are also found when replenishment schemes use a mixture of sand and gravel, often from the shelf, or when gravels are used to protect sandy beaches (López de San Román-Blanco, 2004; Moses and Williams, 2008).

According to Jennings and Shulmeister (2002), two types of mixed sand-gravel beaches can be differentiated: (1) composite beaches, with a gravel high tide beach and a sandy low tide terrace; and (2) MSG beaches, with sand and gravel fractions mixed both cross-shore and at depth. The composite beach type, where the gravel and sand have been sorted by cross-shore

processes, requires a tide range and is more common in meso- and macro-tidal regions, whereas MSG beaches are more common in micro-tidal areas. Among these coastal settings, a distinction can be made between drift-aligned systems (e.g., Shaw et al. (1990); Carter and Orford (1991)), where alongshore sediment exchange plays the main role in driving shoreline dynamics, and swash-aligned areas (e.g., Orford and Carter (1995); Orford et al. (1995)), which are dominated by cross-shore sediment transport (Forbes et al., 1995; Orford et al., 2002).

Despite their societal importance, although they have received increasing attention in recent years, numerous studies have highlighted the discrepancy between the advances made for sandy coasts and the lack of similar progress for pure gravel and MSG coasts (Mason et al., 1997; Mason and Coates, 2001; Jennings and Shulmeister, 2002; Pontee et al., 2004; Buscombe and Masselink, 2006; López de San Román-Blanco et al., 2006; Horn and Walton, 2007). This discrepancy is particularly evident for both experimental studies and numerical approaches (Orford and Anthony, 2011; Masselink et al., 2014), and contrasts strongly with the increasing demand for reliable coastal change models to help mitigate and adapt to global erosion problems (Syvitski et al., 2005; Anthony et al., 2014) and future sea-level rise (Payo et al., 2016; Spencer et al., 2016).

On the one hand, the identification of morphodynamic states and characterization of beach profiles based on field data are important for the correct management of these environments (Bernabeu Tello et al., 2002; González et al., 2010; Díez et al., 2017). Buscombe and Masselink (2006) introduced the concept of *morpho-sedimentary dynamics* as the mutual interactions of morphology, hydro-hydraulics and sediment properties, highlighting that it is the recommended conceptual framework within which to organise further research for gravel environments. This analysis is also relevant for the design of artificial nourishment to combat beach erosion (Li et al., 2006). Previous studies on MSG coasts focused on specific aspects: Horn and Walton (2007) described the sediment distribution before, during and after a nourishment program along a section of an MSG beach and analysed the effects of sediment recharge with different sedimentary properties. Eikaas and Hemmingsen (2006) performed a field study that focused on some sediment properties of an MSG beach, but did not address the morphological characteristics of the beach profile. Ivamy and Kench (2006) and Bramato et al. (2012) analysed the recovery of MSG beaches after storms, but did not study the sedimentological aspects.

On the other hand, several efforts have been made over the last decade to develop a morphodynamic storm response model specific to gravel and MSG beaches (Pedrozo-Acuña, 2005; Pedrozo-Acuna et al., 2006; Pedrozo-Acuña et al., 2007; Van Rijn and Sutherland, 2011; Jamal et al., 2011; Jamal et al., 2014; Williams et al., 2012b), resulting in the development of a 1D process-based model (XBeach-G) for the prediction of storm hydro- and morphodynamics of the beach profile (McCall et al., 2012; McCall et al., 2013; McCall, 2015), which has been successfully validated on cross-shore dominated gravel beaches (McCall et al., 2014; McCall et al., 2015; Almeida et al., 2017). However, in drift-aligned systems, where longshore sediment transport (LST) plays a key role in controlling the coastal behaviour (Orford et al., 1991; Muñoz-Pérez et al., 2010), a cross-shore profile model is clearly not sufficient to model storm response. Drift-aligned systems could be coastlines with a highly variable shoreline orientation and a uni-directional, but spatially-variable LST (López-Ruiz et al., 2012b; López-Ruiz et al., 2014). Alternatively, they could be coastlines subjected to a bi-directional wave climate characterized by temporal variations in the frequency of the incoming wave directions and, as a consequence, in the net littoral drift (French and Burningham, 2015; Bergillos et al., 2016b).

In these coastal areas, it is particularly important to consider not only the cross-shore sediment transport, but also the effects of LST (De Alegría-Arzaburu and Masselink, 2010; Masselink et al., 2016b). Recent advances are available to estimate LST on sand, gravel and shingle beaches (Van Rijn, 2014); but the cross-shore distribution of LST, widely studied on sandy beaches (e.g., Berek and Dean (1982); Komar (1983); Kamphuis (1991b); Bayram et al. (2001)) and relevant for modelling coastal response, has not been investigated in depth on gravel and MSG beaches (Van Wellen et al., 1998; Van Wellen et al., 2000).

Hence, neither the morphological evolution of the beach as a result of wave and water-level forcing, nor its characteristic morpho-sedimentary states have been studied in depth for MSG beaches. In addition, the contribution of wave run-up, astronomical tide and storm surge to the total run-up, and their roles in the beach response has not been explored in detail on micro-tidal coasts. There are also significant gaps related to beach nourishment: (1) the amount of morphological measurements performed after replenishment projects remains limited for MSG coasts, and (2) relatively few numerical models have been applied and compared with field data in reference to these beaches as a means of developing engineering tools for coastal managers. Finally, numerical approaches to model storm response by including cross-shore and longshore sediment transport have not been applied and validated using field data on MSG coasts highly influenced by both components of sediment transport, such as beaches with different coastline orientations and/or forced by varying wave directions (Elshinnawy et al., 2017). These facts, along with the presence of MSG beaches on many worldwide coasts, the frequent use of gravel to protect eroded sandy beaches (Van Wellen et al., 2000; Mason and Coates, 2001) and the expected sea-level rise in the coming years also attest to the importance of this thesis.

1.2 Objectives

The overall objective of this thesis is to characterize and model the dynamics of mixed sand and gravel deltaic coasts at different spatio-temporal scales through the analysis of field observations and the application of different numerical approaches.

To accomplish this global objective, the following specific objectives were addressed based on a case study in southern Spain (Guadalfeo delta):

I. To quantify the effects of the construction of a reservoir on the evolution of the deltaic coast on a decadal scale.

II. To study the implications of nearshore morphological changes around the river mouth on wave propagation and longshore sediment transport on a decadal scale.

III. To characterize the morphological and sedimentary dynamics of the deltaic beach under varying wave and water-level conditions on a yearly scale.

IV. To analyse the morphological response of the deltaic coast forced by an artificial nourishment project on an seasonal scale.

V. To investigate the morphological storm response of the deltaic beach under varying wave directions on a monthly scale.

1.3 Thesis outline

The thesis is structured as follows. Chapter 2 details the study site selected to carry out this research, from the Mediterranean coastal region to the Guadalfeo basin and its deltaic coast. Chapter 3 (specific objective I) quantifies the influence of Guadalfeo river regulation on the recent evolution (1999 - 2014) of the deltaic coast by comparing two scenarios: a managed (real) scenario, based on the flows drained by the dam, and an unmanaged scenario, based on the simulation of the flows without such regulation. Chapter 4 (specific objective II) describes the spatial and temporal variability of the nearshore morphology around the river mouth over a 15-year period (1999 - 2014) and focuses on the influence of these morphological changes on wave propagation and longshore sediment transport. Chapter 5 (specific objective III) addresses the morphological and sedimentary dynamics of the beach profile over a 1-year period (October 2013 - September 2014), focusing on the contribution of wave run-up, storm surge and astronomical tide to natural beach response, as well as its behaviour after an artificial nourishment project. The coastal response forced by nourishment during a six-month period (December 2014 - June 2015) is investigated with more detail in Chapter 6 (specific objective IV), including the modelling of the coastline evolution. Chapter 7 (specific objective V) analyses and models the profile response of the deltaic beach forced by storm waves from varying directions over a 36-day period between January and February 2015. Finally, the conclusions of the thesis and some future research lines are summarized in Chapter 8.

1.4 Publications

Journal papers

- **Bergillos, R.J.**, Rodríguez-Delgado, C., Millares, A., Ortega-Sánchez, M., and Losada, M.A. (2016). Impact of river regulation on a Mediterranean delta: Assessment of managed versus unmanaged scenarios. Water Resources Research 52, 5132-5148.
- **Bergillos, R.J.**, López-Ruiz, A., Ortega-Sánchez, M., Masselink, G., and Losada, M.A. (2016). Implications of delta retreat on wave propagation and longshore sediment transport - Guadalfeo case study (southern Spain). Marine Geology 382, 1-16.
- **Bergillos, R.J.**, Ortega-Sánchez, M., Masselink, G., and Losada, M.A. (2016). Morpho-sedimentary dynamics of a micro-tidal mixed sand and gravel beach, Playa Granada, southern Spain. Marine Geology 379, 28-38.
- **Bergillos, R.J.**, and Ortega-Sánchez, M. (2017). Assessing and mitigating the landscape effects of river damming on the Guadalfeo River delta, southern Spain. Landscape and Urban Planning 165, 117-129.
- **Bergillos, R.J.**, Rodríguez-Delgado, C., and Ortega-Sánchez, M. (2017). Advances in management tools for modeling artificial nourishments in mixed beaches. Journal of Marine Systems 172, 1-13.
- **Bergillos, R.J.**, Masselink, G., and Ortega-Sánchez, M. (2017). Coupling cross-shore and longshore sediment transport to model storm response along a mixed sand-gravel coast under varying wave directions. Coastal Engineering 129C, 93-104.

Books and chapters in books

- Ortega-Sánchez, M., **Bergillos, R.J.**, López-Ruiz, A., and Losada, M.A (2017). Morphodynamics of Mediterranean mixed sand and gravel coasts. SpringerBriefs in Earth Sciences, Springer, ISBN: 978-3-319-52439-9.

International conferences

- **Bergillos, R.J.**, Ortega-Sánchez, M., and Losada M.A. (2015). Foreshore evolution of a mixed sand and gravel beach: The case of Playa Granada (Southern Spain). 8th Coastal Sediments, San Diego (United States).
- **Bergillos, R.J.**, López-Ruiz, A., Millares, A., Rodríguez-Delgado, C., Ortega-Sánchez, M., and Losada, M.A. (2015). Human-driven coast changes in the Guadalfeo River deltaic system (Southern Spain). 36th IAHR-International Association for Hydro-Environment Engineering and Research World Congress, The Hague (The Netherlands).
- **Bergillos, R.J.**, Luengo, J.M., Rodríguez-Delgado C and Ortega-Sánchez M (2015). Massive urbanization and coastal management in Mediterranean deltaic systems: the unsustainable growth model of southern Spain. ECSA 55 - Unbounded boundaries and shifting baselines, London (UK).
- **Bergillos, R.J.**, Ortega-Sánchez, M., Masselink, G., and Losada M.A. (2015). Urban planning analysis of Mediterranean deltas – Guadalfeo case study. 12th International Conference on the Mediterranean Coastal Environment, Varna (Bulgaria).
- **Bergillos, R.J.**, and Ortega-Sánchez, M. (2016). Impact of humans on deltaic coasts – a sustainable management plan to face climate change. 6th Sustainable Development Symposium, Granada (Spain).
- **Bergillos, R.J.**, Masselink, G., McCall, R.T., and Ortega-Sánchez, M. (2016). Modelling overwash vulnerability along mixed sand-gravel coastlines with XBeach-G: Case study of Playa Granada, southern Spain. 35th International Conference on Coastal Engineering, Istanbul (Turkey).

National conferences

- **Bergillos, R.J.**, Rodríguez-Delgado, C., López-Ruiz, A., Ortega-Sánchez, M., and Losada, M.A. (2015). Variabilidad espacio-temporal de la morfología sumergida de un sistema deltáico heterogéneo: playa Granada (Sur de España). XIII Jornadas Españolas de Ingeniería de Costas y Puertos, Avilés (Spain).
- Rodríguez-Delgado, C., **Bergillos, R.J.**, and Ortega-Sánchez, M. (2015). Modelado de sistemas deltaicos altamente alterados: El caso del Guadalfeo (Sur de España). VIII Simposio Internacional sobre el Margen Ibérico Atlántico, Málaga (Spain).

- López-Ruiz, A., **Bergillos, R.J.**, Rodríguez-Delgado, C., Ortega-Sánchez, M., and Losada, M.A. (2015). Variación temporal y espacial del transporte longitudinal de sedimentos en un sistema deltaico alterado. VIII Simposio Internacional sobre el Margen Ibérico Atlántico, Málaga (Spain).

- **Bergillos, R.J.**, Rodríguez-Delgado, C., Reyes-Merlo, M.A., López-Ruiz, A., Ortega-Sánchez, M., and Losada, M.A. (2015). Morfodinámica de playas heterogéneas en el litoral del mar de Alborán: análisis experimental y modelado numérico. XII Jornadas Técnicas de Jóvenes Profesionales de la Asociación Técnica de Puertos y Costas, Motril (Spain).

- **Bergillos, R.J.**, Reyes-Merlo, M.A., Ortega-Sánchez, M., and Masselink, G. (2016). Campañas de campo, modelos numéricos y simulación de agentes como herramientas para la gestión de playas heterogéneas. I Jornadas de Investigadores en Formación: Fomentando la Interdisciplinariedad, Granada (Spain).

- **Bergillos, R.J.**, Millares, A., and Ortega-Sánchez, M. (2016). Development of a sustainable methodology to avoid coastal erosion in Mediterranean deltas. I Foro de Ingeniería para el Desarrollo Sostenible, Granada (Spain).

CHAPTER 2

STUDY SITE

2.1 The Mediterranean region

The Mediterranean basin is almost 2.6 million km^2 with its overall coastline enclosed by mountainous terrain, except for part of the north African margin (Rohling et al., 2009). The length is approximately 3,800 km from east to west and 900 km from north to south at its maximum between France and Algeria. The average water depth is approximately 1,500 m, with a maximum depth of 5,121 m (southwestern Greece). It can be divided into two sub-basins: the western and the eastern Mediterranean, which in turn are composed of a series of small basins (Rohling et al., 2009). The western Mediterranean has an area of approximately 0.9 million km^2 and includes the Alborán Sea (Figure 2.1.1A), which allocates the study site of this thesis (Figure 2.1.1B). The Mediterranean basin comprises a vast set of coastal and marine ecosystems that deliver valuable benefits to all of its coastal inhabitants, including different types of nearshore coastal areas (Liquete et al., 2004).

The evolution of the Mediterranean basin has been analysed in detail in the past (e.g., Maldonado and Comas (1992) and Comas et al. (1999)). The present configuration of the Mediterranean zone represents the final stages of a continent-continent collisional orogeny. The resulting crustal context is characterized by active and passive margins, by isostasy and tectonics that have imprinted marked variations in relief, and by present-day tectonics and coastal geomorphic diversity (Comas et al., 1999; Cavazza and Wezel, 2003; Anthony et al., 2014). The present-day geological configuration of the Mediterranean domain is dominated by a system of connected fold-and-thrust belts and associated foreland and back-arc basins (Cavazza and Wezel, 2003). As a result, small rivers drain approximately 50% of the total Mediterranean Sea catchments (Poulos and Collins, 2002).

The Mediterranean drainage system comprises more than 160 rivers with individual catchment areas < 200 km^2 that bring out the abundance and importance of small rivers in supplying sediment to the coast (Liquete et al., 2004; Lobo et al., 2006; Vanmaercke et al., 2011; Maetens et al., 2012; Anthony et al., 2014; Bergillos et al., 2016a). The morphology of river channels

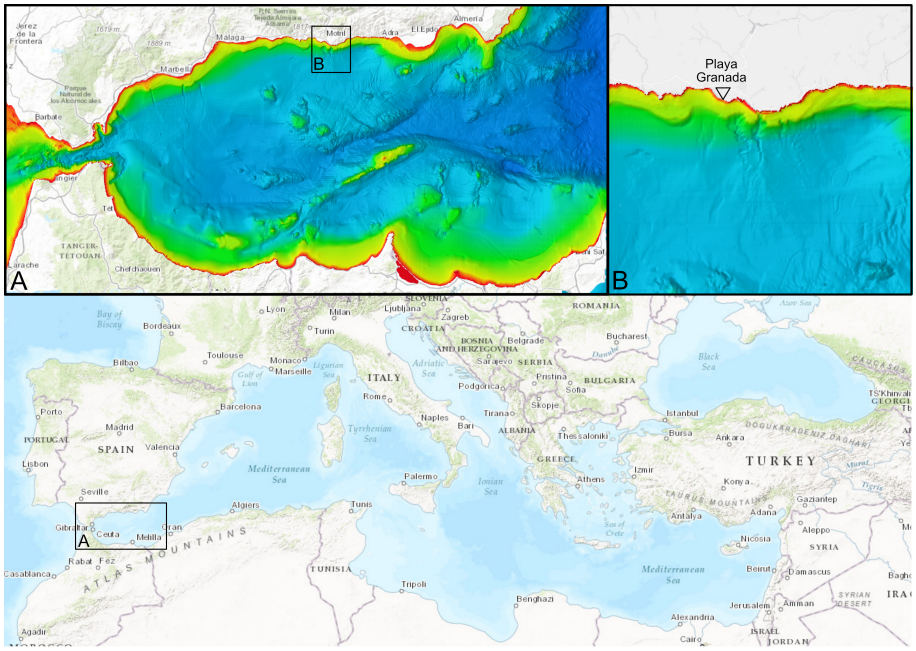

Figure 2.1.1: Topographic and bathymetric map of the Mediterranean basin. Panel A highlights the Alborán basin and panel B depicts the study site of this thesis.

ranges from confined narrow channels in canyons within upland areas to wide, braided channels in piedmont areas and large valleys (Hooke, 2006). Although numerous Mediterranean river systems formed deltas during the Holocene, over the last several and present centuries, most of the deltas have been experiencing erosion because of human impacts (McManus, 2002). Consequently, there is a strong dependence between sediment disposal by Mediterranean rivers and the evolution of the coastal zone with a determinant influence on the type of sediments forming the resulting beaches.

Along the Mediterranean basin, the continental shelves are generally narrow and mountain slopes drop almost straight into the sea (Ortega-Sánchez et al., 2014); remarkable examples occur at the southern and northern Iberian Peninsula and at the Maritime Alps (Figure 2.1.1). Larger continental shelves are present at locations of seaward extension of deltaic systems, such as off the Ebro and Rhône Rivers (Amblas et al., 2004). The supply of riverine sediment has been fundamental for the geomorphic development of these open-coast barrier systems, where coastal morphology and wave fetch conditions favour unimpeded longshore drift (Bergillos et al., 2016b).

The Mediterranean coastline is approximately 46,000 km long (Stewart and Morhange, 2009) and has nearly 19,000 km of island coastline; 54% of the coastline is rocky, and the remaining 46% includes important and fragile habitats and ecosystems such as beaches, dunes, reefs, lagoons, swamps, estuaries and deltas. Rocky coasts commonly exhibit cliffs cut into different terranes (Ortega-Sánchez et al., 2003) with an increasing occupation by settlements over the last several decades but with a morphology that remains largely unaltered. Conversely, low-lying sedimentary coasts are more dynamic than rocky coasts, and the balance among sea-level rise, sediment supply, and wave and coastal current regimes determine whether the coastline advances, remains stable, or retreats (Stewart and Morhange, 2009; UNEP/MAP, 2012; Anthony et al., 2014).

Compared to the Atlantic or Pacific open coasts, wave processes are generally of much lower energy (limited fetch), and the tidal range is generally below a meter (micro-tidal conditions). Therefore, coastline evolution and shoreline features are generally the result of the river sediment supply, the redistribution of this sediment by nearshore processes and the oscillations of the mean sea-level (Stewart and Morhange, 2009). The dynamics of these environments are highly linked to the sediment yield of nearby rivers because LST is not a primary forcing but a key process in modelling and re-shaping the coast (Bergillos et al., 2016b). Therefore, the variety of coastal environments results in a wide range of beaches, from sandy to MSG and pure gravel beaches (Bergillos et al., 2016d).

The Mediterranean region has a long history of human settlements and impacts (Marriner and Morhange, 2007; Hooke, 2006). The total population of the Mediterranean countries grew from 276 million in 1970 to 466 million in 2010 and is predicted to reach 529 million by 2025 (UNEP/MAP, 2012). Overall, more than half of the population lives in countries on the southern shores of the Mediterranean, a proportion that is expected to grow to three quarters by 2025 (UNEP/MAP, 2012). If it is considered as a single area, the Mediterranean basin is by far the largest global tourism destination, attracting almost a third of the world tourists and generating more than a quarter of international tourism receipts. Anthropogenic modification of sedimentary processes and patterns constitutes both adjustments to natural sedimentary environments (e.g., delta irrigation, coastal reclamation) and the creation of novel sedimentary environments articulated around man-made structures. River damming is needed not only to control extreme events but also to underpin the rise in water demand due to increasing tourist exploitation of the beaches. Many complementary attractions and services were developed to enhance these activities: marinas, promenade waterfronts, resorts and golf courses, among others.

As highlighted by recent works (e.g., Semeoshenkova and Newton (2015) and Bergillos and Ortega-Sánchez (2017)), tourist development is placing the littoral zone under unprecedented pressures, resulting in a deep alteration of the natural physical processes that typically control the dynamics of these systems. The direct consequence of this unsustainable pressure on the coast is the development and application of a wide range of management practices (e.g., Palanqués and Guillén (1998), Ibáñez et al. (2014), and Semeoshenkova and Newton (2015)), from coastal structures to artificial replenishments. Despite these efforts, the success of many of these practices, mainly artificial nourishments, is temporary and frequently lasts no more than a winter period (Bergillos et al., 2017a; Bergillos and Ortega-Sánchez, 2017).

2.2 Guadalfeo River basin

The Guadalfeo River basin, with an area of $1,252$ km^2, is located in southern Spain and drains into the Alborán Sea (Figure 2.1.1). It includes the highest peaks on the Iberian Peninsula ($\sim 3,400$ m.a.s.l.) and is fed by one of the most high-energy drainage systems along the Spanish Mediterranean coast. The northern catchment divide corresponds to the crest line of the Sierra Nevada, whereas the southern divide corresponds to the crest lines of the Sierra de la Contraviesa and the Sierra de Lújar (Figure 2.2.1).

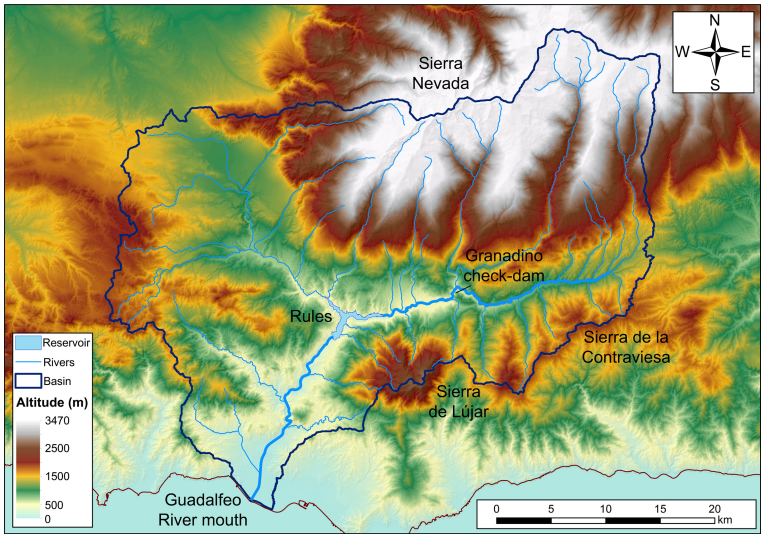

Figure 2.2.1: Delimitation of the basin and locations of the Rules Reservoir, the Granadino check-dam, the Sierra Nevada, the Sierra de la Contraviesa and the Sierra de Lújar. (Source: Adapted from Bergillos and Ortega-Sánchez (2017). Reproduced with permission of Elsevier).

The mountainous influence of the Sierra Nevada conditions the hydrological dynamics and the pluvio-nival character of this semi-arid and high-mountain basin. This sub-basin is mainly composed of Nevado-Filábride complex (mica-schist and graphitic mica-schist). The high altitude guarantees the presence of snow from November to June, which allows a near-perennial flow despite its aridity (Herrero et al., 2009). The nival contributions condition this quasi-perennial flow, which allows the development of an armor layer and separates a surface layer ($D_{50} \sim 60$ mm) from a substrate layer ($D_{50} \sim 2.5$ mm). The periodic occurrence of intense precipitation and snowmelt events reshape this drainage network and release a large amount of sediment (Millares et al., 2014b).

The Sierra de la Contraviesa presents a more ephemeral nature with the absence of snowmelt cycles and sub-surface storage. It is composed of Alpujárride complex (quartzites, phyllites and schists). The evolution of erosion processes is clearly influenced by changes in vegetation and land use. This area was originally dominated by forest and Mediterranean shrubs, and large areas of almond and olive orchards are currently pre-eminent (Millares et al., 2012). This change has led to the emergence and development of different types of incisions in the form of rills, gullies and more developed channels. Here, the tributary channels lead to important bedload contributions during intense events that accumulate in the Guadalfeo River.

The annual precipitation data show significant spatial gradients (Table 2.2.1) and the average annual rainfall in the basin is 586 mm, with minimum and maximum values of 500 and 1,000 mm, respectively (Millares et al., 2012; Millares et al., 2014a). The pre-regulation hydrological regime of the Guadalfeo River had peak discharges that exceeded 1,000 m^3/s (Capel-Molina, 1974). The river longitudinal profile is variable: the slope is greater than 2% in the southern Sierra Nevada and Sierra de la Contraviesa, approximately 1% upstream of the Granadino check-dam, equal to 2.5% between the Órgiva gauge station and the Rules Reservoir, and approximately 0.9% downstream of the dam (Figure 2.2.1). This relatively steep topographic gradients lead to large contributions from a wide range of sediment sizes (Millares et al., 2014a). As a result, the particle size distribution on the coast is particularly complex with varying proportions of sand and gravel (Figure 2.3.1b).

Table 2.2.1: Minimum, maximum, mean and standard deviation (SD) of the annual precipitation (in mm/y) in 11 meteorological stations of the Guadalfeo basin (Millares et al., 2014a).

Station	Minimum	Maximum	Mean	SD
Albuñol	210	1026	456	179
Bérchules	301	1617	658	249
Cádiar	218	1217	429	186
Contraviesa	312	1062	627	285
Órgiva	207	1434	482	195
Poqueira	434	1485	829	379
Pórtugos	326	1719	726	286
Soportújar	336	1810	692	261
Tajos Breca	413	1474	793	381
Torvizcón	262	1265	539	188
Trevélez	307	1635	663	258

The river was dammed 19 km upstream from the mouth in 2004, regulating 85% of the basin runoff (Losada et al., 2011). The total capacity of the Rules Reservoir (117 hm^3) was planned to be used for the following purposes: irrigation (40%), supplies for residential developments along the coast (19%), energy generation (9%), flood control (30%) and environmental flow (2%). However, the river damming modified the natural flow regime and altered the behaviour of the system downstream of the dam (Bergillos et al., 2016a).

Previous works on the Guadalfeo delta focused on the description of the submarine geomorphology and sedimentology (Liquete et al., 2005; Lobo et al., 2006; Fernández-Salas et al., 2007), the determination of marine intrusion (Duque et al., 2008), the characterization of the delta aquifer's hydrology (Duque et al., 2010) and the study of the delta at the millennial temporal scale (Jabaloy-Sánchez et al., 2014). Given its characteristics, recent history and similarities with many other worldwide deltas (Syvitski and Saito, 2007; Syvitski et al., 2009; Anthony et al., 2014; Anthony, 2015), the Guadalfeo delta represents a valuable example to investigate the multi-scale dynamics of deltaic coasts, including the analysis of human-induced morphological changes and their effects on coastal processes.

2.3 Guadalfeo deltaic coast: Playa Granada

Playa Granada is a 3-km-long MSG beach located on the southern coast of Spain that faces the Mediterranean Sea (Figure 2.3.1). The beach corresponds to the central stretch of the Guadalfeo deltaic coast and is bounded to the west by the Guadalfeo River mouth and to the east by *Punta del Santo*, the former location of the river mouth. The deltaic coast is bounded to the west by Salobreña Rock and to the east by Motril Port. This port is an artificial barrier that prevents eastward longshore sediment transport (Félix et al., 2012).

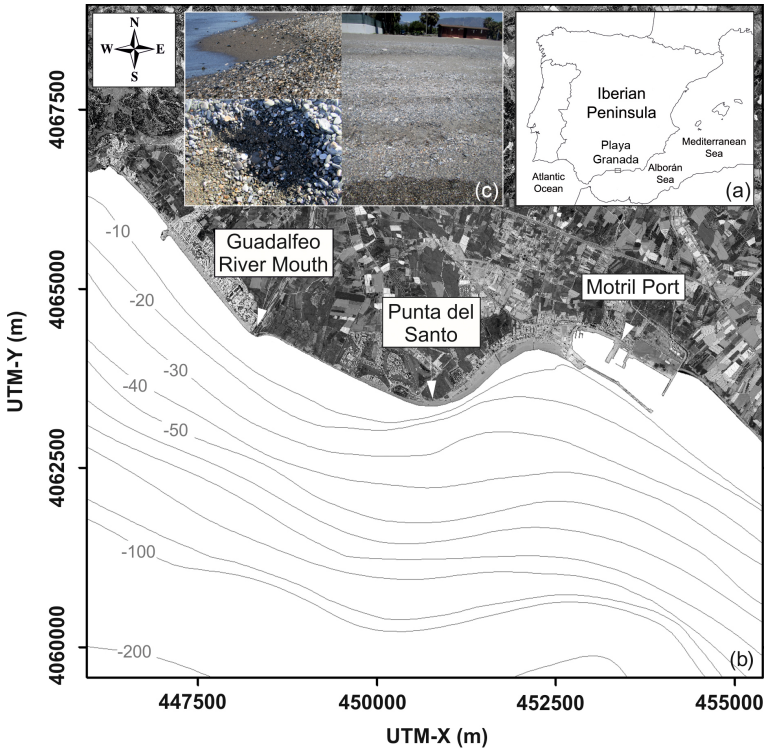

Figure 2.3.1: (a) Location of Playa Granada (southern Spain). (b) Plan view of Playa Granada and bathymetric contours (in meters below the present sea-level). (c) Sediment variability on the beach. (Source: Adapted from Bergillos et al. (2016d). Reproduced with permission of Elsevier).

The continental shelf of the Guadalfeo River is narrow with an average width of less than 5 km. The shelf break is located at a depth of 100 m and is approximately parallel to the main coastline orientation of the delta front (Lobo et al., 2015). The shelf gradient is $> 3\,^{\circ}$ in the delta foreset region and then decreases seaward to $< 1.5\,^{\circ}$ in the bottomset region (Jabaloy-Sánchez et al., 2014). The Guadalfeo River pro-delta extends seaward almost 3.5 km and is characterised by an undulating pro-delta surface due to the presence of bedforms (Lobo et al., 2015). An off-lap break is identified proximally over the pro-delta, at water depths of 8-14 m and up to 0.5 km from the coast (Fernández-Salas et al., 2007). Medium sands with some muddy intercalations are found in the Guadalfeo pro-delta, whereas the sediment composition in shallower water across the foreset region is dominated by sandy sediments (Lobo et al., 2006). The emerged deltaic area of the fluvial system covers $8.6 \cdot 10^6$ m^2 and is composed of coarse-grained sediments ranging from medium sands to boulders (Jabaloy-Sánchez et al., 2014).

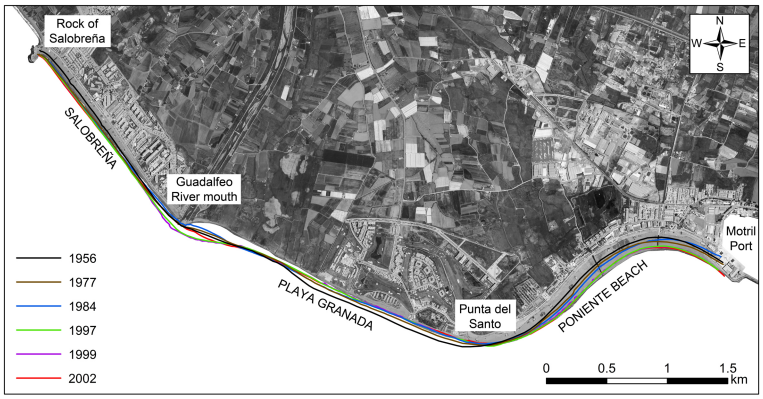

Figure 2.3.2: Evolution of the coastline position before the entry into operation of the dam. The background aerial image is from 2013. (Source: Adapted from Bergillos and Ortega-Sánchez (2017). Reproduced with permission of Elsevier).

The dynamics of the deltaic coastline has been historically governed by the sediment supply of the river during intense events; the coastline evolution at the millennial temporal scale is detailed in Hoffmann (1987) and Jabaloy-Sánchez et al. (2014). The beach extension increased by approximately $150,000$ m^2 since 1956 until the entry into operation of Rules Dam in 2004. Over this period, the stretch of beach between Punta del Santo and Motril Port advanced seaward, whereas erosion persisted in the section between Salobreña Rock and *Punta del Santo* (Figure 2.3.2). Therefore, the studied stretch of beach has been particularly affected and has presented higher levels of coastline retreat in recent years than both western and eastern stretches of the deltaic coast, known as Salobreña and Poniente Beach, respectively (Figure 2.3.3).

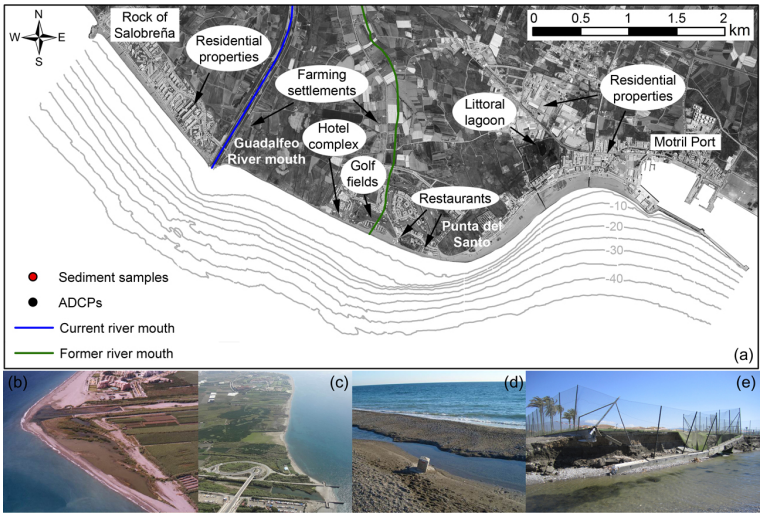

Figure 2.3.3: (a) Locations of former and current river mouths, principal occupations and bathymetric contours in 1999. Plan views of the delta before (b) and after (c) the river damming. (d) Boundary marker of the public domain in Playa Granada, which is located few meters from the shoreline. (e) Storm-induced erosion problems in the hotel complex indicated in panel a. (Source: Adapted from Bergillos and Ortega-Sánchez (2017). Reproduced with permission of Elsevier).

The built-up area at a distance of less than 2 km from the coastline has increased by more than 6 times since 1956, with the growth being especially significant between 2002 and 2008 (Figure 2.3.4). However, it reduced in recent years due to economic downturn (Figure 2.3.4a), avoiding new urban development at the southeast of the river mouth (Figure 2.3.4e). The buildings between Rock of Salobreña and *Punta del Santo* are located within a distance of 50 m from the coastline and most of them were built on areas of great environmental value (Félix et al., 2012). Playa Granada is occupied by an exclusive leisure resort, golf courses, restaurants and summer homes, and has urban lots, at the south of the river mouth, that have not been developed yet. In light of these facts, it is clear that the coast has a high environmental and tourist value, and its exploitation requires a large area of dry beach (Félix et al., 2012). For this reason, artificial nourishment projects in this MSG coastal environment have been frequent since the entry into operation of the dam (Bergillos et al., 2015b).

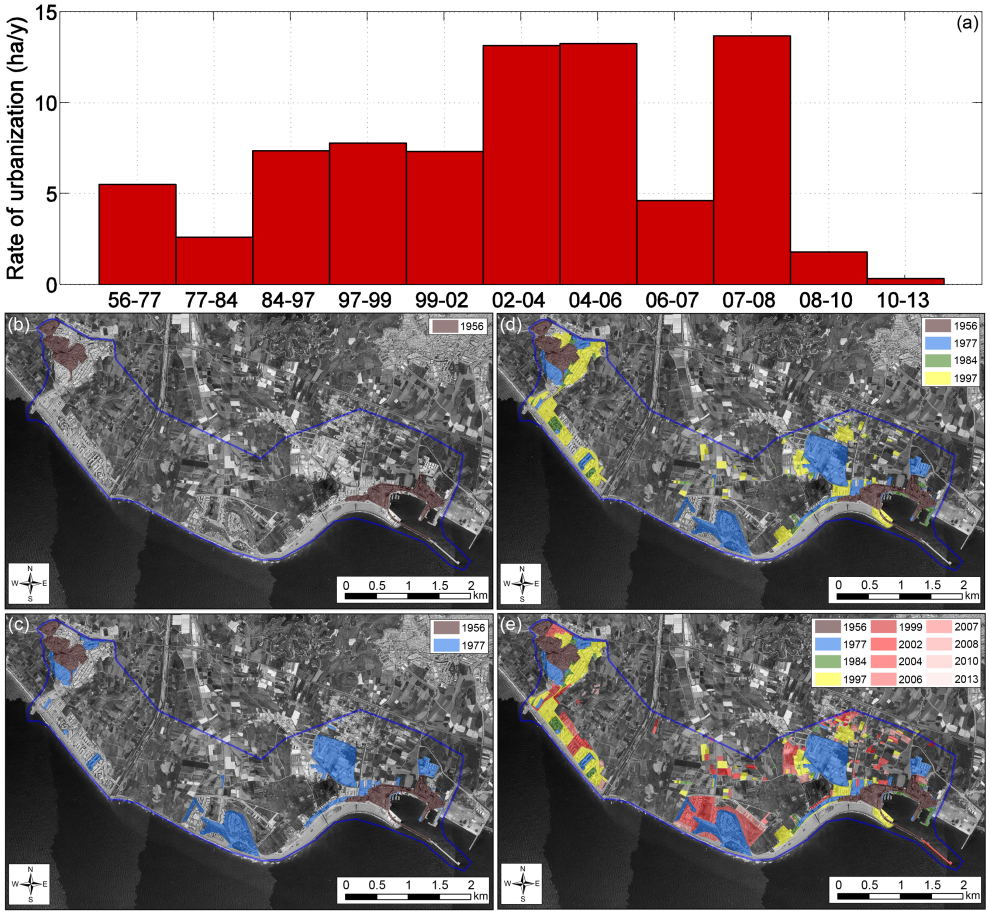

Figure 2.3.4: (a) Rate of urbanization at a distance of less than 2 km from the coastline from 1956 to 2013. Developed areas in 1956 (b), 1977 (c), 1997 (d) and 2013 (e). The background aerial image is from 2013. (Source: Adapted from Bergillos and Ortega-Sánchez (2017). Reproduced with permission of Elsevier).

Climatic patterns at the Guadalfeo deltaic coast exhibit a significant contrast between summer and winter. The wave climate is bimodal with prevailing west-southwest and east-southeast directions (Figure 2.3.5). The region is subjected to the passage of extra-tropical Atlantic cyclones and Mediterranean storms, with average wind speeds of 18–22 m/s (Ortega-Sánchez et al., 2003), which generate wind waves under fetch-limited conditions (approximately 200 to 300 km). Under south Atlantic storm conditions, swell waves generated in the Gulf of Cadiz propagate through the Strait of Gibraltar. These swell waves impinge the coast simultaneously with the local wind waves, but with slightly different angles (Ortega-Sánchez et al., 2008). The 50%, 90%, 99% and 99.9% not exceedance significant wave heights in deep water are 0.5 m, 1.2 m, 2.1 m and 3.1 m, respectively. The astronomical tidal range is ~ 0.6 m, whereas typical storm surge levels can exceed 0.5 m (Bergillos et al., 2016d).

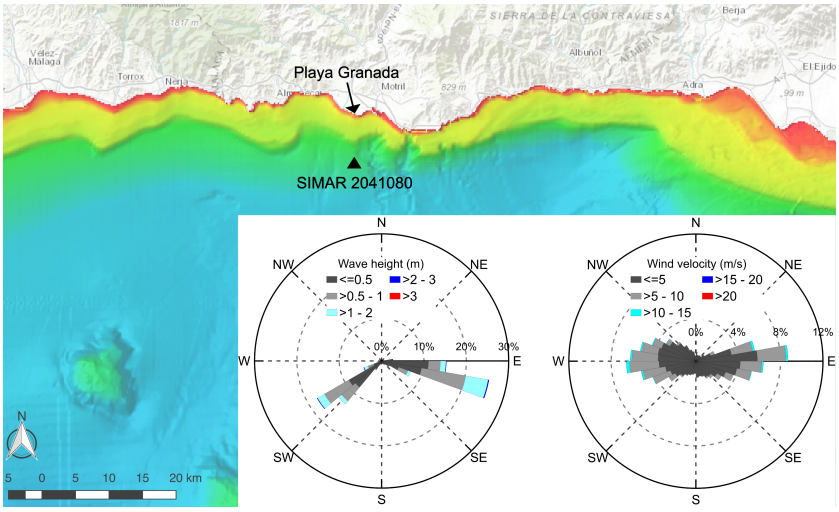

Figure 2.3.5: Polar diagram showing the occurrence frequency of deep-water significant wave heights and wave directions, and wind velocity and directions. Data from SIMAR 2041080 were provided by *Puertos del Estado*.

CHAPTER 3

INFLUENCE OF RIVER REGULATION ON THE DELTA

This chapter addresses the effects of the construction of a reservoir 19 km from the mouth on the dynamics of the Guadalfeo delta, a Mediterranean delta in a semi-arid and high-mountain basin. The sediment volume transported as bedload and accumulated in the delta was estimated under two scenarios by means of a calibrated hydrological model: a managed scenario, considering the flows drained by the dam, and an unmanaged scenario, considering the absence of such infrastructure. Bathymetric and topographic measurements were analysed and correlated with the fluvial and maritime forcing agents. Results indicate that the reservoir has significantly modified the dynamics downstream: the coast has lost almost 0.3 hm^3 of sediments since the entry into operation of the dam, generating a 1.4-km coastline retreat around the mouth, with a maximum retreat of 87 m (92% of the initial). The beach profile decreased by up to 820 m^2, whereas the average decrease around the mouth was equal to 214 m^2. Under unmanaged conditions, more than 2 hm^3 of bedload would have reached the coast. Based on the results, three new management scenarios of flows drained by the dam, in combination with bypassed sediment from the reservoir, were proposed to prevent more severe consequences in the delta and the silting of the reservoir. The proposed methodology for new management scenarios can be extended to other worldwide deltas, especially to those in semi-arid and Mediterranean basins, and it represents an advanced tool for decision making.

3.1 Objective

The main objective of this chapter is to analyse and quantify the influence of the construction of a reservoir on the recent evolution (1999-2014) of the Guadalfeo River delta by comparing two scenarios: a managed (real) scenario, based on the flows drained by the dam, and an unmanaged scenario, based on the simulation of the flows without such regulation. A calibrated physically based hydrological model was used for both scenarios. Changes in sediment volume for different control volumes at the delta were calculated and related to bedload inputs modelled stochastically under both scenarios and the deltaic deposits retained at the tail of the Rules Reservoir (Millares et al., 2014b). These results were correlated with the maritime climate and both regulated and unmanaged flow regimes. The evolution of the coastline and beach profile was also analysed Finally, three new management scenarios were proposed. These scenarios were based on the constant or seasonal flows drained by the dam required to avoid coastal erosion during drought periods. The feasibility of the application of these management scenarios to other deltas was also discussed.

3.2 Methodology

This chapter is mainly based on the analysis and quantification of bedload contributions, coastal changes and their relation to maritime and fluvial forcing agents under two different scenarios: an unmanaged scenario (Q_{unman}) and a managed (real) scenario (Q_{man}). Field measurements were performed between October 1999 and December 2014 (hereafter referred to as the study period).

3.2.1 Data, measurements and modelling of basin dynamics

3.2.1.1 Flow, precipitation and snowmelt

Forcing agents at basin-scale were obtained from the 20 available weather stations, which recorded data of rainfall, temperature, radiation and snow precipitation. Registered flow data for the entire study period were only available at the Órgiva gauge station (Figure 3.2.1). This limitation was overcome by means of simulations with the physically based and distributed hydrological model *Water Integrated Management for Mediterranean Watersheds* (WiMMed), specifically developed for the study basin. Modelling of precipitation, temperature, emissivity and radiation with WiMMed allowed not only assessing the spatial distribution of these variables but also including the dynamic of the snowmelt, important in high-mountain and semi-arid catchments. The structure and calculation scheme of the model are described in detail in Appendix 3.A.

The cross section of Órgiva represents the main hydrological characteristics and responses of the basin due to the great influence of snow and the mountainous torrential nature of this area. These factors allow assuming that the calibrated and validated parameters for this section are valid for the simulation of the whole basin (Millares, 2008). The modeled flows were compared to the measurements at the Órgiva gauge station to validate the unmanaged scenario. For the managed scenario, flows drained by the dam were completed with the modelled contributions from secondary and ephemeral rivers that are joined downstream (Figure 3.2.1).

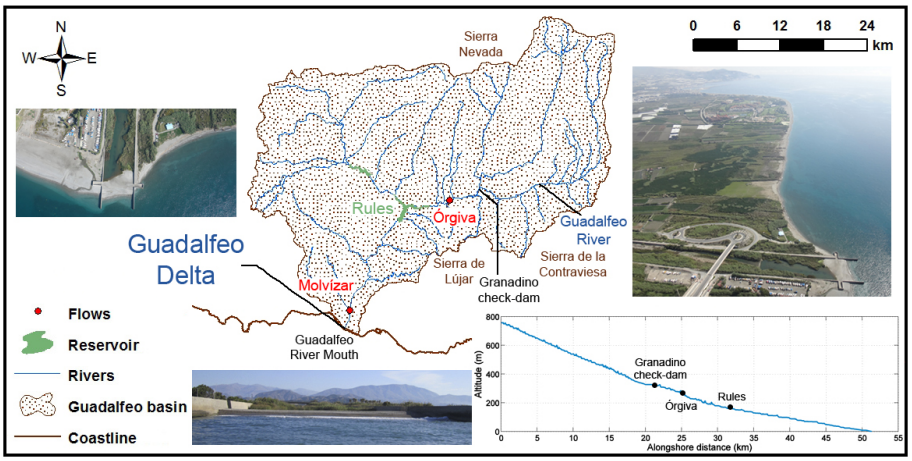

Figure 3.2.1: Delimitation of the basin and location of Rules Reservoir, the flow control points (Órgiva and Molvízar), the Granadino check-dam, the Sierra Nevada, the Sierra de la Contraviesa and the Sierra de Lújar. (Source: Adapted from Bergillos et al. (2016a). Reproduced with permission of Wiley).

3.2.1.2 Sediment delivery assessment

The characterization of the erosive and sedimentary dynamics of the contributing basin was performed using the studies presented in Moñino et al. (2011), Millares et al. (2012), Torres et al. (2013), Millares et al. (2014a), and Millares et al. (2014b). These works were based on monitoring fluvial and hillslope contributions and validating the model through sediment accumulation at the Rules Reservoir, where the trap efficiency was assumed to be close to 100%.

The huge amount of sediment in the floodplain areas allows assuming that the supply of sediment is not limited in the time scale of this chapter. Actually, the measured and estimated volumes of sediment accumulated upstream of the Granadino check-dam (Millares et al., 2014a), where the river slope is similar to that of the reservoir - river mouth stretch, and upstream of the Rules Reservoir (Millares et al., 2014b) coincided at 0.14 hm^3 and 1.8 hm^3, respectively, inspiring confidence in the validated bedload transport model.

3.2.1.3 Modelling sediment transport rates to the mouth

Due to the inherent uncertainty associated with bedload estimations four types of conceptually differentiated models (detailed in Appendix 3.B) were used. First, the model proposed by Schoklitsch (1962) is based on the critical flow that produces bedload transport and has been widely applied in steep gravel bed rivers due to the difficulty in accurately estimating the shear stress (Rickenmann, 2001). This model requires the calibration of the critical flow (Q_c), an empirical coefficient (α), and an exponent (β) that varies between 1.5 and 2. Although the model has been calibrated in different river stretches along the study basin (Millares et al., 2014a; Millares et al., 2014b), this chapter used the optimized values upstream of the Granadino check-dam (Appendix 3.B) where the river slope is similar to that of the stretch from the reservoir to the river mouth.

In addition, due to the highly heterogeneous distributions of the sediment sizes and the

Table 3.2.1: Mean values of grain sizes d_{10} to d_{90} (in mm) used for Monte Carlo simulations.

	d_{10}	d_{20}	d_{30}	d_{40}	d_{50}	d_{60}	d_{70}	d_{80}	d_{90}
Surface	4.18	16.41	33.44	51.23	68.79	85.92	103.04	120.17	179.75
Substrate	0.31	0.6	0.92	1.49	2.59	5.42	9.31	24.25	44.17

existence of armored and unarmored stretches in the river, alternative formulations, based on surface and substrate layers, were considered to model the effects of near-equal mobility in transport. The first model is the surface-based model from Wilcock and Crowe (2003), which incorporates the particle size distribution of all sediment fractions and considers the role of the sand fraction in the beginning of sediment motion. The second model corresponds to the substrate-based model of Powell et al. (2001), widely used in unarmored ephemeral channels in semi-arid environments. Finally, the model from Meyer-Peter and Müller (1948), based on the grain size of the surface layer, corrected by Wong and Parker (2006) and widely applied in gravel and sandy rivers, was also considered.

These sediment transport models were tested through 20,000 Monte Carlo simulations to consider the aforementioned uncertainty associated with bedload calculations due to the sediment heterogeneity (Chen and Stone, 2008) and to the changes in both river slope and critical flow (Millares et al., 2014b). The grain-size distributions of both surface and substrate layers were obtained from the analysis of 390 sediment samples taken upstream of the Granadino check-dam (Millares et al., 2014a), upstream of Rules Reservoir (Millares et al., 2014b) and in the reach between the reservoir and the river mouth (Rodero et al., 2005). The variability of the river slope was addressed using different topographic measurements of the longitudinal river profile (Figure 3.2.1), detailed in Ávila (2007).

The Monte Carlo simulations were based on the probability functions of these random variables. For both scenarios, log-normal distribution functions were used, considering grain sizes of d_{10} to d_{90} (mm), with the mean values shown in Table 3.2.1; whereas normal distribution functions were assumed for the slope (S) and critical flow (Q_c), with $\mu = 0.01$, $\sigma^2 = 0.005$ and $\mu = 5$, $\sigma^2 = 1$ m^3/s, respectively. The number of simulations provides sufficient statistical representativeness of the generated variables. The validity of this methodology to address the intrinsic uncertainty of natural processes has been widely proven in previous works both at basin (e.g., Gómez-Beas et al. (2012)) and coastal (e.g., Baquerizo and Losada (2008)) environments.

3.2.2 Data, measurements and analysis of coastal dynamics

3.2.2.1 Wave and wind conditions

A series of 133,704 data records (hourly sea states from the study period), that corresponds to hindcasting SIMAR point number 2041080 (Figure 3.2.1), was used to study the evolution of deep-water significant wave height (H_0), deep-water incident wave direction (θ), spectral peak period (T_p), wind velocity (V_w) and incident wind direction (θ_w). The storms were identified by means of the peaks over threshold (POT) method (Goda, 2010) considering H_0 higher than 3.1 m and storm durations lasting longer than 6 hours, according to Bergillos et al. (2016d).

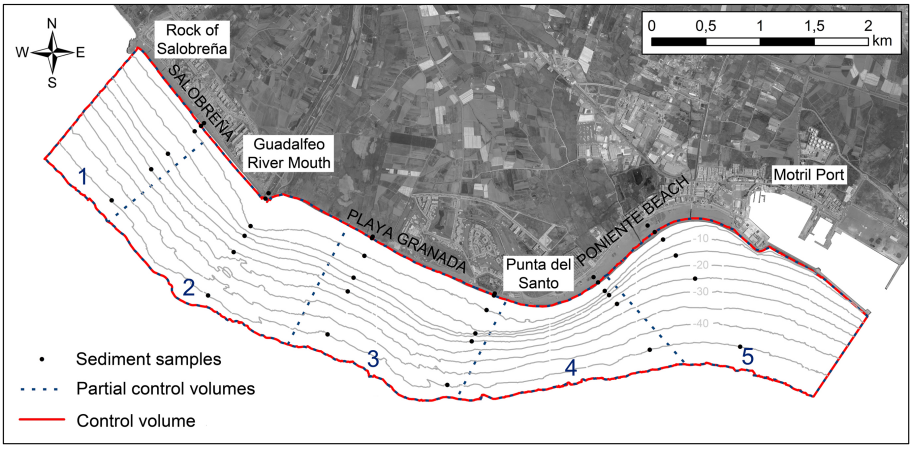

Figure 3.2.2: Delimitation of the control volume (CV) and partial control volumes (CVps); location of the Rock of Salobreña, the Guadalfeo River mouth, Playa Granada, *Punta del Santo*, Poniente beach, Motril Port and sediment samples taken; and bathymetric contours in 1999. (Source: Bergillos et al. (2016a). Reproduced with permission of Wiley).

3.2.2.2 Bathymetric and topographic surveys

High-resolution multibeam bathymetries were carried out in September 1999, October 2004, September 2008 and December 2014 on the coast. The data were acquired using Differential Global Positioning System (DGPS) navigation referring to the WGS-84 ellipsoid. Accurate navigation and real-time pitch, roll and heave were corrected. The multibeam data were also corrected for the water column velocity. At least one velocity profile was executed per day. In addition, topographic surveys were carried out with a highly accurate DGPS to complement the aforementioned multibeam bathymetries. Both bathymetric and topographic measurements were used to calculate the evolution of sediment volumes in the deltaic system.

3.2.2.3 Sediment volume, coastline and beach profile evolution

The differences between the sediment volumes of the four bathymetries described in Section 3.2.2.2 were calculated through the definition of a control volume (CV) bounded to the west by Rock of Salobreña, to the east by Motril Port, to the south by the maximum cross-shore distance common in the four bathymetries (approximately 1 km from the coastline) and to the north by the land-side envelope of the four coastlines (Figure 3.2.2). Five partial control volumes (CVps) were also defined (Figure 3.2.2) to study the alongshore variability in sediment distribution and artificial nourishments during the study period were considered.

In addition, the coastlines of the years 1999, 2001, 2004, 2007, 2008, 2009, 2010, 2013 and 2014 were analysed through aerial photographs with a resolution of 0.5 m/pixel. The coastlines of 1999, 2004, 2008 and 2014 were compared with field measurements, obtaining differences less than 5%. The difference in areas between each pair of consecutive coastlines and the rate of change was also calculated. The beach profile evolution in the river mouth was studied by means of the bathymetric data (Section 3.2.2.2).

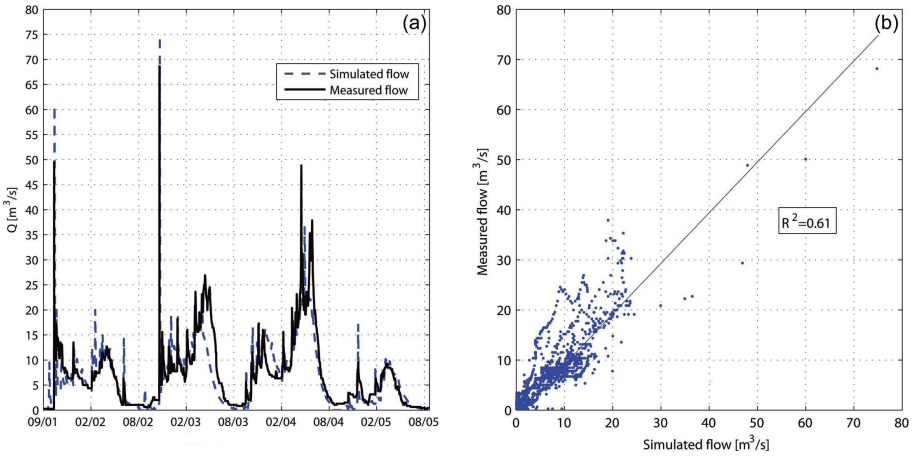

Figure 3.3.1: Validation results of the hydrological model WiMMed in the Órgiva gauge station during 2001-2005 (a). Relationship between the observed and simulated flow and the obtained Nash-Sutcliffe efficiency coefficient (b). (Source: Bergillos et al. (2016a). Reproduced with permission of Wiley).

3.3 Results

3.3.1 Flows and sediment inputs under managed and unmanaged scenarios

Figure 3.3.1 depicts the comparison between the hydrological modelling and the measurements at the Órgiva station during the calibration period (2001-2005). As noted, the main differences are associated with periods of snowmelt due to anthropogenic use of this resource in the area. Peak flows are properly represented by the model with an efficiency Nash-Sutcliffe coefficient equal to 0.61.

Through these simulations, non-gauged flow contributions were estimated for both managed and unmanaged scenarios (Figure 3.3.2). This was especially important at the ephemeral river of Molvízar (Figure 3.2.1) due to its contribution during storms events (Figure 3.3.2b). Both simulated and measured flows exhibit the pulse nature of the hydrological regime associated with intense events. Additionally, irregular contribution periods, which combine cycles of drought and intense events, are clearly identified for the different stages considered in this study. Figure 3.3.2c-d also presents the differences in magnitude and temporal pattern of the flow between the two scenarios. Peak flow in the river mouth was 5 times higher than the average during the study period under managed conditions, whereas it would have been more than 55 times higher than the average and almost 65 times higher than the critical flow under unmanaged conditions.

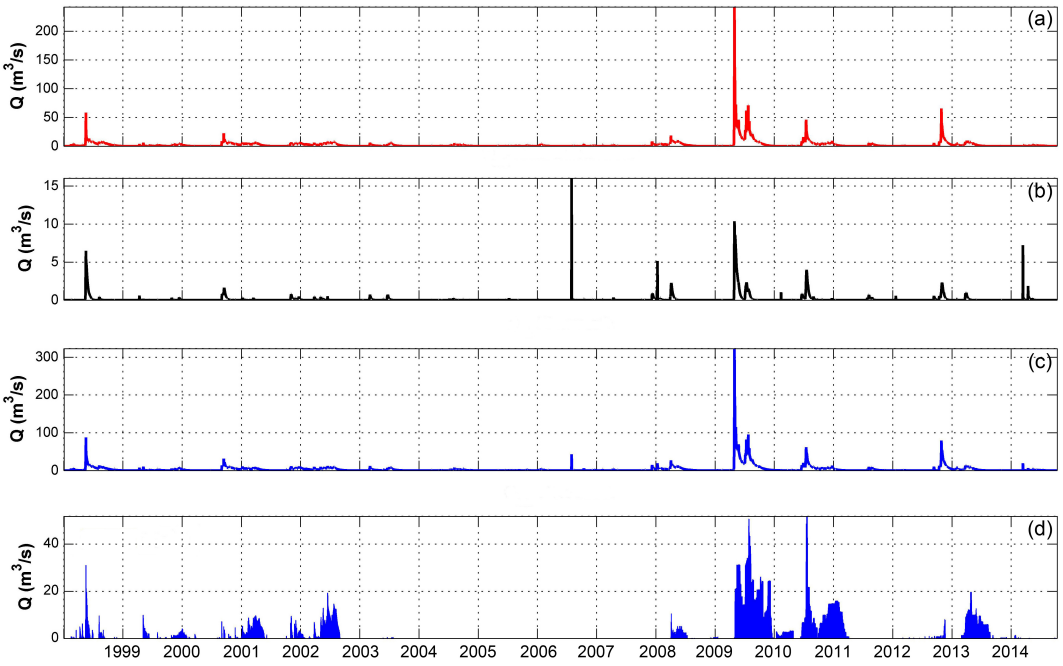

Figure 3.3.2: Simulated flows under the unmanaged scenario in Órgiva (a), Molvízar (b) and the river mouth (c). Real (managed) flow downstream of Rules Dam (d). (Source: Bergillos et al. (2016a). Reproduced with permission of Wiley).

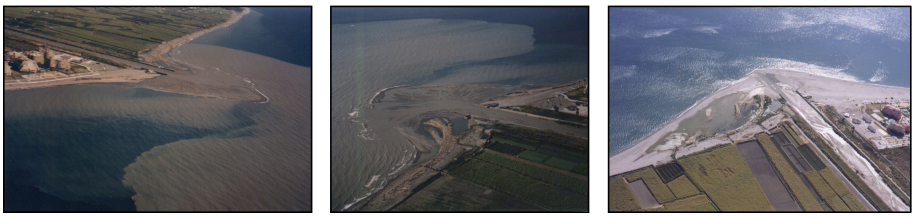

Figure 3.3.3: Aerial photographs of the river mouth during a sediment pulse before the entry into operation of the dam.

These differences, an expected consequence of the regulation of the system against floods, point to a significant change in the sediment contribution to the river mouth. The stochastic results for the four transport models using the Monte Carlo approach (Figure 3.3.4) show a clear regression if the estimations of the mean value (μ) of the fitted distribution function for the two scenarios are compared. Differences of 0.97, 1.49, 1.13 and 0.76 hm^3 were estimated for the study period (Figure 3.3.4). As mentioned in Section 3.2.1.3, modelling uncertainties are associated with these values; however, all of them reveal the significant impact of river regulation on the amount of sediment supplied to the coast. The greater dispersion under unmanaged conditions, with substantially higher values of σ, is related to the lower variability in the flow regime under regulation. The average estimated rate of bedload input under real/managed conditions (~ 0.09 hm^3/year) was significantly lower than those calculated in the Rhône delta (between 0.87 and 2.6 hm^3/year) by Sabatier et al. (2006).

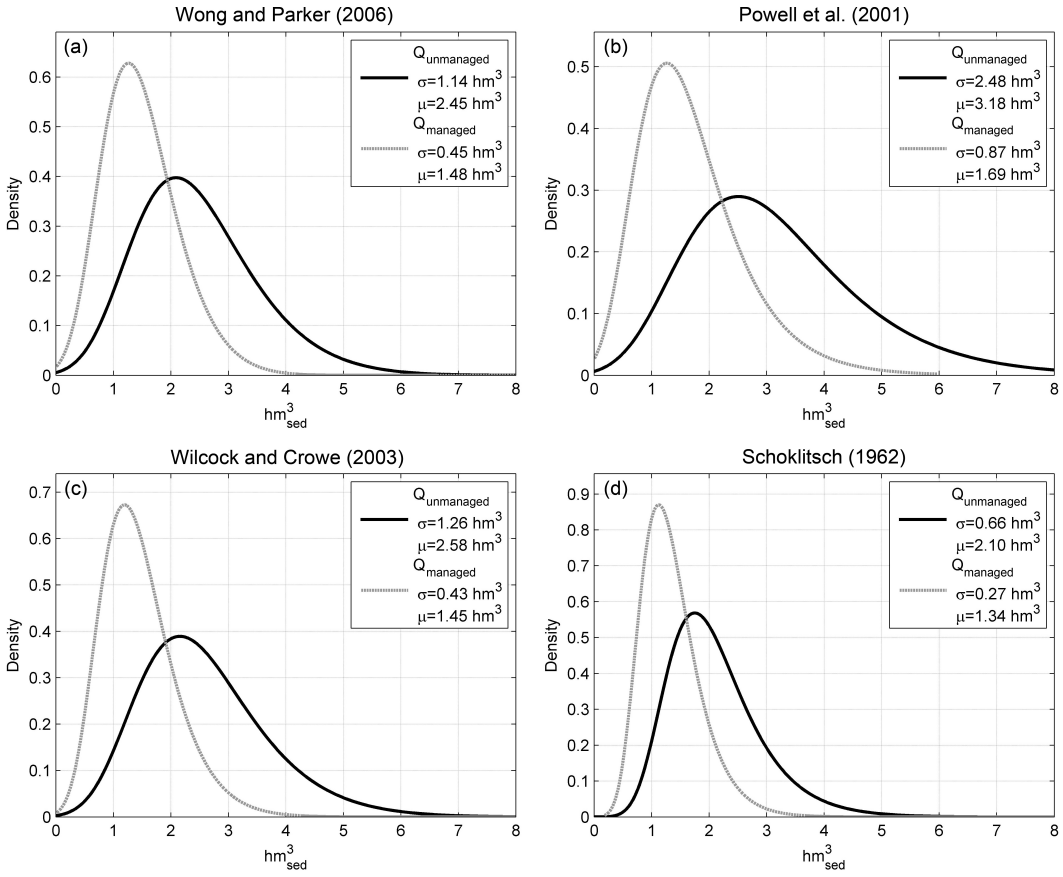

Figure 3.3.4: Density functions of the sediment volumes estimated by Monte Carlo simulations for the different transport models described in Appendix B: (a) Wong and Parker (2006), (b) Powell et al. (2001), (c) Wilcock and Crowe (2003) and (d) Schoklitsch (1962). (Source: Bergillos et al. (2016a). Reproduced with permission of Wiley).

3.3.2 Maritime climate evolution

Waves are an important agent in the construction, shaping and destruction of river deltas (Anthony, 2015). The significant wave heights in deep-water and spectral peak periods were generally $H_0 < 1$ m and $T_p < 6$ s during the study period (Figure 3.3.5), indicating that the deltaic system was predominantly forced by low-energy waves. The predominant θ were west-southwest and east-southeast (Figure 3.3.6a), whereas the prevailing V_w were less than 10 m/s, with θ_w from the east-southeast and west-southwest (Figure 3.3.6b).

Considering the three periods defined by the bathymetries performed (1999–2004, 2004–2008, 2008 – 2014), the last one was subjected to a greater number of storms: 14. In contrast, only 1 storm occurred in the period 2004 – 2008 (Figure 3.3.5a). Medium- to high-energy sea states were frequently associated with θ from the southwest-west (Figure 3.3.5e). The maximum V_w also occurred in the period 2008-2014 (Figure 3.3.5c), incoming predominantly from the west (Figure 3.3.6b).

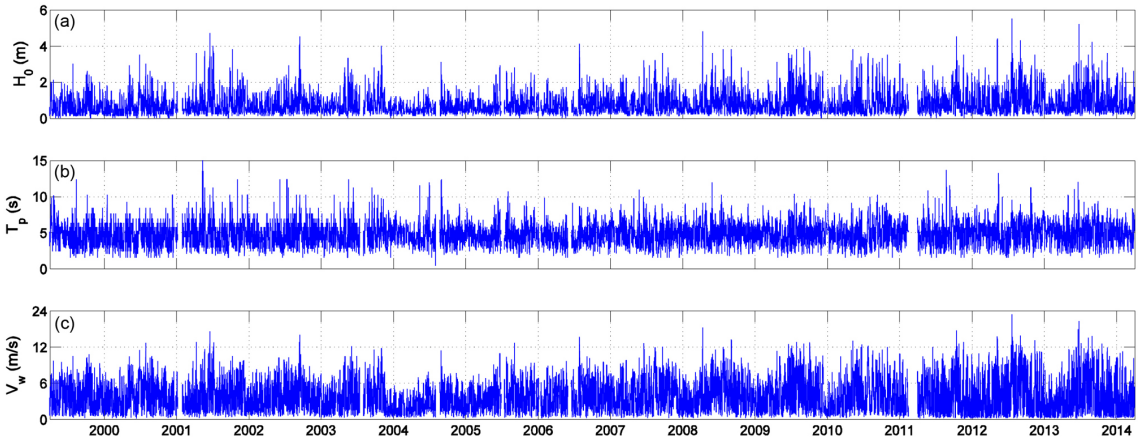

Figure 3.3.5: Evolution of the deep-water significant wave height (a), spectral peak period (b) and wind velocity (c) during the study period. (Source: Adapted from Bergillos et al. (2016a). Reproduced with permission of Wiley).

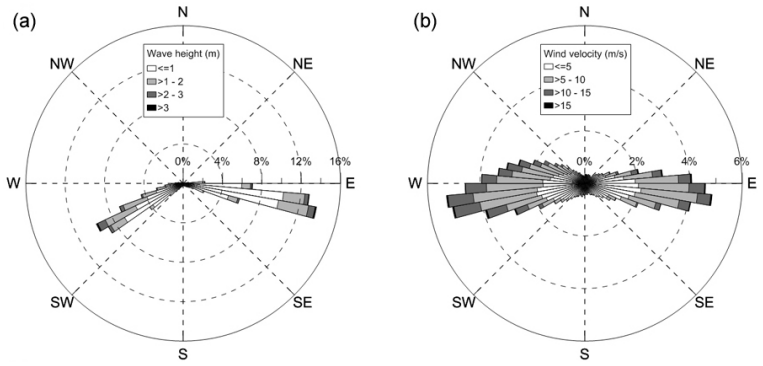

Figure 3.3.6: Polar diagram showing the occurrence frequency of deep-water significant wave heights and wave directions (a) and wind velocity and directions (b). (Source: Adapted from Bergillos et al. (2016a). Reproduced with permission of Wiley).

3.3.3 Sediment volume: temporal and spatial evolution

Volume differences between bathymetries both in the CV and in the five CVps are shown in Table 3.3.1; whereas volumes, origins and destinations of artificial nourishments performed during the study period are detailed in Table 3.3.2. In 1999, the sediment volume (initial volume) above the 50 m isobath was approximately 215.4 hm^3 in the CV, whereas the volume of the active delta (defined as the part of the delta in which changes occurred between bathymetric measurements) was approximately 12.3 hm^3.

Regarding the temporal evolution, the difference in sediment volume between 1999 and 2004 was approximately +2,000 m^3. Considering that almost 0.4 hm^3 of sediments from the Rules Reservoir were artificially deposited on the coast (Table 3.3.2 and Figure 3.3.7a), despite the flows during this period (Figure 3.3.2d), the rate of erosion was about 75,000 m^3/year during this period whereas the eroded sediment volume was equal to 0.17% of the initial total volume and 3.07% of the initial volume of the active delta.

Table 3.3.1: Differences in volume of sediment (in m^3) based on bathymetric measurements: control volume and partial control volumes.

	1999 – 2004	2004 – 2008	2008 – 2014
CV	+1,968.43	−394,892.32	+105,430.58
CVp 1	−24,757.37	−66,372.27	−15,195.64
CVp 2	−76,189.02	−294,362.59	−11,185.11
CVp 3	−49,172.79	−84,371.71	−114,361.96
CVp 4	+9,592.63	+2,071.41	+5,854.83
CVp 5	+142,494.97	+48,142.84	+240,318.45

Table 3.3.2: Artificial replenishment projects carried out during the study period: year, volume (in m^3), origin and destination.

Year	Volume	Origin	Destination
2002	379,352	Rules Reservoir	CV
2006	70,950	CVp 5	CVp 3
2009	51,375.26	CVp 5	CVp 3
2010	1,654	CVp 5	CVp 3
2014	19,436	CVp 5	CVp 3

Between 2004 and 2008, the total loss was equal to 0.18% of the initial volume and 3.21% of the active volume. During this period, the rate of erosion was about 98,700 m^3/year (Figure 3.3.7a), i.e., higher than that of the period 1999-2004. This could well be due to the low rainfall and the resulting negligible flow drained by Rules Dam (Figure 3.3.2d). The measured erosion rates are greater than that observed by Jabaloy-Sánchez et al. (2010) in the Adra delta (69,500 m^3/year) but are significantly lower than those found in the Ebro (up to 241,000 m^3/year in the vicinity of Cap Tortosa) and Rhône (1,340,000 m^3/year) deltas by Jiménez and Sánchez-Arcilla (1993) and Sabatier et al. (2006), respectively.

Finally, between 2008 and 2014, there was a gain of approximately 0.05% of the initial volume in the CV and 0.86% in the active delta due to the fluvial sediment supplies during storms in that period, representing a rate of accretion higher than 16,800 m^3/year (Figure 3.3.7a). Bedload inputs under unmanaged conditions would have been more than 0.75 hm^3 higher than the real ones (Figure 3.3.4) and would have avoided the loss of almost 0.3 hm^3 of sediment from the CV between 1999 and 2014 (Table 3.3.1).

The analysis of CVps reveals that during the first period, sediment losses approximately equal to 0.08%, 0.13% and 0.1% were produced in the CVps 1, 2 and 3, respectively, despite the artificial nourishment performed (Table 3.3.2). These losses represent percentages equal to 1.4%, 2.28% and 1.75% of their respective active volumes and contrast with the accumulation of sediments in CVp 5 during this period (~ 0.29% of the total volume in CVp 5 and more than 5% of its active volume). Between 2004 and 2008, sediment losses in the CVps 1, 2 and 3 were higher than those in the previous period (especially in CVp 2, Table 3.3.1) due to the low flows during that time (Figure 3.3.2d). Although the CV decreased by almost 0.4 hm^3, sediment accumulation occurred in CVps 4 and 5 mainly due to the prevailing wave directions (Figure 3.3.5e). Additionally, the sediment loss during this period was concentrated on the western alignment (Table 3.3.1).

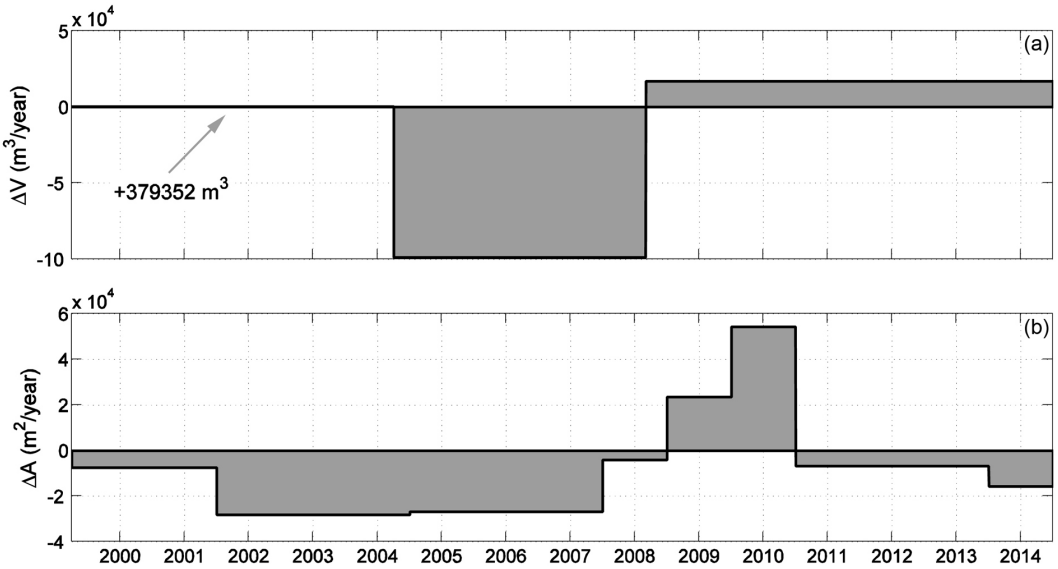

Figure 3.3.7: (a) Evolution of the sediment volume difference in the control volume shown in Figure 3.2.2. The only artificial nourishment proceeding from outside of the coastal system is indicated. (b) Evolution of the area difference between coastlines. (Source: Bergillos et al. (2016a). Reproduced with permission of Wiley).

Finally, CVps 1, 2 and 3 again lost sediment between 2008 and 2014, with the loss being particularly significant in CVp 3. Conversely, despite the sediment bypass made during this period from the eastern section of the beach to the western one (Table 3.3.2), sediment gain approximately equal to 0.49% occurred in CVp 5, representing 8.57% of its active volume. This might be due to the flows drained by Rules Dam (Figure 3.3.2d) in December 2009, December 2010 and March 2013 (Figure 3.3.2d), and the resulting sediment inputs in the coastal system. Maritime storms during that period (Figure 3.3.5a), often associated with westerly incoming directions (Figure 3.3.5e), could transport the sediment to CVp 5. Under unmanaged conditions, the inputs of sediment to the coast would have prevented losses in CVps 1, 2 and 3 (Figure 3.3.4).

3.3.4 Coastline and beach profile evolution

Despite the artificial sediment bypass carried out during the study period (Table 3.3.2), Poniente beach advanced seaward, whereas, in Playa Granada, erosion persisted (Figure 3.3.8a-b). This was partly due to the aforementioned relationship between maritime storms and incoming west direction (Figure 3.3.5e). The difference in the area of the coastlines was approximately $-183,000$ m^2 between 1999 and 2008, representing 28.5% of the initial area and an average rate of erosion higher than $20,000$ m^2/year (Table 3.3.3). During the period 2009-2010, as a consequence of the flow drained by Rules Dam (Figure 3.3.2d) and the resulting sediment transport (Figure 3.3.4), the beach area increased by almost $55,000$ m^2 (Figure 3.3.7b), that is, 8.5% of the initial area. The average rate of erosion during the study period, approximately equal to $9,330$ m^2/year, was significantly lower than those observed in the Aliakmonas ($24,960$ m^2/year) and Axios ($50,480$ m^2/year) deltas by Petropoulos et al. (2015).

Table 3.3.3: Differences in areas (in m^2) between coastlines, percentage of variation compared to the initial area, and annual rate (in m^2/year) of sediment loss (negative) or gain (positive).

Period	Area difference	% Variation	Rate
1999 – 2001	−14,832	−2.3	−7,416
2001 – 2004	−84,351	−13.1	−28,117
2004 – 2007	−80,445	−12.5	−26,815
2007 – 2008	−4,062	−0.6	−4,062
2008 – 2009	23,518	3.7	23,518
2009 – 2010	54,175	8.4	54,175
2010 – 2013	−20,612	−3.2	−6,871
2013 – 2014	−15,686	−2.4	−15,686

Since the entry into operation of Rules Dam, the beach area has been reduced by approximately 43,000 m^2, resulting in an average coastline retreat greater than 6 m (~ 0.6 m/year, on average) between the Rock of Salobreña and the Motril Port. The coastline retreat was particularly significant over a length of 1.4 km around the river mouth (Figure 3.3.8a-b), with a maximum retreat of 87 m between 2004 and 2014, that is, an approximately rate of retreat of 9 m/year. This coastline retreat represents 92% of the initial cross-shore length of the beach. The maximum rate of coastline retreat (40 m/year between 2010 and 2013) was greater than those observed in the Adra (3.5 m/year) and Po (9 m/year) deltas by Jabaloy-Sánchez et al. (2010) and Simeoni et al. (2007), respectively. Conversely, it was lower than that measured in both the Ebro delta, with a maximum coastline retreat of more than 50 m/year at Cap Tortosa (Jiménez and Sánchez-Arcilla, 1993) and the Nile delta, with a maximum rate of coastline retreat larger than 100 m/year in the down-drift side of Damietta Port (Frihy and Komar, 1993).

Considering the bedload model calibrated in this basin (Figure 3.3.4d) and the same ratio bedload input/area increase observed for the managed scenario, the area balance between September 2004 and December 2014 would have been approximately +3,500 m^2 under unmanaged conditions, corresponding to a rate of gain equal to 341.5 m^2/year and an average coastline advance approximately equal to 0.5 m between the Rock of Salobreña and the Motril Port. Under these conditions, artificial nourishment would not have been necessary.

Finally, Figure 3.3.9a shows the alongshore-averaged beach profile in CVp 2 (Figure 3.2.2). It is observed that the beach profile variation is consistent with the coastline evolution (Figure 3.3.8b) and with the volumes obtained in Section 3.3.3. Thus, the evolution of the beach profile in CVp 2 denotes a constant loss of sediment in the delta, reaching maximum unit volumes of 820 m^2 (0.75% of the total and 13% of the active profile). The average decrease in the beach profile in CVp 2 since the entry into operation of the reservoir was equal to 214 m^2, i.e., erosion rate of 20.9 m^2/year. It was lower than that observed in the Ebro delta by Jiménez and Sánchez-Arcilla (1993), who measured an erosion rate of 56 m^3/year per meter of coastline around the Cap Tortosa.

The decrease in delta profile contrasts with the accumulation of sediment as delta deposits in the reservoir upstream (Figure 3.3.9b), detailed in Millares et al. (2014b), demonstrating the barrier effect of the dam. The sediment volume trapped into Rules Reservoir is also significantly lower than those in the Mequinensa and Riba-Roja reservoirs, upstream of the Ebro delta, with a total stored volume of 280 hm^3 according to Rovira and Ibáñez (2007).

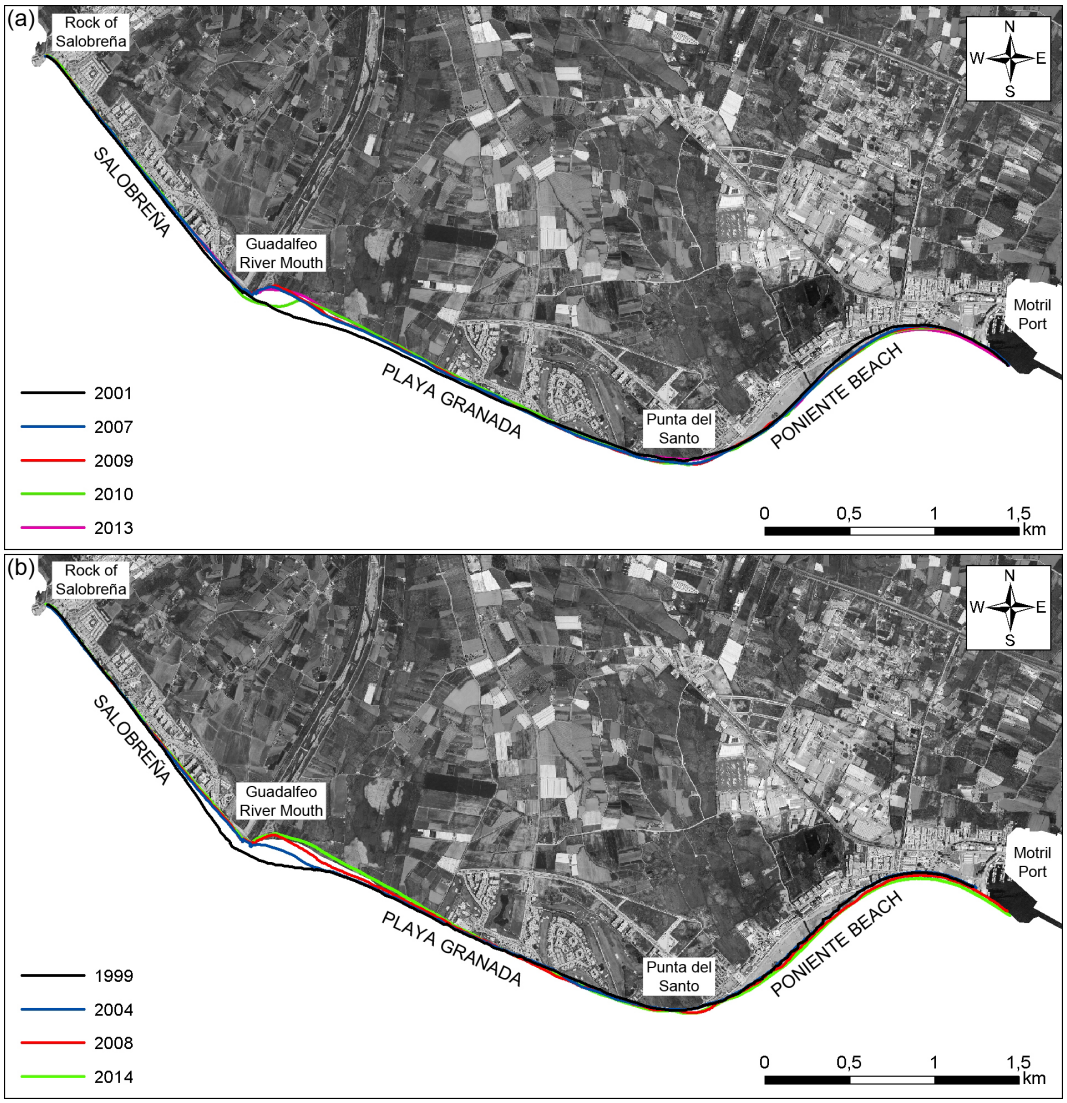

Figure 3.3.8: (a) Coastlines of the years 2001, 2007, 2009, 2010 and 2013 based on aerial photographs and (b) coastlines measured through topographic surveys. (Source: Bergillos et al. (2016a). Reproduced with permission of Wiley).

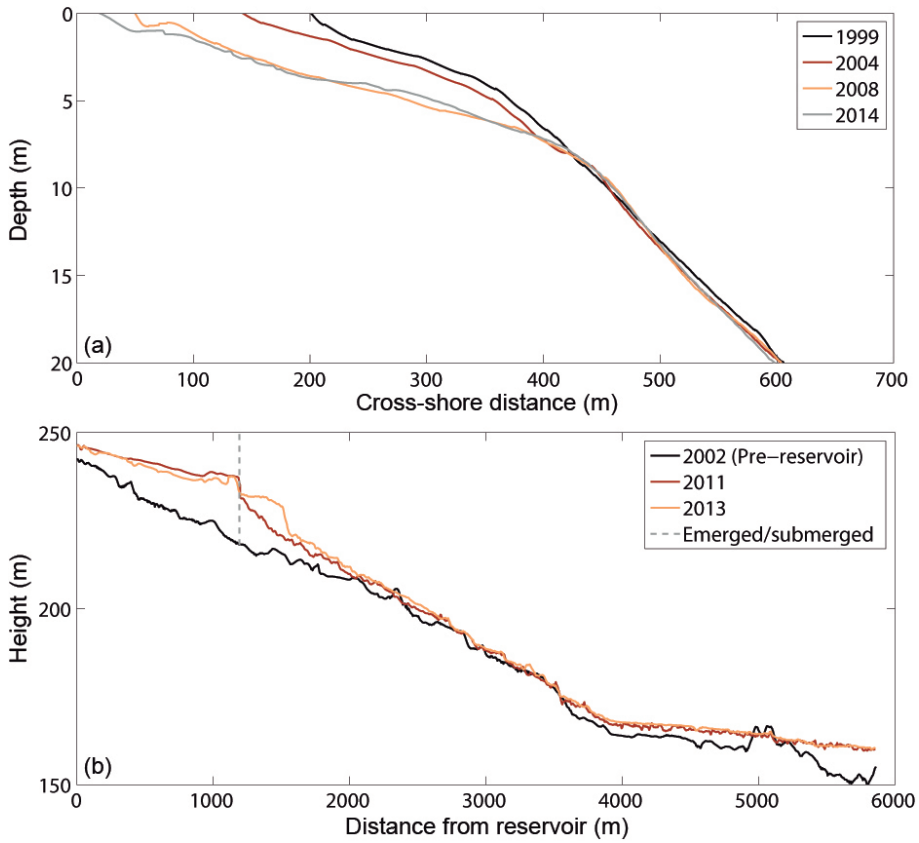

Figure 3.3.9: (a) Beach profiles in partial control volume 2, (b) deltaic deposits at the Reservoir's tail: longitudinal cross sections. (Source: Bergillos et al. (2016a). Reproduced with permission of Wiley).

3.3.5 Management scenarios: uncertainties

Considering the transport models defined in Appendix 3.B, a constant flow drained by the dam ($Q_{man,C}$) equal to 6 m^3/s between 2004 and 2008, along with sediment bypass from the reservoir, would have avoided the coastal erosion during this period. Alternatively, the drainage of seasonal flows equal to 7 m^3/s ($Q_{man,S1}$) or 6.5 m^3/s ($Q_{man,S2}$) during the six months (October-March) or nine months (September-May) per year with a higher occurrence probability of both pluvial and maritime storms, respectively, would also have avoided delta erosion.

The seasonal strategies require less water resource per year (total volume of $Q_{man,S1}$ and $Q_{man,S2}$ are 58.33% and 81.25% of the total volume of $Q_{man,C}$, respectively), allowing also a higher availability of water in the reservoir upstream during spring and summer. Through these seasonal strategies, the beach area would be larger during the more tourist (summer) periods and the bedload input would be greater during stormy periods, contributing to coastal protection. However, the $Q_{man,C}$ would contribute to protect the river ecosystem downstream of the dam. Comparing both seasonal scenarios, the first one requires less water resource, whereas the second could be more useful for protection against spring maritime storms.

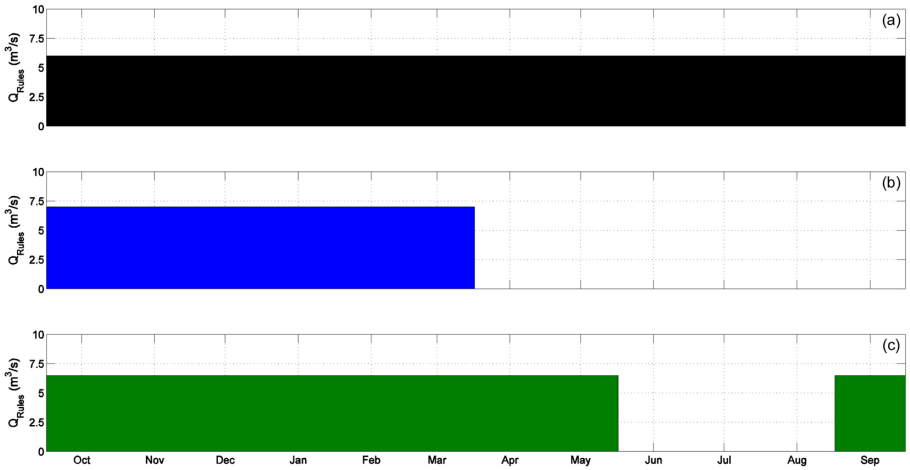

Figure 3.3.10: Management scenarios of flow drained by the dam to reduce coastal erosion.

The proposed scenarios have the logical uncertainties associated with these types of estimations, where both fluvial and maritime forcing agents present intra- and inter-annual variabilities. In addition to the recognized uncertainty associated with bedload calculations (Section 3.3.1), there are others related with the variable frequency of occurrence of maritime storms, fluvial pulses, snowmelt, etc. However, this management methodology, based on the required flow and amount of sediment through the quantification of sediment volume on the coast and bedload contributions by the river, could be considered during future drought periods. In particular, a more severe erosion in both the downstream reach (due to sediment starvation and increased clear water erosion of river beds and banks) and on the coast could be reduced by operating the reservoir as proposed. Sediment bypassing would also reduce the loss of reservoir storage and avoid, in the long term, the impacts of silting. Other management strategies could be designed through the combination of the proposed scenarios to optimize regulation and fulfil any requirements, including those imposed by law.

Therefore, this methodology represents a tool for decision making that can be feasibly extended to other deltas worldwide using a three-step procedure. First, bathymetric, topographic and grain size data both on the coast and in the reservoir upstream are analysed. Second, hydrological and sediment transport models are calibrated in the basin. Third, the parameters that define the management scenarios (flow distribution drained by the dam and characteristics and volume of sediment bypassed from the reservoir upstream) are proposed based on both the measurements and the results of the simulations.

For rivers with two or more dams, such as the Ebro, coordination between the drainages of the different dams would be required. In addition, sediment samples should be analysed in every reservoir to test the sediment most susceptible to transport and to remain close to the river mouth in order to contribute to the reduction of coastal erosion. These strategies are especially useful in semi-arid environments that are characterized by water scarcity, and Mediterranean deltas, which are particularly sensitive to both sea-level rise and coastline retreat (Jeftic et al., 1996; Nicholls and Hoozemans, 1996).

3.4 Discussion and conclusions

Although it is well known that coastal evolution is strongly dependent on the sediment supplied by nearby rivers, the quantification of this interaction is still not well described. In particular, few studies to date have addressed how the system would have evolved without regulation interventions. This chapter analyses, compares and quantifies the real (managed) evolution of the Guadalfeo deltaic system (southern Spain) after the construction of a reservoir with a simulated (unmanaged) scenario without regulation. The study is based on bathymetric and topographic measurements correlated with the maritime and fluvial forcing agents. Based on the results, three new management scenarios were proposed, consisting of the constant or seasonal flow that should be drained by the dam, in combination with the required sediment bypass from the reservoir upstream, to avoid coastal erosion during drought periods. The length of the study period, the quality of measurements carried out, the application of a calibrated hydrological model, the interpretation of both maritime and fluvial variables, and the proposed scenarios make the results interesting and valuable for management purposes.

The analysis of fluvial and coastal observations reveals that the dynamics of the Guadalfeo deltaic system is governed by the sediment supplies of the river during intense events. These sediments are then transported along the coast due to the directionality of the wind and waves (Figure 3.3.5e-f). Both the river bedload and the coastal system have heterogeneous distributions of sediments, with the same three prevailing fractions (sand, fine gravel and coarse gravel) and with similar mineralogical composition (Bergillos et al., 2016a).

The coastal system has lost almost 0.3 hm^3 of sediments (0.13% of the total volume and 2.34% of the initial volume in the active delta) since the entry into operation of the dam in 2004, whereas the area surrounding the river mouth has lost almost 0.31 hm^3 (0.63% of its initial volume and 11% of its initial active volume). These losses have generated a coastline retreat of up to 87 m (92% of the total) and a beach profile decrease down to 820 m^2 (13% of the active zone). These sediment losses contrast with the accumulation of 0.14 hm^3 in the Granadino check-dam (Millares et al., 2014a) and 1.8 hm^3 in Rules Reservoir (Millares et al., 2014b). Thus, the sediment availability in the stretch between Rules Dam and the Guadalfeo River mouth, without a renewal rate, will diminishes and the erosion on the coast will increase in the near future, with direct implications on the management.

The results obtained from hydrological modelling confirm the importance of the regulation produced by the reservoir: peak flows in the river mouth were 5 times higher than the average, whereas they would have been more than 55 times higher than the average under unmanaged conditions. In addition, peak flows during storms under managed conditions were more than 6 times lower than those under unmanaged conditions. Consequently, bedload contributions higher than 2 hm^3 would have reached the deltaic system under unmanaged conditions, representing more than 150% of the real situation. The difference between scenarios is greater than 0.75 hm^3; accordingly, Rules Reservoir has prevented the advance of a delta that was prograding before the construction of the dam (Hoffmann, 1987; Jabaloy-Sánchez et al., 2014). This change in the pattern of delta dynamics due to human activities has also been observed in the Ebro (Jiménez and Sánchez-Arcilla, 1993), Po (Simeoni and Corbau, 2009), Nile (El Banna and Frihy, 2009), Rhône (Sabatier et al., 2009) Adra (Jabaloy-Sánchez et al., 2010), Axios and Aliakmonas (Petropoulos et al., 2015) deltas.

Therefore, despite the benefits in flood control and water resource storage, strategic in semi-arid environments, the results of this study underline the real cost of this type of infrastructure. In the short term, the increasing erosion processes downstream and the coastline retreat require costly management projects. In the long term, the cost associated with the loss of reservoir volume by siltation should be added. This suggests that new management scenarios of the flow drained by the dam, along with sediment bypass from the reservoir upstream to the stretch downstream, would be necessary to prevent the erosion of both the coastal system and the stretch between Rules Reservoir and the Guadalfeo River mouth, as well as the silting of the reservoir. The significance of this study mainly lies in: (1) the exploration and demonstration of the evolution of a delta with and without river regulation; (2) the comparison to other Mediterranean deltas; and (3) the proposal of new management methodologies, based on both field data and numerical modelling, to control coastal erosion problems.

Appendix 3.A WiMMed model

WiMMed (Polo et al., 2009; Herrero et al., 2014) is a physically based and fully distributed model, specifically designed to reproduce the spatial and temporal variability of the forcing agents and processes that are particularly relevant in mountainous and semi-arid environments. It has been widely tested in the study basin (e.g., Herrero (2007), Millares (2008), Aguilar (2008), and Egüen et al. (2009)).

This model is based on the overlap of different maps with information on the distributions of vegetation, soil and aquifers, using the digital elevation model as a reference for topographical and hydrological calculations. For meteorological inputs, WiMMed includes specific algorithms for the spatial and temporal interpolation of rainfall and snowfall, temperature, solar radiation, wind and relative humidity, accounting for topographical corrections (Aguilar et al., 2010; Aguilar et al., 2014). The calculation for each cell is implemented as a cascade of reservoirs for the considered subsystem, vegetation cover, snow pack, vadose zone and aquifers. The water excess is circulated along the hillslope cells and linked for each sub-basin at different points across the main drainage network.

The model identifies event and inter-event periods, adapting the time step to the requirements of each sub-process. At each cell, WiMMed implements rainfall interception by vegetation cover. The snow dynamics is incorporated using a 1D thermodynamic model of energy and water balance in the snow cover (Herrero et al., 2009). Infiltration flux is calculated by Green and Ampt's physical approach for soil water movement considering Sherman's flood time, the Darcy-Buckingham equation and the conductivity of the unsaturated flow from the Van-Genuchten-Mualem equation. The spatial distributions of the physical-chemical and hydraulic properties of the soil were obtained from Rodríguez et al. (2008).

For runoff modelling, WiMMed considers Hortonian flow and localizes the subsurface contribution at a predefined discharge point for each sub-basin. Baseflow contribution is included based on recession pre-analysis and slow water responses from a linear reservoir approach by considering different aquifer units, which are linked to the sub-basin discharge points (Millares et al., 2009). The resulting hydrographs in each sub-basin are the input data for flow propagation, water depth and velocities along the river cross sections using the Muskingum-Cunge method for the general network and a 1-D hydrodynamic model for the main channel (Ávila, 2007).

Appendix 3.B Bedload transport models

Schoklitsch (1962) proposed the following empirical model based on water flow:

$$Q_b = \alpha S^{\beta}(Q_m - Q_c) \tag{3.1}$$

where Q_b is the average bedload for the duration of the event, Q_m is the average flow for the event, Q_c is the critical flow for bedload transport, S is the river bed slope, α is an empirical coefficient, and β is an exponent that varies between 1.5 and 2.0. This model was calibrated at the stretch of river upstream of the Granadino check-dam (Millares et al., 2014a), with a similar slope to that of the stretch reservoir-river mouth, considering Q_c = 5 m^3/s, α = 6.3 and β = 2.

These values are in agreement with the range of values proposed in previous works (Mizuyama, 1981; Smart, 1984; Rickenmann, 1990).

By considering the relationship between the average sediment size and incipient motion, Meyer-Peter and Müller (1948) proposed:

$$Q_b = Bc(\tau^* - \tau_c^*)^{1.5}\left[(s-1)d_s^3\right]^{0.5} \tag{3.2}$$

where B is the channel width, c is an empirical coefficient, τ_c^* is the dimensionless critical shear stress, and τ^* is the dimensionless shear stress ($\tau^* = \tau/[(s-1)\rho g d_s]$), with τ the shear stress (Pa): $\tau = \rho g R_h S_f$, where R_h is the hydraulic radius, g the acceleration of gravity, and S_f the friction slope. Wong and Parker (2006) proposed values equal to $c = 3.97$ and $\tau_c^* = 0.0495$. The particle size is noted as d_s, and s is the specific gravity: $s = \rho_s/\rho$, where ρ_s is the mass density of the solid particles ($\rho_s = 2650$ kg/m^3), and ρ is the water density ($\rho = 1{,}000$ kg/m^3).

Finally, models based on every size fraction i by considering a dimensionless transport function W_i were calculated through:

$$W_i = 11.2\left(1 - \frac{1}{\Phi_i}\right)^{4.5} \tag{3.3}$$

with:

$$\Phi_i = \frac{\tau_{50}^*}{\tau_{c_{50}}^*}\left(\frac{d_i}{d_{50}}\right)^{-0.26} \tag{3.4}$$

from the substrate-based model proposed by Powell et al. (2001), specifically designed for intense floods events and unarmored semi-arid rivers, where $\tau_{c_{50}}^* = 0.03$; and as:

$$W_i = \begin{cases} 0.002\Phi_i^{7.5} & \text{for } \Phi_i < 1.35 \\ 14\left[1 - \frac{0.984}{\Phi_i^{0.5}}\right]^{4.5} & \text{for } \Phi_i \geq 1.35 \end{cases} \tag{3.5}$$

following the Wilcock and Crowe (2003) surface-based model, where $\Phi_i = \tau_i^*/\tau_{c_i}^*$ with $\tau_{c_i}^* = 0.021 + 0.015e^{20F_s}$, and F_s is the sand fraction of the river bed. The amount of sediment transported as bedload for each fraction is calculated as:

$$Q_{b_i} = \frac{W_i f_i B(gR_hS)^{3/2}}{(s-1)g} \tag{3.6}$$

where f_i is the mass proportion of the size fraction i. The porosity p_0, estimated through the expression $p_0 = (1 - \rho_d/\rho_s)$ where ρ_d is the measured dry specific mass of the mixture, was used to derive the final volume.

CHAPTER 4

IMPLICATIONS OF DELTA RETREAT ON COASTAL PROCESSES

This chapter details the spatial and temporal variability of the mouth of the Guadalfeo River and focuses on the influence of submerged morphological changes, partly due to watershed regulation in 2004, on wave propagation and longshore sediment transport (LST). Bathymetric measurements were carried out over a 15-year period (1999-2014), a wave propagation model was calibrated and applied, and the complete littoral drift time series were obtained using statistical downscaling techniques. The results show that the river damming led to coastline retreat and bed-level erosion up to 3 m along a 1-km section around the river mouth, with maximum erosion rates in excess of 760 m^3/m. These subtidal morphological changes reduced wave refraction and led to higher breaking wave energy. Variations in wave climate during the study period have also played a role in influencing the coastline dynamics. Although the erosion around the river mouth has decreased since 2008, partly due to a sediment pulse in 2010, eastward LST rates under westerly storm wave conditions have significantly increased since then. This has led to the propagation of the sediment deficit towards the east of the mouth, endangering urban developments at this location. This chapter provides insights into the shift from wave-river dominated deltas towards deltaic coasts increasingly controlled by wave directionality and LST, and represents an advance on the understanding of the dynamics of many worldwide deltas where the river sediment supply has decreased due to human activities.

4.1 Objective

The main objective of this chapter is to study the spatial and temporal variability of the river mouth of the Guadalfeo deltaic system. The chapter describes the changes on the submerged morphology and quantifies their impact on wave propagation and longshore sediment transport (LST) near the coast. Firstly, multibeam bathymetric measurements over a period of 15 years (1999-2014) are analysed and a wave propagation model is calibrated and applied to the study site. Secondly, an LST formulation was applied to help explain the coastal changes. Finally, advanced wave climate downscaling techniques are used to further explore the feedbacks between nearshore morphology, wave directionality and LST.

4.2 Methodology

This chapter addresses the evolution of the submerged morphology and the influence on coastal processes mainly by means of multibeam bathymetric surveys carried out in 1999, 2004, 2008 and 2014 (Section 4.2.1.2). Accordingly, three epochs are considered: 1999-2004 (Epoch 1), 2004-2008 (Epoch 2) and 2008-2014 (Epoch 3). The period 1999-2014 is hereafter referred to as the full study period.

4.2.1 Data

4.2.1.1 Wave climate

Fifty-seven years of hourly hindcasted wave data, corresponding to SIMAR point number 2041080 (depth ~ 630 m) and provided by *Puertos del Estado*, were used to study the evolution of the following deep-water wave variables: significant wave height (H_0), wave direction (θ, $N = 0\,^\circ$, $E = 90\,^\circ$) and spectral peak period (T_p). Typical and extreme storms were identified by means of the peaks over threshold (POT) method considering: (1) H_0 higher than 2.1 m ($H_{99\%}$) and 3.1 m ($H_{99.9\%}$), respectively, (2) storm durations lasting longer than 6 hours and (3) separation between storms longer than 6 hours.

4.2.1.2 Bathymetries and sediment samples

High-resolution multibeam bathymetric surveys were carried out in September 1999, October 2004, September 2008 and December 2014 by the Provincial Coastal Service of Granada, the University of Granada, the Spanish Ministry of Environment and Rural and Marine, and the Andalusian Institute for Earth System Research, respectively. The data were acquired using Differential Global Positioning System navigation referring to the WGS-84 ellipsoid. Accurate navigation and real-time pitch, roll and heave were corrected. The multibeam data were also corrected for the sound velocity. In addition, 18 sediment samples along the active zone (at depths ~0, ~5 and ~10 m) of 6 selected beach profiles (Figure 4.2.1) were collected during each survey to be used in the calculation of the LST rates.

4.2.2 Wave propagation: model description and calibration

For each of the four bathymetries, frequently occurring sea states at the study site (Table 4.2.1), under both low energy and storm conditions, and for both easterly and westerly waves, were propagated from deep water to the nearshore using the WAVE module of the Delft3D model (Lesser et al., 2004; Lesser, 2009). This module is based on the SWAN model (Holthuijsen et al., 1993). The influence of the changes in the submerged morphology on the nearshore wave propagation patterns was thus addressed and these results were subsequently used to estimate the alongshore and temporal variation in the LST.

Table 4.2.1: Sea states propagated with Delft3D to study the effect of the morphology changes on wave propagation and LST.

	Low energy		Storm	
	East	West	East	West
H_0 (m)	0.4	0.4	3.2	3.2
T_p (s)	4.5	4.5	8.4	8.4
θ (°)	112	245	112	245

The model domain consists of two different grids, shown in Figure 4.2.1. The first is a coarse curvilinear 82x82-cell grid covering the entire deltaic region, with cell sizes that decrease with decreasing depth from 88x60 to 48x35 m. The second is a nested grid covering the beach with 144 and 82 cells in the alongshore and cross-shore directions, respectively, and cell sizes of about 25x14 m. For the spectral resolution of the frequency space, 37 logarithmically-distributed frequencies ranging from 0.03 to 1 Hz were used; for the directional space, 72 directions covering 360 ° in increments of 5 ° were defined.

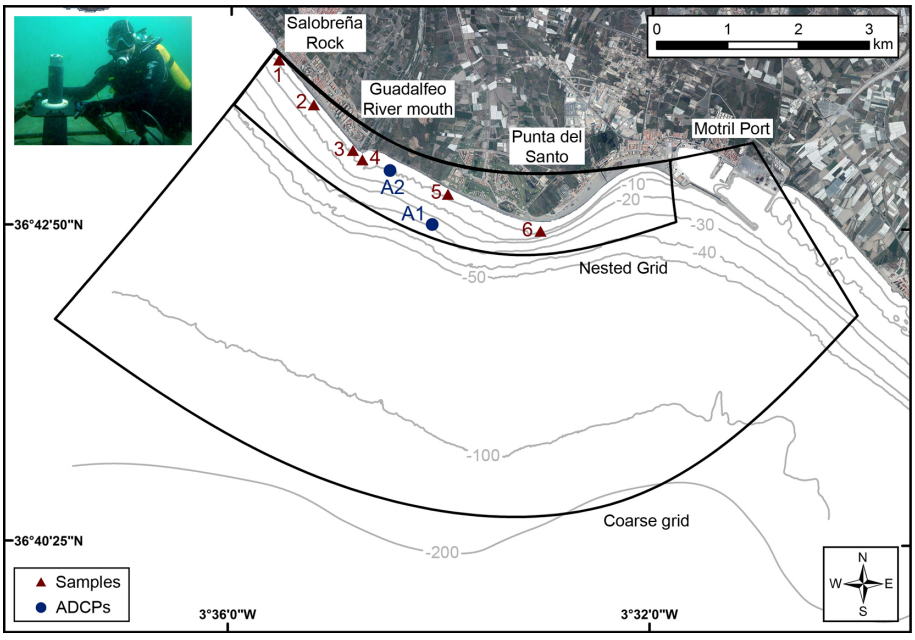

Figure 4.2.1: Bathymetry of the study site, profiles where the sediment samples were taken (red numbered triangles), ADCPs (blue circles A1 and A2) and grids used in the numerical model. (Source: Adapted from Bergillos et al. (2016b). Reproduced with permission of Elsevier).

The model was calibrated through comparison with field data collected from 20 December 2014 to 30 January 2015 by means of two ADCPs (Figure 4.2.1). The wave model was forced with the SIMAR point data (Section 4.2.1.1) using the bathymetry of 2014 and considering the following physical processes: wind effects, refraction, white-capping, depth-induced breaking ($\alpha = 1$, $\gamma = 0.73$), non-linear triad interactions ($\alpha = 0.1$, $\beta = 2.2$), bottom friction (Type *Collins*, coefficient = 0.02) and diffraction (smoothing coefficient = 0.6, smoothing steps = 600). Significant wave heights measured by the instruments were compared with the equivalent wave heights propagated with the model for the same locations. Coefficients of determination (R^2) higher than 0.86 were obtained, providing confidence that the wave model is reproducing the actual wave conditions (Figure 4.2.2).

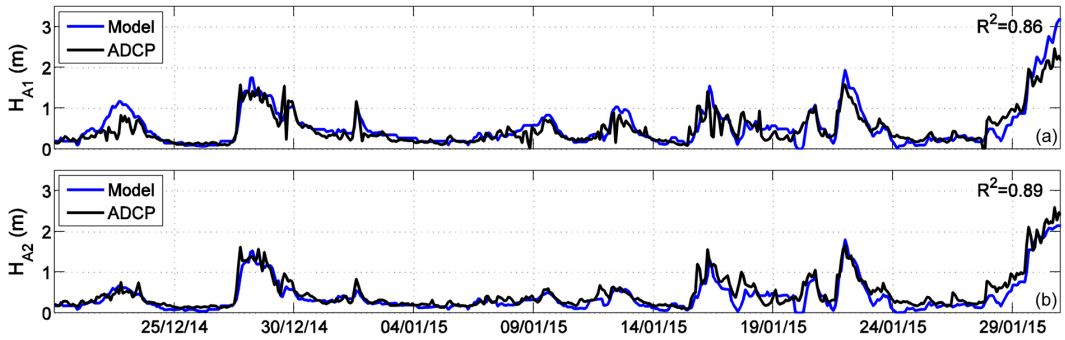

Figure 4.2.2: Comparison of time series measured and modelled wave heights in locations A1 (a) and A2 (b), according to Figure 4.2.1. (Source: Bergillos et al. (2016b). Reproduced with permission of Elsevier).

4.2.3 Longshore sediment transport

LST is a key process in coastal morphodynamics because alongshore gradients in LST drive changes in the coastline position (Dean and Dalrymple, 2002). Although cross-shore processes are important on coasts like the Guadalfeo River deltaic system, it is assumed that the redistribution of the sediment delivered by the river, and the ensuing response of the coastline, is mainly dependent on LST. The alongshore and temporal variations of LST were analysed using the different bathymetries to estimate how the shoreline plan view has evolved as a consequence of the evolution of the submerged delta.

4.2.3.1 LST formulation

In this chapter, the energetic approach proposed by López-Ruiz et al. (2014) was applied. This expression uses a framework specifically defined for curvilinear coasts, considering alongshore variations of the shoreline and wave angles, and also gradients in the wave energy characterized by the surf zone width. It was obtained without the assumption of alongshore-uniform beach characteristics. This expression accounts for the potential LST that can be transported for specific wave energy conditions, and predicts the LST rate if there is enough sediment to be mobilized.

4.2.3.2 Time series of LST along the shoreline of the delta

The LST distribution for the three epochs (1999-2004, 2004-2008 and 2008-2014) was correlated with changes in the submerged morphology and variations in wave climate between the epochs to give insight into the role of these factors in driving the recent morphological evolution of the delta.

To obtain the LST time series for the full study period, the following methodology was applied. Firstly, a database of representative wave conditions (H_0, T_p and θ) is generated using the downscaling method presented by Camus et al. (2011) and Camus et al. (2014). This first step synthesizes the complete data set of the deep-water wave climate in a group of 280 sea states representing mild, mean and extreme wave conditions. These sea states ranged in the intervals $H_0 \in (0.1, 5.2)$ m, $T_p \in (2.5, 15)$ s, and $\theta \in (0, 360)^\circ$, un-equally distributed to account for the most likely sea states. Secondly, all sea states in this database are propagated over the initial bathymetry for each epoch (Section 4.2.1.2) using the calibrated wave propagation model described in Section 4.2.2. With these propagations, nearshore breaking wave parameters are obtained to compute LST for every sea state. Finally, these results are used to reconstruct the LST time series along the coast during the full study period by means of interpolation. This methodology significantly reduces the computational effort and new LST results can be obtained without performing new wave propagations.

The main limitation of this analysis is related to the lack of bathymetric information between the epoch dates. Hence, the bathymetry at the beginning of each epoch is assumed to be constant during this epoch. After obtaining the temporal evolution of LST, an analysis of the role of wave directionality (prevailing wave and LST directions and intensities) on the morphological evolution of the delta was carried out from a simple statistical treatment of the deep-water wave data and LST results. The time series of LST was also used to obtain the alongshore evolution of both the LST rates and the sediment volumetric changes induced by LST for the three epochs.

4.3 Results

4.3.1 Evolution of the wave climate

The delta was predominantly forced by low-energy waves during the full study period, with the average deep-water wave height H_0 less than 1 m during all three epochs (Table 4.3.1). Epoch 3 was the most energetic period with the average H_0 and T_p during this period, respectively, 25% and 6% higher than during the other epochs.

By applying the POT method, four extreme storms associated with easterly waves occurred during 1999-2004, with maximum H_0 of 4.7, 4, 3.7 and 4.5 m (Figures 4.3.1a and 4.3.2a). Only one easterly extreme storm took place during 2004-2008, with a maximum H_0 of 4.1 m (Figures 4.3.1a and 4.3.3a). Fourteen extreme storms occurred during 2008-2014, with maximum H_0 between 3.6 and 5.4 m; six of these storms were associated with easterly waves and eight were associated with south-westerly waves (Figures 4.3.1a and 4.3.4a). In addition, 27 typical storms took place during Epoch 1 (14 from the east and 13 from the southwest), 14 during Epoch 2 (10 from the east and 4 from the southwest) and 100 during Epoch 3 (34 from the east and 66 from the southwest).

Table 4.3.1: Average deep-water wave height and spectral peak period; and number of extreme and typical storms during the study epochs.

Epoch	H_0 (m)	T_p (s)	Extreme storms	Typical storms
1999-2004	0.67	4.76	4	27
2004-2008	0.67	4.77	1	14
2008-2014	0.84	5.05	14	100

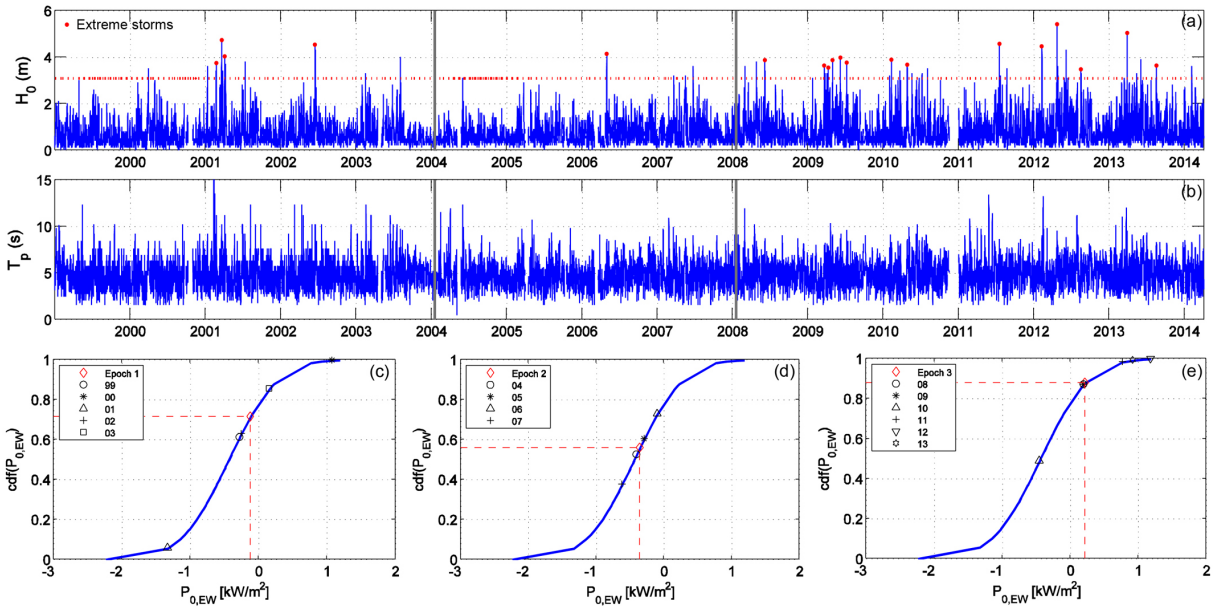

Figure 4.3.1: Evolution of the deep-water wave height (a) and spectral peak period (b) from 1999 to 2014. Fitted cumulative distribution function (cdf) of the yearly averaged $P_{0,EW}$ (Normal distribution, $\mu = -0.45$ kW/m^2, $\sigma = 0.56$ kW/m^2). Black markers correspond to values of the years in the Epoch 1 (c), Epoch 2 (d) and Epoch 3 (e). Red markers indicate the mean value for each epoch. (Source: Bergillos et al. (2016b). Reproduced with permission of Elsevier).

To analyse the importance of wave directionality on the evolution of the delta, the east-west (EW) component of the offshore wave power $P_{0,EW}$ was obtained using linear wave theory (Dean and Dalrymple, 2002):

$$P_{0,EW} = \frac{1}{64\pi}\rho g^2 T_p H_0^2 \sin\theta \tag{4.1}$$

where g is the acceleration of gravity, $\rho = 1.025$ kg/m^3 is the density of salt water and θ is the wave angle measured over the EW direction. With the angle definition considered, positive (negative) values of $P_{0,EW}$ correspond to westerly (easterly) waves. Note that $P_{0,EW}$ is not a measure of the wave energy content, but a characterization of its asymmetry with respect to the EW direction. The average value of $P_{0,EW}$ for each epoch and the cumulative distribution function (cdf) of the yearly-averaged values were calculated to provide insight into the temporal variability of the wave power asymmetry (Figure 4.3.1c-e).

The average value for the cumulative distribution function (cdf = 0.5), considering all epochs, is approximately $P_{0,EW} = -0.5$ W/m^2, which implies an asymmetrical distribution of the wave power directionality, with prevailing easterly wave conditions. When the averaged values for every particular epoch and year are analysed, important differences are observed (Figure 4.3.1c-e). For Epoch 1, offshore wave power of easterly waves was slightly predominant ($P_{0,EW} \simeq -0.12$ W/m^2), but there was a significant variability between the yearly values. During Epoch 2, the directionality was closer to its mean value (cdf $\simeq$ 0.56), with a dominance of easterly waves ($P_{0,EW} \simeq -0.35$ W/m^2), and yearly values showed limited variability. However, during Epoch 3, westerly waves dominated with an average value for $P_{0,EW} = 0.22$ W/m^2 and a cdf > 0.87. Besides, five of the six years in this epoch had a cdf > 0.85.

Considering only (typical) storm conditions, the values of $P_{0,EW}$ are -22.71, -17.67 and 0.21 W/m^2 for Epochs 1, 2 and 3, respectively. The directionality of the values for Epochs 1 and 2 differ slightly from those obtained for the complete range of conditions due to the higher intensity and longer duration of the easterly storms during Epoch 1 (Figure 4.3.1c-e). These results are further analysed and correlated with LST distributions in Section 4.3.4.2.

4.3.2 Evolution of the submerged morphology – A comparative analysis

4.3.2.1 Epoch 1: 1999-2004

During this epoch, before the establishment of Rules Reservoir, there was a change in the coastline orientation around the river mouth and a maximum coastline retreat equal to 99 m, i.e., the rate of retreat was about 20 m/year (Figure 4.3.2a). Aerial images, with a resolution equal to 0.5 m/pixel, show that the erosive processes were evident at the east side of the Guadalfeo River mouth in 2004 (Figure 4.3.5). This erosion generated a single shoreline undulation 300 m at the east of the mouth (green triangle, Figure 4.3.5c).

The submerged morphology was eroded up to 2 m below mean sea-level (MSL), reaching maximum bed-level erosion of 1 m (Figure 4.3.2a). Accretion took place in deeper water, reaching maximum (positive) bed-level changes of approximately 1.5 m. This accretion was most likely fed by the sediment supply from the river, detailed in Bergillos et al. (2016a). The relationship between sediment input from the river and bed elevation changes in deep water has been widely demonstrated in this part of the Mediterranean Spanish coast (e.g., Lobo et al. (2006)).

Volume differences per meter of coastline, obtained as the integral of the change from the shoreline to 10 m water depth across the beach profile, are shown in Figure 4.3.2b. Maximum erosion occurred at the eastern flank of the mouth (up to 140 m^3/m) with less erosion along the eastern region (< 60 m^3/m) and hardly erosion along the western region (< 15 m^3/m). As a whole, the eroded volume along the whole study area was about $130 \cdot 10^3$ m^3, i.e., an erosion rate of $26 \cdot 10^3$ m^3/year.

4.3.2.2 Epoch 2: 2004-2008

The maximum coastline retreat southeast of the river mouth during this epoch was 76 m and mainly occurred before 2007 (Figure 4.3.3d-e), thus corresponding to a retreat rate of 25.3 m/year. According to the aerial image of 2008, a slight eastward movement of the horn (blue rhombus, Figure 4.3.5f) and a reduction of the prominence of the undulation took place.

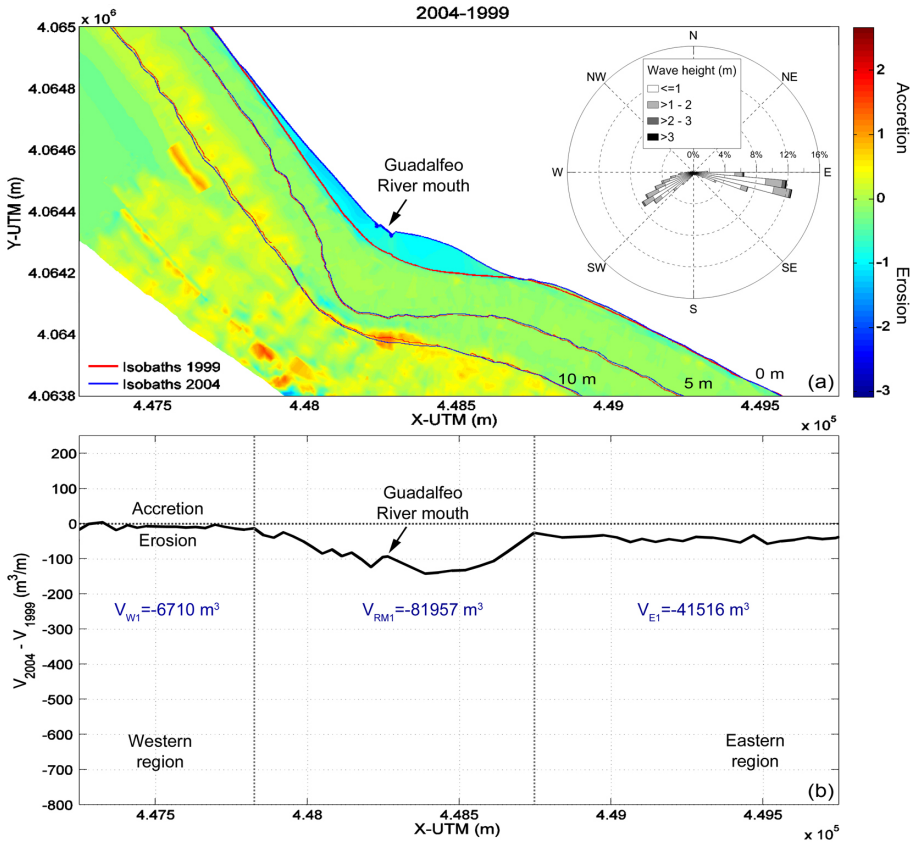

Figure 4.3.2: (a) Difference in bed-level between 2004 and 1999 bathymetries and polar diagram showing the frequency of occurrence and the incoming wave directions over the first epoch. (b) Difference in sediment volume per meter of coastline –from the shoreline to 10 m water depth– during Epoch 1. (Source: Bergillos et al. (2016b). Reproduced with permission of Elsevier).

The river regulation in 2004 (river flow discharges during this epoch were lower than 4 m^3/s), and the resulting reduction in the sediment supply to the coast, generated a significant deficit of submerged sediment around the river mouth (Figure 4.3.3a) and, as a consequence, delta shoreface retreat. Despite the fact that only one extreme storm took place during this epoch, bed-level erosion up to 3 m occurred along a 1-km section around the river mouth. Unlike the relatively shallow morphological changes during the previous epoch, significant bed-level changes during Epoch 2 occurred from the coastline to depths up to 8 m below MSL. Maximum sediment erosion, with values higher than 760 m^3/m, took place at the eastern flank of the mouth, but erosion rates in excess of 300 m^3/m occurred along a 500-m section around the river mouth (Figure 4.3.3b).

The reduction in sediment volume around the river mouth from the coastline to 10 m water depth was almost $360 \cdot 10^3$ m^3 during this epoch. Conversely, sediment accretion of up to 212.5 m^3/m and 112.4 m^3/m occurred in the western and eastern regions, respectively (Figure 4.3.3b). Therefore, the sediment eroded in the mouth appears to have been redistributed towards the neighbouring stretches of coast, especially towards the western region due to the dominance of easterly waves during this epoch (Figure 4.3.1d). Altogether, the sediment erosion along the

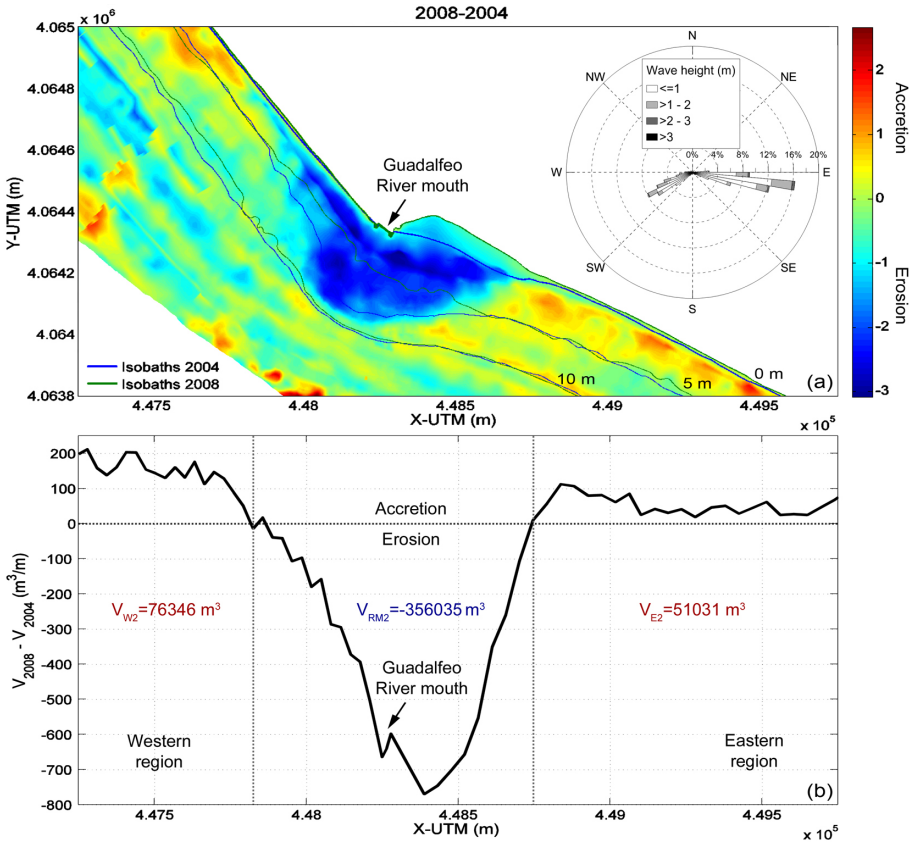

Figure 4.3.3: (a) Difference in bed-level between 2008 and 2004 bathymetries and polar diagram showing the frequency of occurrence and the incoming wave directions over the second epoch. (b) Difference in sediment volume per meter of coastline –from the shoreline to 10 m water depth– during Epoch 2. (Source: Bergillos et al. (2016b). Reproduced with permission of Elsevier).

study area was almost $230 \cdot 10^3$ m^3, corresponding to an erosion rate of $57 \cdot 10^3$ m^3/year.

4.3.2.3 Epoch 3: 2008-2014

Changes in coastline position and beach orientation around the mouth between 2008 and 2014 were mainly influenced by the dominance of westerly waves (Figure 4.3.4e) and the water drainages of the dam in January 2010 (up to 53 m^3/s). The latter generated a sudden change (accretion) in coastline position and orientation (Figure 4.3.5g). After that, a severe coastline retreat of approximately 120 m took place in the southeast of the river mouth, corresponding to a rate of erosion equal to 40 m/year between 2010 and 2013 (Figure 4.3.5g-h).

During this epoch, the erosion around the river mouth was significantly lower than that of the previous epoch, influenced by the drainages of the dam in January 2010. These river discharges contributed to the positive bed-level changes in deep water during this epoch (Figure 4.3.4a). These bands of accretion are distributed parallel to the shoreline and reaching maximum values of 2 m which are within the range of heights of undulations previously measured in the study site (e.g., Fernández-Salas et al. (2007)).

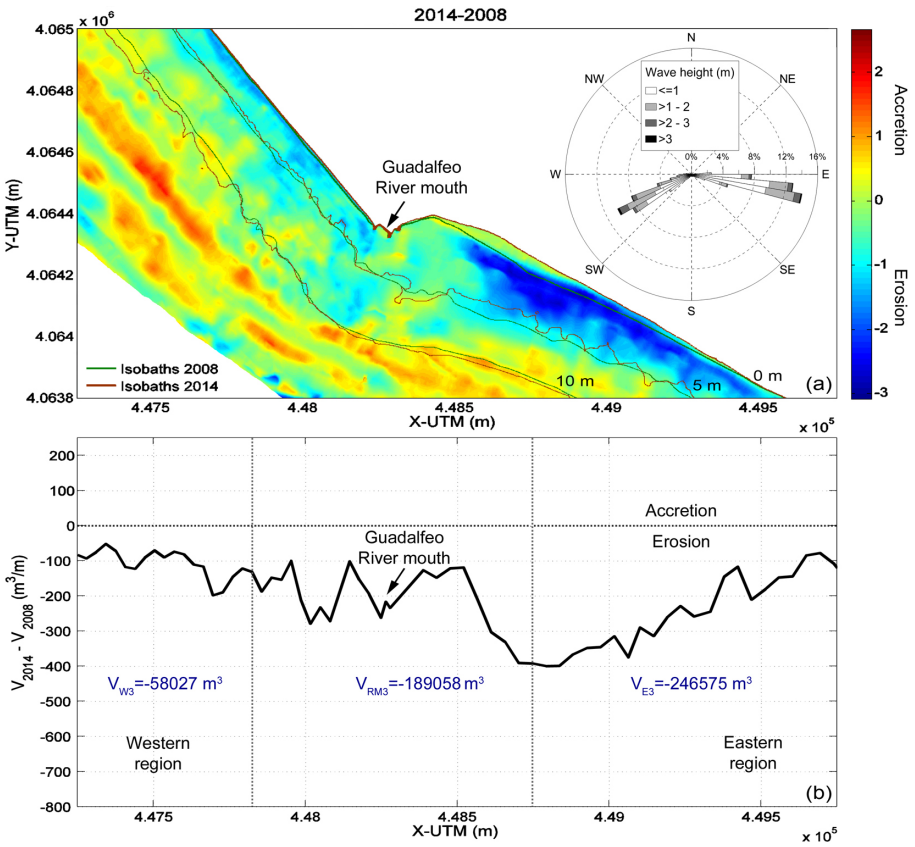

Figure 4.3.4: (a) Difference in bed-level between 2014 and 2008 bathymetries and polar diagram showing the frequency of occurrence and the incoming wave directions over the third epoch. (b) Difference in sediment volume per meter of coastline –from the shoreline to 10 m water depth– during Epoch 3. (Source: Bergillos et al. (2016b). Reproduced with permission of Elsevier).

Erosion took place in the neighbouring stretches of coast, especially stern region, where maximum bed-level changes exceeded 2 m and sediment volumetric losses of up to 400 m^3/m occurred (Figure 4.3.4). Hence, it appears that the erosion generated in the delta between 2004 and 2008 was propagated mainly towards the east during Epoch 3, influenced by the predominance of westerly waves (Figure 4.3.1e). As a whole, the reduction in sediment volume along the study section was almost $494 \cdot 10^3$ m^3, corresponding to an erosion rate of $79 \cdot 10^3$ m^3/year.

4.3.2.4 Summary of morphological changes

The erosion rate per meter of coastline has been increasing in the entire study area: the increase in Epoch 2 was attributed to the negligible sediment discharge during this epoch due to flow regulation in 2004, whereas the increase in Epoch 3 was, in addition to the reduced fluvial sediment discharge, also induced by the higher number of storms and the predominant westerly waves during this epoch (Table 4.3.1 and Figure 4.3.1), inducing greater volumes of LST, as will be show in Section 4.3.4.

Figure 4.3.5: Aerial images of the Guadalfeo River mouth in 1999 (a), 2002 (b), 2004 (c), 2006 (d), 2007 (e), 2008 (f), 2010 (g) and 2013 (h). The shorelines are highlighted in colours (Source: Bergillos et al. (2016b). Reproduced with permission of Elsevier).

The lowest sediment losses took place along the western region (higher accretion rate in Epoch 2 and lower erosion rates in Epochs 1 and 3), whereas the highest erosional rates occurred around the river mouth in Epochs 1-2 and in the eastern region over Epoch 3. In Section 4.3.4, this alongshore variability in the sediment volumetric changes will be related to the differences in wave directionality and the wave direction dependent LST gradients.

Table 4.3.2: Rates of volumetric change (in m^3/year), length of the coastline (in m) and rates of change per meter of coastline (in m^3/year/m) during the study epochs in the three regions indicated in Figures 4.3.2-4.3.4 and in the entire study area.

	Western region			River mouth			Eastern region			Entire area		
	V	L	V/L	V	V/L	L	V	L	V/L	V	L	V/L
Epoch 1	-1,342	850	-1.6	-16,391.4	1,082.3	-15.1	-8,303.2	1,072.1	-7.8	-26,036.6	3,004.4	-8.7
Epoch 2	19,086.4	850	22.4	-89,008.8	1,082.3	-82.2	12,757.8	1,072.1	11.9	-57,164.6	3,004.4	-19
Epoch 3	-9,284.3	850	-10.9	-30,249.3	1,082.3	-28	-39,452	1,072.1	-36.8	-78,985.6	3,004.4	-26.3

4.3.3 Changes in wave propagation induced by delta erosion

To understand the delta mouth dynamics in terms of nearshore wave propagation and LST patterns, the spatial and temporal variation in the breaking wave height (H_b) and the LST rates were analysed under low energy and storm conditions (Table 4.2.1). Figure 4.3.6 depicts the alongshore distribution of H_b for the four bathymetries detailed in Section 4.2.1.2 under both westerly and easterly waves.

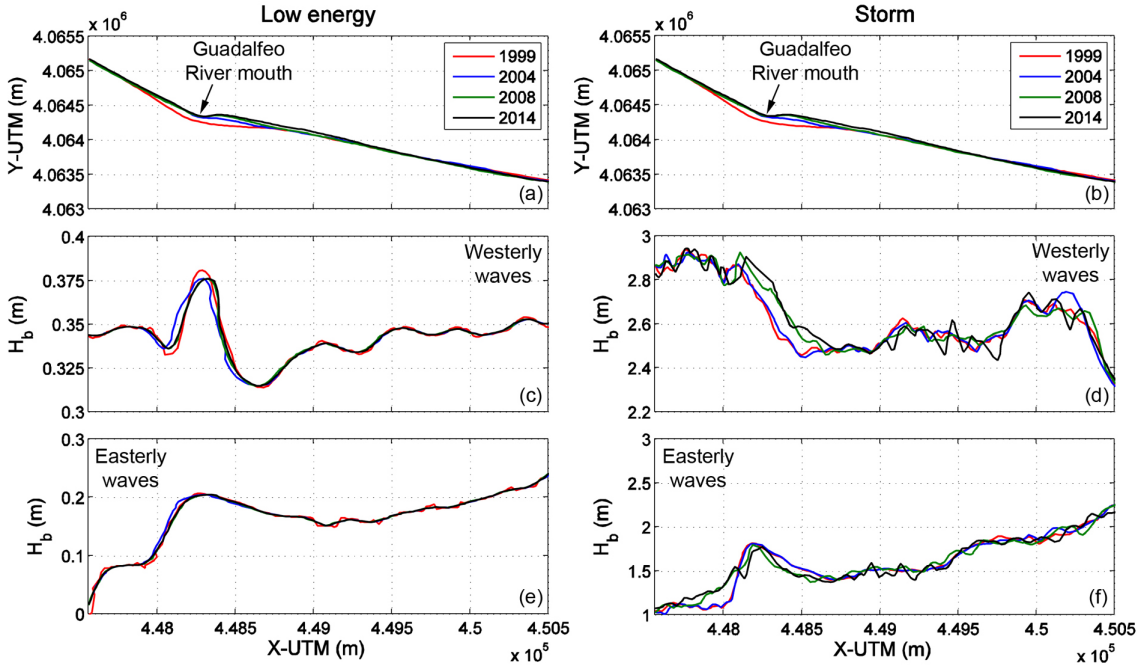

Figure 4.3.6: Alongshore evolution of the breaking wave height: low energy conditions for south-westerly (c) and easterly waves (e); storm conditions for south-westerly waves (d) and easterly waves (f). The shorelines of the four bathymetries are shown in panels a and b. (Source: Bergillos et al. (2016b). Reproduced with permission of Elsevier).

Under low energy conditions, the H_b values, and their alongshore variation, are similar for the four bathymetries under both westerly and easterly waves (Figure 4.3.6c-e); however, significant differences are observed for typical storm conditions (Figure 4.3.6d-f). Under westerly storm waves it is observed how the delta retreat during Epoch 2 (Figure 4.3.3), and the reduction in wave refraction, induced significantly larger values of H_b at the eastern flank of the mouth. The maximum difference represents an increase of almost 10% (difference in H_b of 0.22 m).

Under easterly storm conditions (Figure 4.3.6f), higher H_b values are observed in 1999 and 2004 at the eastern flank of the mouth, probably due to the advanced seaward coastline position in 1999 and the shoreline undulation in 2004 at this location (Figure 4.3.5a-c). However, the delta retreat during this epoch led to greater values of H_b at the western flank of the mouth, with differences up to 21% and 0.25 m. During the 2008-2014 epoch, changes in the wave breaking conditions were significantly less than during the preceding period (increases of 2% and 10% in H_b for westerly and easterly storm conditions, respectively). This is attributed to the lower erosion rates during Epoch 3 at this location (Figure 4.3.4) and the ensuing more stable nearshore morphology in terms of wave propagation.

4.3.4 Relationship between morphological changes and LST

4.3.4.1 Influence of delta evolution on the LST rates

LST rates under both low energy and storm conditions were computed based on the data shown in Table 4.2.1. The shoreline angle and beach slope distributions were obtained from the bathymetric data of 1999, 2004, 2008 and 2014. Figure 4.3.7 depicts the results of LST obtained under low energy and storm conditions and demonstrates that transport rates are generally largest in the vicinity of the Guadalfeo River mouth. It is also observed that the largest values for LST are obtained under westerly waves for both low energy and storm conditions.

Under low energy conditions and for westerly waves (Figure 4.3.7c), LST gradients at the Guadalfeo River mouth are insignificant except for 2004. In this case, LST is almost one order of magnitude larger than for the other bathymetries. Under easterly waves (Figure 4.3.7c), the LST gradients for 2004 are also much more significant than for the other bathymetries. These higher rates in 2004 were induced by the different coastline configuration (shoreline angles) and nearshore bathymetry (slope and surf zone width), and contributed to the delta retreat during Epoch 2 (Figure 4.3.3).

For storm conditions (Figure 4.3.7d-f), significant differences are observed between westerly and easterly waves. Under westerly storms, LST is significantly larger than those obtained under easterly storms, particularly for the 2008 and 2014 bathymetries. However, for easterly storms the largest LST occurred for the 1999 and 2004 bathymetries with significantly lower LST values for 2008 and 2014. It appears that by 2008 the shoreline is much more in equilibrium with easterly storm wave conditions, and, overall, Figure 4.3.7c-f suggests that the delta has acquired a shape that minimizes LST for all wave conditions except for westerly storms, which are the most energetic and were more frequent during Epoch 3 (Figures 4.3.1a and 4.3.4a).

4.3.4.2 LST and wave directionality

To further explore the relationships between the directionality distribution of waves and LST, the complete time series of LST was obtained for Epochs 1, 2 and 3 using the downscaling methodology described in Section 4.2.3.2. The results are shown in Figure 4.3.8, where the probability distribution functions (pdfs) of LST are depicted for each epoch, depending on the location along the shoreline (plotted on the x-axis). To help with interpreting this figure, the colour bar representing the probability values (left panels) was adjusted to enable consideration of the low pdf values and the pdf for a single cross-shore profile in the vicinity of the river mouth where LST is maximum is presented separately (right panels).

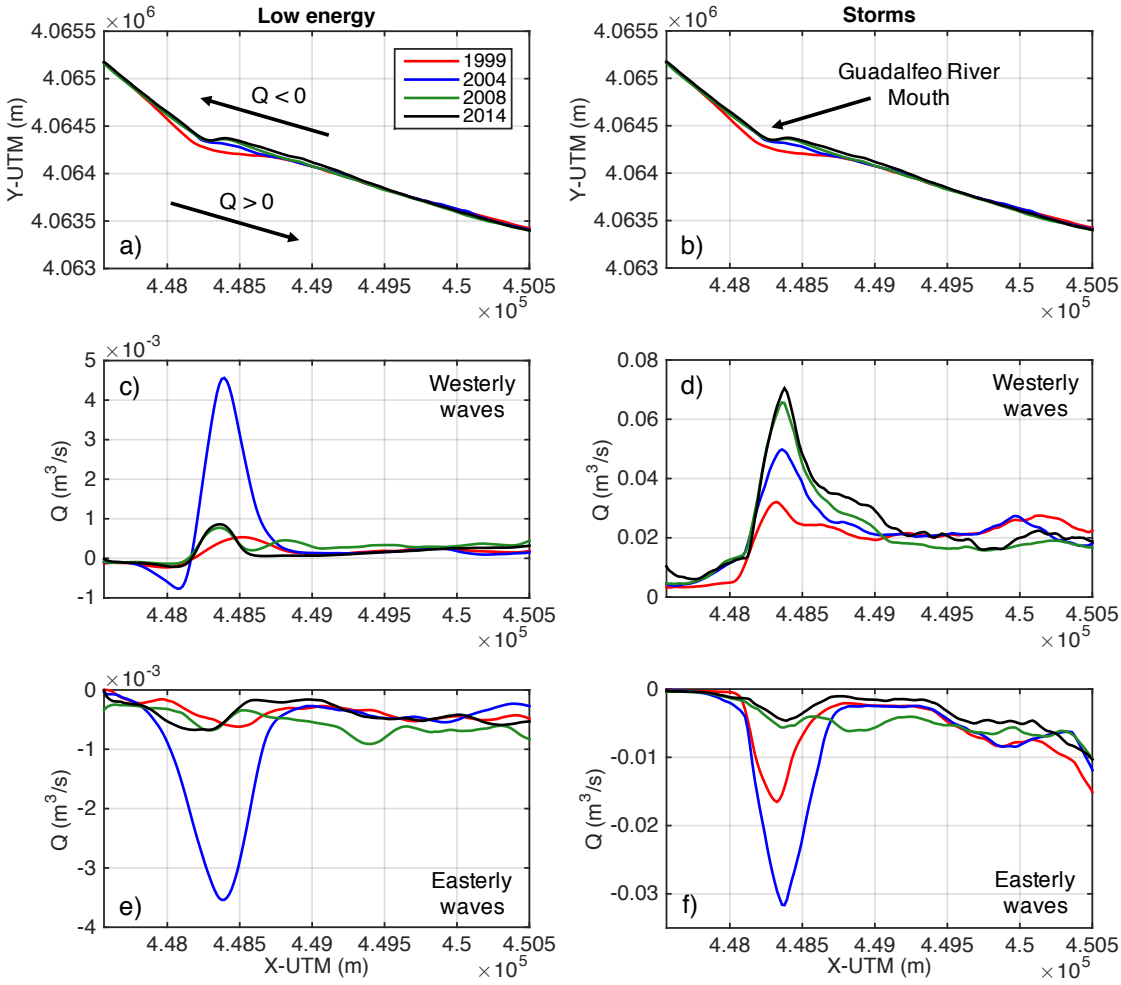

Figure 4.3.7: Alongshore evolution of the longshore sediment transport: low energy conditions for south-westerly (c) and easterly waves (e); storm conditions for south-westerly waves (d) and easterly waves (f). The shorelines of the four bathymetries are depicted in panels a and b. (Source: Bergillos et al. (2016b). Reproduced with permission of Elsevier).

The highest LST values for both drift directions are found around the river mouth; however, some differences in the pdfs are observed between the three epochs. During Epoch 1 (Figure 4.3.8c-d), LST values with probabilities over 0.035 (red colours) barely present significant alongshore gradients. On the contrary, LST with probabilities around 0.01 present significant gradients and values of $Q \simeq 0.02$ m^3/s for westerly drifts close to the river mouth. Hence, westerly drift ($Q > 0$) was more frequent and intense than easterly drift, influenced by the higher LST rates under westerly waves (Figure 4.3.7). These results are also in agreement with those of wave directionality, as the value of the mean $P_{0,EW}$ for this epoch was over the mean for the entire dataset, indicating that this epoch was less easterly dominated than the average.

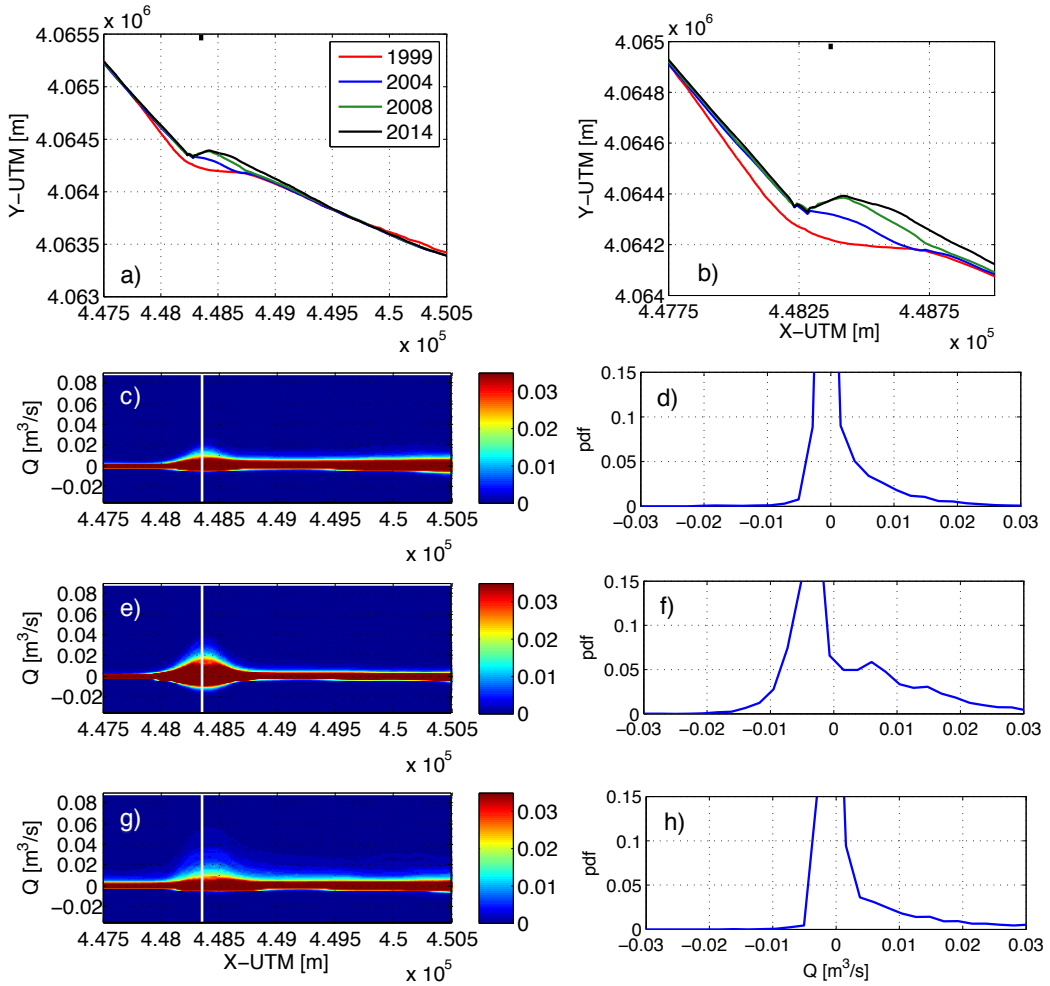

Figure 4.3.8: Probability distribution functions (pdfs) for the LST during Epochs 1 (c), 2 (e) and 3 (g). Colours correspond to the probability of LST rates (vertical axis) in its alongshore location (horizontal axis). Panels d, f and h show the pdfs for a cross-shore section located at the vicinity of the river mouth and depicted in panels a and b. (Source: Bergillos et al. (2016b). Reproduced with permission of Elsevier).

For Epoch 2, higher values of LST and alongshore gradients around the river mouth were clearly more frequent than for Epoch 1. Although during this epoch LST with absolute values over 0.02 m^3/s were more likely for westerly drifts, implying that significant alongshore gradients in LST were more frequent under westerly waves, the symmetry of the deep red colours around the river mouth indicates that the majority of the LST values in this area were concentrated in $Q \in (-0.015, 0.015)$ m^3/s. This implies that easterly waves were more important during this epoch, from a morphodynamic point of view, than in previous one. This is in agreement with the results shown in Figure 4.3.1c-e, as this epoch was the one with the lowest mean $P_{0,EW}$ value. For Epoch 3, the LST distribution is very asymmetric with a dominance of westerly drifts. The highest LST rates ($Q > 0.03$ m^3/s) were much more likely than in the previous epochs (pdf > 0.01), contributing to the significant sediment deficit measured in the study area (Figure 4.3.4b).

4.3.4.3 Volumetric changes induced by LST – Comparison with delta evolution

Figure 4.3.9 shows the observed coastline changes, the average LST rates and the volumetric differences based on the gradient in the LST for the three epochs. Since the LST formulation accounts for sediment transport in the breaking zone, the modelled differences indicate changes in this zone.

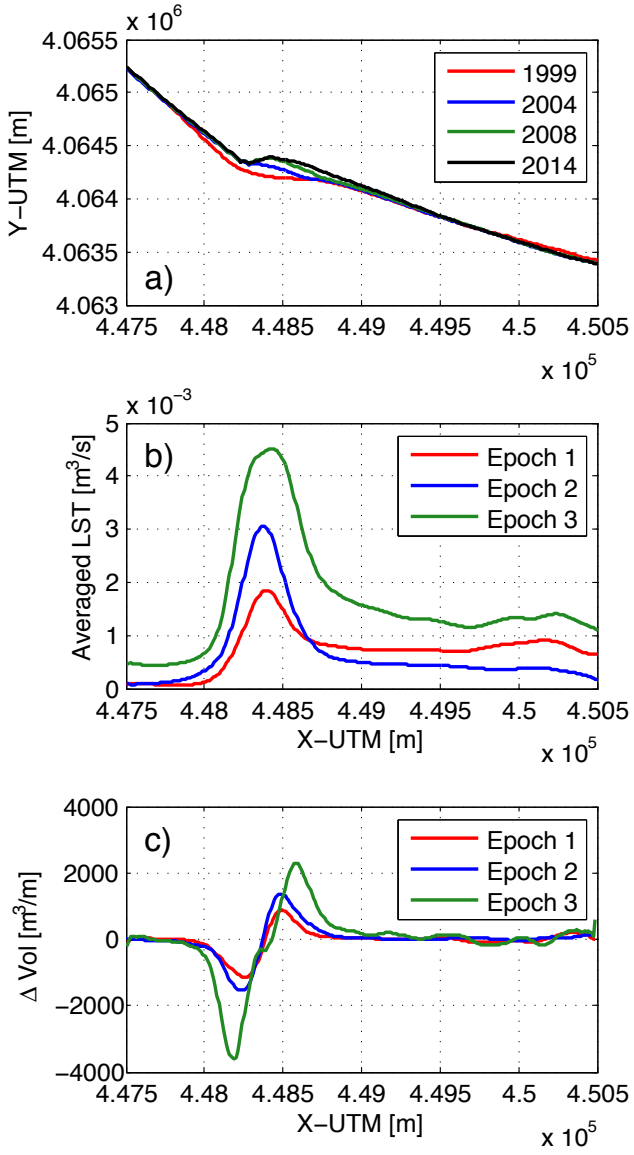

Figure 4.3.9: (a) Shoreline at the beginning of each Epoch. (b) Averaged LST rates for Epochs 1 (red), 2 (blue) and 3 (green). (c) Alongshore evolution of LST volumetric changes in the nearshore during Epochs 1 (red), 2 (blue) and 3 (green). (Source: Bergillos et al. (2016b). Reproduced with permission of Elsevier).

The LST volume gradients, which are based on the potential littoral drift rates (Figure 4.3.9b), predict erosion of the western flank of the delta and accretion of the eastern flank for all epochs (Figure 4.3.9c). However, higher eroded volumes were measured on the eastern flank during the three epochs (Figures 4.3.2-4.3.4). The discrepancy between observed changes and those expected on the basis of LST rates can be attributed to the trapping of eastward moving sediment by the river jetties, resulting in erosion rather than accretion on the eastern flank and reducing erosion on the western flank. This highlights the importance of the river jetties in reversing the morphodynamic behaviour expected for an unmodified beach.

The total sediment volume losses along the stretch of beach between Salobreña Rock and *Punta del Santo* (Figure 4.2.1) induced by LST were approximately $90 \cdot 10^3$, $12 \cdot 10^3$ and $120 \cdot 10^3$ m^3 for Epochs 1, 2 and 3, respectively. As shown in Table 4.3.3, these modelled values are similar (differences lower than 35%) to the measured erosion between the shoreline and the maximum breaking depth for each epoch (3.5, 3.7 and 5.9 m for Epochs 1, 2, 3, respectively) and indicate that LST is the main contributor to coastal changes. The uncertainty associated with both measurements and modelling (Brad Murray et al., 2016), particularly the lack of available multibeam bathymetries at a larger temporal resolution, should be considered to understand the obtained differences.

Table 4.3.3: Sediment volumes (in m^3) during the study epochs: gross LST, net LST, and measured between the shoreline and the maximum breaking depth (h_b).

	Epoch 1	Epoch 2	Epoch 3
Gross LST	480,870	64,0790	1,315,000
Net LST	-89,997	-12,016	-119,623
Measured	-71,461	-18,198	-175,310

The negative sediment balance in the studied stretch of beach (Figures 4.3.2-4.3.4 and Table 4.3.3) contrasts with the accumulation of sediments and the advance seaward of the coastline in the section *Punta del Santo* - Motril Port (Figure 4.2.1), detailed by Bergillos et al. (2015a). This indicates that most of the eroded sediment in the surveyed area was transported eastward and accumulated in the section *Punta del Santo* - Motril Port, mainly due to the greater LST rates under westerly waves (Figure 4.3.7) and the resulting dominance of westerly drift (Figure 4.3.9b). Due to the wave directional variability, the net LST is a relatively small fraction of the gross LST (< 20%). These gross LST volumes modelled for each epoch ($V_3 > V_2 > V_1$, Table 4.3.3) are also consistent with both the wave directionality analysis performed (Figure 4.3.1c-e) and the nearshore volumetric changes observed (Figures 4.3.2-4.3.4).

4.4 Discussion

Although the influence of both natural and human-induced changes on the evolution of deltas has been widely addressed, much still remains to be known of the interactions between waves and deltaic river mouths (Anthony, 2015). This chapter provides insights into the relationship between wave climate, submerged morphological changes, wave propagation patterns and longshore sediment transport.

The Guadalfeo has been historically a mixed wave-river to river dominated delta, that is, the delta response was mainly dominated by the sediment supplies of the river (Hoffmann, 1987; Jabaloy-Sánchez et al., 2014), but the redistribution of this sediment input along the coast was influenced by wave directionality and LST (López-Ruiz et al., 2012a). Thus, the delta evolution between 1999 and 2004, when no significant sediment pulses from the river occurred (Bergillos et al., 2016a) and the offshore wave power was almost balanced between easterly and westerly waves (Figure 4.3.1c), is summarized in Figure 4.4.1a considering the weak river jet. The observed coastline retreat and erosion of the shallow nearshore during this epoch could be attributed to the advanced seaward position of the initial coastline (Figure 4.3.5a) due to sediment pulses over previous years (Losada et al., 2011). The delta response during these years (before 1999) was thus similar to the conceptual model shown in Figure 4.4.1a considering the strong river jet, that is, fluvial delivery of sediment exceeding the capacity for LST to remove sediment from regions proximal to the river mouth (Anthony, 2015).

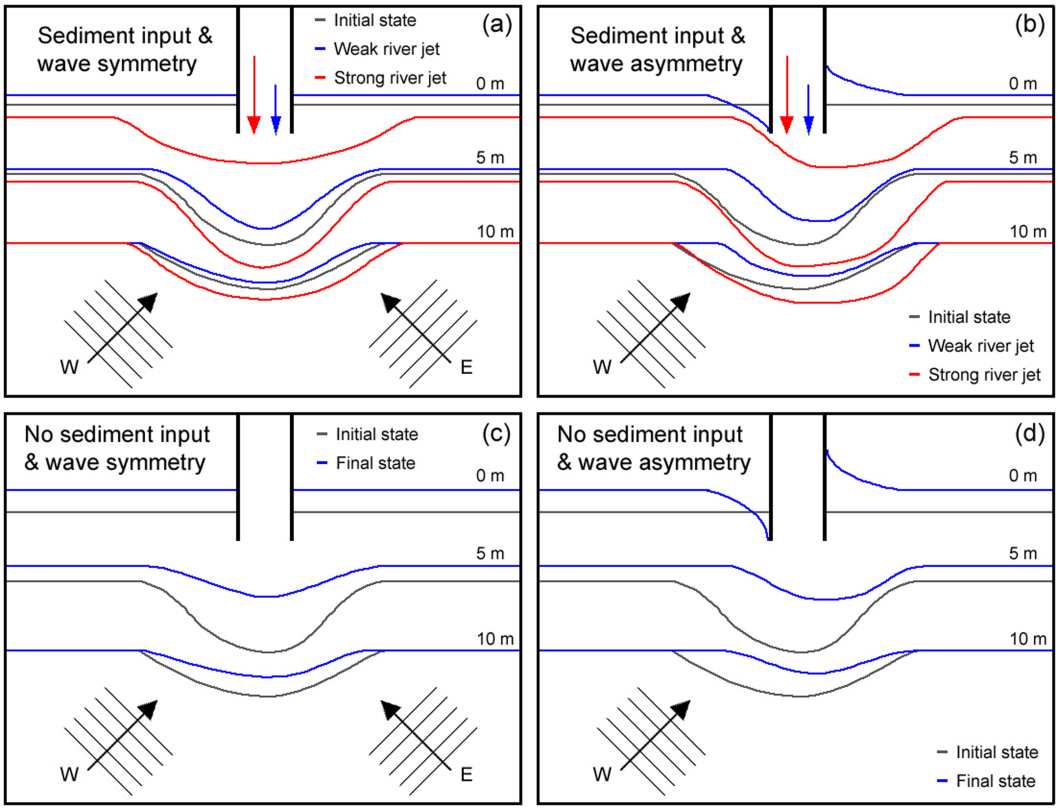

Figure 4.4.1: Conceptual model describing the delta response forced by: (a) sediment input from the river and symmetric wave climate; (b) sediment input and asymmetric wave climate; (c) symmetric wave climate without sediment input; and (d) asymmetric wave climate without sediment input. (Source: Bergillos et al. (2016b). Reproduced with permission of Elsevier).

However, the river mouth has been subjected to strong coastal erosion since 2004 as a result of reduction in river and sediment discharge due to flow regulation (Figure 4.4.1c-d). Although this response has been reported widely from other deltas (Syvitski and Saito, 2007; Syvitski et al., 2009), the maximum measured rate of coastline retreat for the Guadalfeo (40 m/year between 2010 and 2013) was larger than those observed in the Adra (3.5 m/year), Po (9 m/year), Ombrone (11 m/year), Rhône (15 m/year), Danube (20 m/year) and Arno (20 m/year) deltas by Jabaloy-Sánchez et al. (2010), Simeoni et al. (2007), Pranzini (1994), Sabatier and Suanez (2003), Vespremeanu-Stroe et al. (2007) and Pranzini (2001), but lower than those found in the Ebro (> 50 m/year) and Nile (> 100 m/year) deltas by Jiménez and Sánchez-Arcilla (1993) and Frihy and Komar (1993), respectively. A wide variety of factors, such as the different flows (drainages of dams), wave conditions (especially wave direction), shoreline orientations, grain sizes and/or beach slopes in these deltas, in combination with the different time-scales considered to estimate these rates, are important contributors to the reported differences.

In addition to coastline retreat, sediment losses across the delta front were measured: the maximum erosion rate along the surveyed area during Epoch 3 ($\sim 79 \cdot 10^3$ m^3/year) was similar to that detailed by Jabaloy-Sánchez et al. (2010) in the Adra delta ($69.5 \cdot 10^3$ m^3/year), but significantly lower than those reported in the Ebro (up to $241 \cdot 10^3$ m^3/year), Ombrone ($630 \cdot 10^3$ m^3/year), Rhône ($1.94 \cdot 10^6$ m^3/year) and Nile ($19 \cdot 10^6$ m^3/year) deltas by Jiménez and Sánchez-Arcilla (1993), Pranzini (1994), Sabatier et al. (2006) and Inman and Jenkins (1984), respectively. These significant differences are mainly due to the smaller (alongshore) length of the studied stretch of beach, since the erosion rates per meter of coastline in the Guadalfeo during Epoch 3 (26.3 m^2/year), Ebro (56 m^2/year), Ombrone (42 m^2/year), Rhône (27.7 m^2/year) and Nile (95 m^2/year) deltas are of the same order of magnitude.

The observed changes in the coastal morphology and nearshore bathymetry generated significant variations in wave propagation patterns. In particular, the delta retreat during Epoch 2 led to lower refraction and higher wave energy content, with increases in breaking wave height up to 10% and 21% under westerly and easterly storms, respectively (Figure 4.3.6d,f). The role of the river deltas in the reduction of wave energy, highlighted by Pranzini (2001) and Anthony (2015), was thus reduced significantly after river damming. Such quantifications of reduced protection from wave action (i.e., higher breaking wave heights) due to delta erosion based on calibrated wave propagation models have so far been limited. The coupling of increasing erosion and decreasing protection from waves around the Guadalfeo delta has led to the shift towards an increasingly wave-dominated situation. This change, mainly induced by human activities, has been observed in numerous Mediterranean deltas over last decades (Anthony et al., 2014).

Among these human interventions, channelization through river jetties plays a significant role in the deltaic response (Arnaud-Fassetta, 2003; Fan et al., 2006). When the jetties are filled up (most of Epoch 1), LST is not interrupted and sediment is passed around the river mouth; whereas if they extend into the sea (Epoch 2 and most of Epoch 3), they interrupt the LST and reverse the expected morphological response in the plan view. The reported interruption of LST by river jetties is in agreement with previous works in the Nile delta, where higher erosion rates were measured to the east of the jetties under prevailing westerly drift (Frihy et al., 1991; Frihy et al., 2003), and in the Guadiana ebb-tide delta, where erosion was observed along down-drift coasts in response to jetty construction (Garel et al., 2014; Garel et al., 2015). The influence of river jetties on LST is especially relevant under asymmetric wave conditions (Figure 4.4.1b,d).

The results obtained in Sections 4.3.1 and 4.3.4 indicate that the erosion rate in the study area increases as a function of westerly LST (Figure 4.3.1 and Table 4.3.3). The maximum LST rates around the Guadalfeo River mouth ($\sim 4.5 \cdot 10^{-3}$ m^3/s, Figure 4.3.9b) are similar (same order of magnitude) to those found in the Ombrone ($\sim 4.8 \cdot 10^{-3}$ m^3/s), Ebro ($\sim 5.4 \cdot 10^{-3}$ m^3/s) and Nile ($\sim 9.5 \cdot 10^{-3}$ m^3/s) deltas by Pranzini (2001), Jiménez and Sánchez-Arcilla (1993) and Frihy et al. (2003), respectively. The coarser sediments in the Guadalfeo and Ombrone deltas compared to those of the Ebro and Nile surely contribute to these differences in LST rates, which are in agreement with the reported erosion rates per meter of coastline (Guadalfeo < Ombrone < Ebro < Nile).

The relationship between measured erosion and LST rates documented for the Guadelfeo delta serves as an example for the increasing importance of wave action for the evolution of Mediterranean deltas characterised by decreased river sediment supplies. Comparison between the reduction in fluvial sediment discharge due to river regulation in 1999 ($\sim 74 \cdot 10^3$ m^3/year) and the sediment volume eroded and transported eastward by LST since then ($\sim 57 \cdot 10^3$ and $\sim 79 \cdot 10^3$ m^3/year during Epochs 2 and 3, respectively) represents clear evidence for a human-induced shift in the dynamics of a hitherto mixed fluvial-wave dominated delta.

4.5 Conclusions

This chapter studies the evolution of the Guafalfeo River mouth (southern Spain), a highly altered Mediterranean delta. The analysis is mainly based on the evolution of the submerged morphology, and its correlation with the maritime climate, wave propagation and LST. Based on the observations and results, the following conclusions were drawn:

1. Coastline retreat (up to 40 m/year) and significant erosion in the submerged morphology around the river mouth (up to $190 \cdot 10^3$ m^3/m/year) have occurred since the entry into operation of Rules Reservoir in 2004. The erosion in the delta wedge has been lower since 2008 but the sediment deficit is being propagated towards the east side of the mouth, influenced by the dominance of westerly waves and the presence of river jetties, and the erosion propagation will probably continue in the coming years.

2. Delft3D-WAVE modelling reveals that the erosion in the delta wedge induced lower refraction and greater wave energy around the mouth. The breaking wave height under storm conditions increased up to 10% (21%) at the eastern (western) flank of the mouth for incoming westerly (easterly) waves.

3. LST on the coast was significantly modified by the combined effect of changes in the nearshore bathymetry (partly induced by river damming) and wave conditions (mainly wave directionality). Volumetric changes obtained through the LST gradients are able to explain quantitatively the majority of the measured volumetric changes (differences lower than 35%), indicating that LST was the main driver of the nearshore changes in the delta.

CHAPTER 5

MORPHO-SEDIMENTARY DYNAMICS OF THE BEACH

This chapter addresses the changes in the morphology and sedimentology of Playa Granada forced by wave and water-level variations, and human intervention through nourishment. Monthly and storm event-driven beach surveys, consisting of topographical measurements and sediment sampling in two selected areas, were carried out over a one-year period. Three prevailing sediment fractions (sand, fine gravel and coarse gravel) and two end-member morphological states of the upper beach profile (convex with multiple berms and concave with a single storm berm) were identified. Between them, several transitional profiles were formed, characterized by developing berms that progressively overlapped, generating sediment variability both across the beach profile and with depth. The results indicate that the total run-up (including water-level) reached during an event represents a more accurate threshold for differentiating between erosional and depositional conditions than wave height. They also suggest that mixed sand and gravel beaches recover faster from storm erosion than sandy beaches. The long-term benefit of the artificial nourishment that took place at the end of the survey period was very limited and this is attributed to the too fine sediment used for the nourishment and its placement too high on the beach. Clearly, nourishment interventions must take into account the natural sediment distribution and the profile shape to avoid rapid losses of the nourished sediment. The results of this chapter allow deepening into the knowledge of the morpho-sedimentary dynamics of MSG beaches under varying wave and water-level conditions.

5.1 Objective

The main objective of the chapter is to characterize the morphological and sedimentary dynamics of a mixed sand and gravel (MSG) beach (Playa Granada), focusing on the contribution of wave run-up, storm surge and astronomical tide to natural beach response, as well as its behaviour after artificial nourishment. To meet this objective, the evolution of wave and wind conditions and total run-up is analysed; the morphological and sedimentary characteristics of the beach are detailed; typical morpho-sedimentary states are identified; and the profile response before, during and after artificial replenishment is investigated. All morphological variability is related to the wave and water-level forcing.

5.2 Methodology

5.2.1 Data

5.2.1.1 Maritime data

One year of hourly hindcasted data, corresponding to SIMAR point number 2041080, was used for driving the wave-induced coastal morphological changes. The SIMAR networks wind fields are obtained through the High Resolution Limited Area Model (Cats and Wolters, 1996) and the wave fields are computed through the WAM model (Booij et al., 1999), on the basis of the wind field data (López et al., 2012). The following variables were extracted from these hindcasted data: deep-water significant wave height (H_0), spectral peak period (T_p), deep-water wave direction (θ_0), wind velocity (V_w) and wind direction (θ_w). Furthermore, the astronomical tide measured by a gauge located in the Motril Port was used to represent the tidal forcing. Both wave and tide data were provided by *Puertos del Estado*.

5.2.1.2 Field surveys

Field surveys were performed from October 2013 to September 2014 (hereafter referred to as the study period). To analyse the beach morphological evolution, two study areas within the study site were selected (Figure 5.2.1) to ensure the results were representative for entire beach section.

Monthly periodic field surveys were performed during the study period, consisting of topographic and sediment sizes measurements of the beach profile. In addition, several specific surveys were carried out before and after two significant storms (December 2013 and March 2014), and before, during and after the artificial replenishment of the beach performed in June 2014 (Table 5.2.1). Each survey was carried out under low tide conditions and the measurements were referenced to the mean low water spring level (MLWS) to avoid negative contributions of the astronomical tide to the total run-up. The two major storms that occurred during the study period were identified by means of the peaks over threshold (POT) method (Goda, 2010) considering $H_T = 3.1$ m ($H_{99.9\%}$) and storm durations lasting longer than 6 hours.

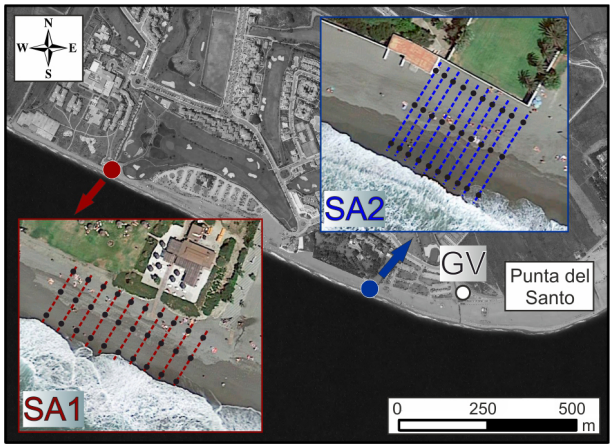

Figure 5.2.1: Selected study areas and geodesic vertex *Punta del Santo*. Ten profiles were measured in both study areas (dashed lines) and samples were taken both at the surface and at depth in each profile (dots). (Source: Bergillos et al. (2016d). Reproduced with permission of Elsevier).

Table 5.2.1: Timeline of the periodic (P) and specific (S) surveys carried out during the study period.

No. Survey	1	2	3	4	5	6	7	8	9
Date	25/10	22/11	20/12	27/12	10/1	21/1	27/2	10/3	17/3
Type of Survey	P	P	P	S	S	P	P	S	S
10	11	12	13	14	15	16	17	18	19
31/3	25/4	19/5	2/6	13/6	17/6	25/6	24/7	21/8	19/9
P	P	P	S	S	S	P	P	P	P

The topography was recorded with a highly accurate DGPS (Javad Maxor) with less than 2 cm of both horizontal and vertical instrument errors. Previously, the geodesic coordinates of the vertex *105582 Punta del Santo* were moved to the positions of the GPS-base in the study areas. Ten profiles were measured at each study area to obtain an alongshore-averaged profile to reduce the uncertainty associated with measurement errors and alongshore variability (Figure 5.2.1). Sediment samples, both at the surface and at depth (0-30 cm), were taken at three points of each profile (Figure 5.2.1) to capture the spatial variability in the sediment distribution. Sieve analyses of the sampled sediments in each study area were performed following the basic methods of Folk (1980) with grain size nomenclature according to Wentworth (1922).

5.2.1.3 Bathymetry

A high-resolution multibeam bathymetric survey was carried out in October 2013 (beginning of the study period) at the study site. The data were acquired using Differential Global Positioning System navigation referring to the WGS-84 ellipsoid. Accurate navigation and real-time pitch, roll, and heave were corrected. The multibeam data were also corrected for the water column velocity. These bathymetric data were used as the bottom boundary condition for the wave propagation model (Section 5.2.2).

5.2.2 Wave propagation model

The WAVE module of the Delft3D model (Lesser et al., 2004; Lesser, 2009), which is based on the spectral wave model SWAN (Holthuijsen et al., 1993), was applied (considering the SIMAR point data) to estimate inshore wave conditions. Simulated wave heights were obtained at points with depth of 8 m ($H_{8\mathrm{m}}$) to avoid the influence of wave breaking and these inshore wave conditions were related to the beach response. The model domain consisted of two different grids, shown in Figure 4.2.1c. The first grid is a coarse curvilinear 82x82 - cell grid covering the entire Playa Granada region, with cell sizes that decrease with depth from 88x60 to 48x35 m. The second grid is a nested grid with 82 and 144 cells in the alongshore and cross-shore directions, respectively, and cell sizes of about 25x14 m. This model was calibrated and successfully validated for the study site through comparison with field data by Bergillos et al. (2016b).

5.2.3 Total run-up and sediment mobility formulations

5.2.3.1 Total run-up

The run-up measured on the beach by means of the DGPS (based on observations of run-up mark) was compared with estimates of the total run-up, obtained as the sum of astronomical tide, storm surge (wind set-up and inverse barometric effect) and wave run-up. The wind set-up was calculated as follows: $\Delta\eta_{\mathrm{wind}} = \tau_{\mathrm{wind}}/\rho g h_0 \cdot \Delta x$ (Bowden, 1983), where the depth of the wave base level is represented by $h_0 = L_0/4$, ΔX is the wave fetch from the centre of the low-pressure system to the coast (estimated through isobar maps) and the tangential wind stress is obtained from $\tau_{\mathrm{wind}} = \rho_a U_*^2$, where ρ_a is the air density and U_* is the friction velocity. The barometric set-up was obtained from $\Delta\eta_{\mathrm{bar}} = \Delta P_a/\rho g$ (Dean and Dalrymple, 2002), where ΔP_a represents the atmospheric pressure variation relative to the long-term average pressure at Motril Port.

Finally, the wave run-up was calculated through the equation $\Delta\eta_{\mathrm{wave}} = 0.36\, g^{0.5} H_{8,0}^{0.5} T_p \tan\beta$ (Nielsen and Hanslow, 1991), where $\tan\beta$ is the intertidal slope and $H_{8,0}$ is the modelled wave height at 8 m water depth ($H_{8\mathrm{m}}$) de-shoaled to deep water using linear theory and assuming parallel bottom contours. This parameter allows accounting for the alongshore variability of the inshore wave height and is consistent with the run-up expression which requires deep-water wave height. This formulation for total run-up was successfully used and compared with high resolution images from a video camera by Bramato et al. (2012) deployed on another nearby mixed sand and gravel beach along the Mediterranean Spanish coast.

5.2.3.2 Sediment mobility

Sunamura and Takeda (1984) derived the following relationship to determine the accretion/erosion states of a beach:

$$\frac{H_{8,0}}{L_0} = C\left(\tan\bar{\beta}\right)^{-0.27}\left(\frac{D}{L_0}\right)^{0.67} \tag{5.1}$$

where $H_{8,0}/L_0$ is the deep-water wave steepness, L_0 is the deep-water wave length, $C = 18$ is an empirical constant, D is the grain size and $\tan\bar{\beta}$ is the average nearshore bottom slope to a water depth of 20 m. According to Sunamura and Takeda (1984), the beach erodes (accretes) when the left-hand side of the equation is greater (smaller) than the right-hand side. The difference (S_r) between both sides of the equation was calculated considering the prevailing sediment sizes measured in Playa Granada for each sea state and the results were related with the beach evolution. This equation, deduced for sandy beaches, was tested in the study site to analyse the role of the different fractions and to discuss its applicability to MSG beaches.

5.3 Results

5.3.1 Wave and wind conditions

Figure 5.3.1 depicts the evolution of the wave and wind conditions during the study period. The deep-water significant wave height and spectral peak period were generally $H_0 < 1$ m (73% of the time) and $T_p < 6$ s (76% of the time), indicating that the beach predominantly experienced low energy waves. This agrees with the generally calm wave climate of this part of the Mediterranean Spanish coast (Ortega-Sánchez et al., 2014). The predominant deep-water wave directions were west-southwest and east-southeast, and the maximum T_p was 12 s and associated with easterly waves (Figure 5.3.1). This relatively high value for T_p (for the Mediterranean) has been exceeded 0.24% of the time since 1958. The prevailing wind velocity was less than 10 m/s with incoming directions from the east-southeast and west-southwest. The latter was more frequent and was generally associated with higher velocities. The wind direction was closely related to the wave direction.

Applying the POT method, two storms occurred that had maximum H_0 of 4.6 m and 4 m, and maximum $H_{8\mathrm{m}}$ of 3.6 m and 3.2 m in study area 1 and $H_{8\mathrm{m}}$ of 3.8 m and 3.3 m in study area 2. Both storms were associated with westerly waves ($\theta_0 \sim 240\,^\circ$), with maximum T_p of 9.6 s and 8.8 s (Figure 5.3.1). The maximum V_w during storms 1 and 2 was 19.4 m/s and the θ_w was $\sim 260\,^\circ$. Both two storm events had a very high energy content compared to other storms that occurred in the Alborán Sea. Specifically, storm 1 was the third most severe since 1958 to the end of the study period, based on the SIMAR 2041080 data.

5.3.2 Water-level conditions: contributions to the total run-up

Figure 5.3.2a shows the time series of the maximum daily total run-up (referenced to the MLWS) in study area 1 estimated using the formulations described in Section 5.2.3.1; the relative contributions of the different contributors (astronomical tide, storm surge and wave run-up) to the total run-up are depicted in Figure 5.3.2b. The results for study area 2 were very similar (differences less than 5%), and are not shown. Comparison of the estimated maximum run-up values with those observed during 21 field measurements (19 during field surveys and 2 during storms) yielded high correlation (differences less than 9%), inspiring confidence in the estimated total run-up time series.

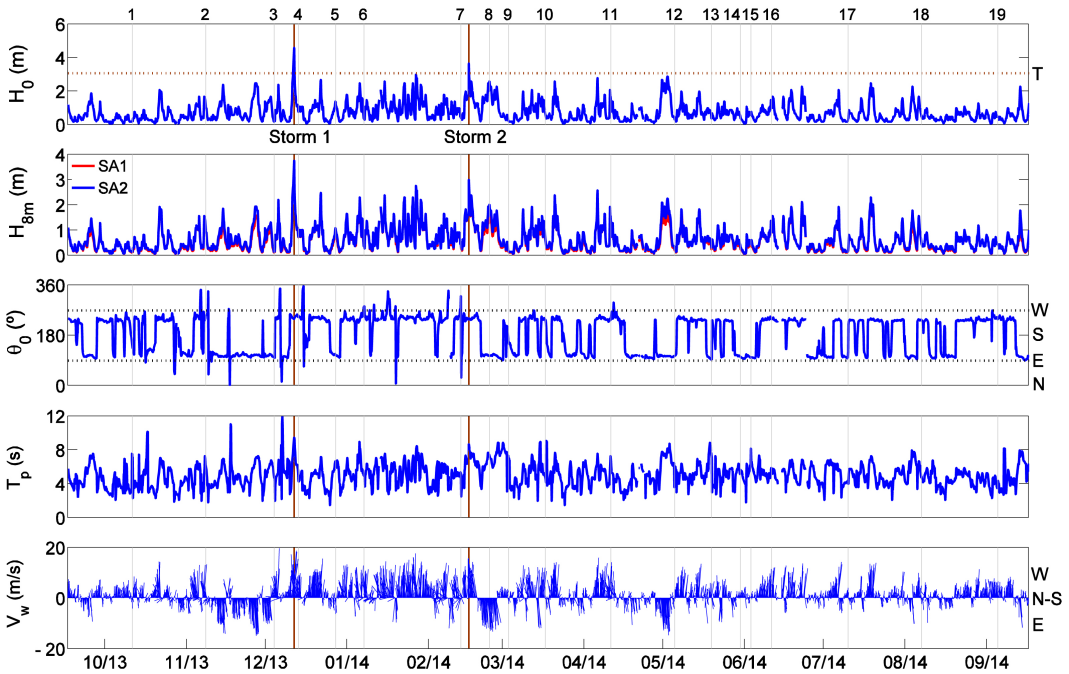

Figure 5.3.1: From top to bottom: evolution of the deep-water wave height, wave height at depths of 8 m (red: study area 1, blue: study area 2), deep-water wave direction, spectral peak period, and wind velocity and direction. The vertical lines (grey) indicate the date of the field surveys and storms are marked in brown. (Source: Bergillos et al. (2016d). Reproduced with permission of Elsevier).

The measured tidal ranges during storms 1 and 2 were 0.2 m and 0.44 m, respectively, and were considerably less than the maximum tide range of 0.6 m (Figure 5.3.2a). This reinforces that the contribution of the astronomical tide to the total run-up under high-energy conditions is relatively minor, representing less than 21% for both storms (Figure 5.3.2b). In addition to wave run-up, storm surge is also a significant contributor to the total run-up, contributing more than 30% during both storms (Figure 5.3.2b). The contribution of wave run-up reached values of almost 55% and 70% after storms 1 and 2 (recovery phases), i.e., between surveys 4-5 and 8-9, respectively (Figure 5.3.2b).

Waves are frequently considered as the main driver of changes in the profile of micro-tidal beaches. However, Figure 5.3.2b indicates that storm surge resulting from low atmospheric pressure and wind stress can also be important contributors to the total elevation under storm conditions and, consequently, to the erosion of the beach. If wind velocities are high enough ($V_w \sim 15$ m/s) and pressure gradients are negative, the resulting large storm surge enables waves to reach the upper parts of the beach profile (backshore), as shown in Figure 5.3.2a.

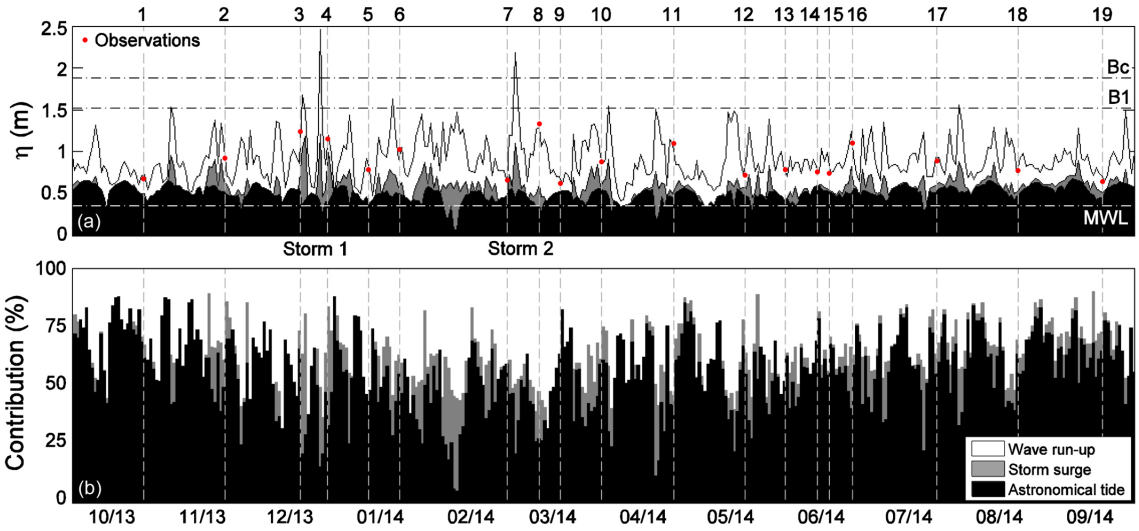

Figure 5.3.2: (a) Evolution of the astronomical tide, storm surge and wave run-up and (b) contribution of each in the study area 1 during the study period. $\eta = 0$ indicates the MLWS level and the vertical lines (grey) indicate the date of the field surveys. The observations of total run-up (red circles), height of the mean water-level (MWL), the beach crest (Bc) and the upper berm (B1) are indicated. (Source: Bergillos et al. (2016d). Reproduced with permission of Elsevier).

5.3.3 Morphological response of the upper profile

A total of 190 upper profiles (beach profile above the MLWS level) were measured during the study period in each study area: 130 before the artificial replenishment (natural profile) and 60 both during the nourishment and afterwards (replenished). Table 5.3.1 shows that the beach width (cross-shore distance between the MLWS level and the nearest building) and unit volume (calculated by the trapezoidal rule) of the beach typically increases under low energy conditions (LE) and decreases after storms (S). The slope of the natural profile, defined by the ratio between the height of beach crest and the beach width, was 0.05 – 0.069 and 0.056 – 0.073 in study areas 1 and 2, respectively.

Table 5.3.1: Morphological characteristics of the natural and replenished profiles in the study areas. LE: low energy conditions, S: storms.

		Study area 1	Study area 2
Natural profiles	Slope	0.05 (LE) – 0.069 (S)	0.056 (LE) – 0.073 (S)
	Beach width (m)	24.74 (S) – 35 (LE)	39.5 (S) – 50 (LE)
	Unit volume (m^2)	27 (S) – 41.40 (LE)	51.19 (S) – 73.56 (LE)
Replenished profiles	Slope	0.057 – 0.059	0.05 – 0.053
	Beach width (m)	33.22 – 34.72	47 – 50
	Unit volume (m^2)	39.17 – 45.38	77.88 – 87.69

Comparing the measured slopes of the natural profiles (Table 5.3.1) with other published data, these slopes are generally steeper than on micro-tidal sandy beaches (Jackson et al., 2005), but gentler than the slope on macro-tidal gravel beaches analysed by Austin and Masselink (2006) and Poate et al. (2013), and the slope on the MSG beach described in Horn and Walton (2007). The observed slope is slightly steeper than that measured on another micro-tidal MSG beach along the southern Spanish coast (Bramato et al., 2012).

Figure 5.3.3 depicts both the maximum wave height and total run-up (including astronomical tide, storm surge and wave run-up) before each survey along with the sediment volume of the upper profile in both study areas (in m^3 per unit m beach length per day, or m^2/day). It is observed that beach erosion/accretion not only depends on wave height, but on the sum of the three components that contribute to the total run-up. Actually, a relationship between the maximum total run-up between surveys and the beach response is clearly observed, specially after the two storms (surveys 4 and 8).

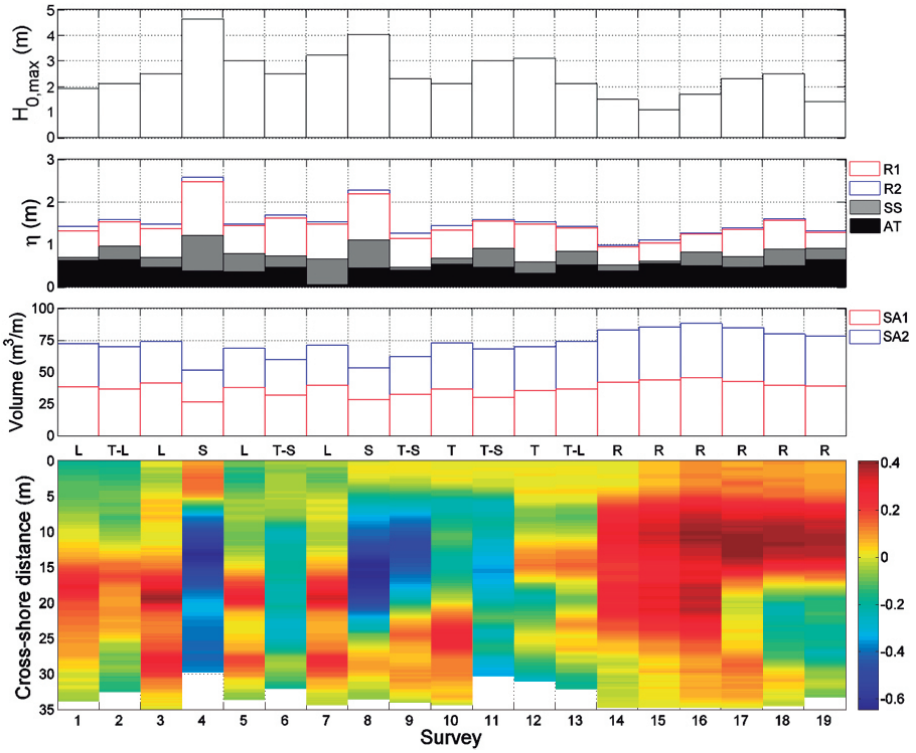

Figure 5.3.3: From top to bottom: maximum deep-water wave height before each survey; astronomical tide (black), storm surge (gray) and wave run-up (red: study area 1, blue: study area 2) contributions to the maximum total run-up before each survey; unit volume of the upper profile (red: study area 1, blue: study area 2); and differences between the profile in each survey and the average profile in study area 1. States of the profile, according to Figure 5.3.9, are shown. (Source: Bergillos et al. (2016d). Reproduced with permission of Elsevier).

The differences between the bed elevation in each survey and the average profile in study area 1 are also shown in Figure 5.3.3 (lower panel). During storms 1 and 2, the erosion rates in study area 1 were 2.06 and 1.09 m^2/day, respectively; whereas they were 3.2 and 1.76 m^2/day in study area 2. If a beach overwashes, erosion tends to be less, because the wave energy is dissipated across the backshore and sediment is retained within the beach in the form of overwash deposit (Matias et al., 2013; Matias et al., 2016). This occurred in both study areas during storms, as the entire beach was overwashed. On the other hand, the recovery rates after the storm 1 and 2 were at least 0.79 and 0.51 m^2/day in study area 1, and 1.76 and 0.94 in study area 2, respectively. It is important to highlight that these values are average rates between surveys, so the maximum erosion/accretion rates were most likely higher.

The profiles of both study areas were flattened due to the artificial nourishment carried out in June 2014. It consisted of an input of 8.4 m^3/m and 14 m^3/m in study areas 1 and 2 over beach lengths equal to 500 and 300 m, respectively. The slope of the replenished profiles was slightly milder than those of the pre-nourished beach, but higher than the slope under low energy conditions (Table 5.3.1). The sediment volume of the replenished profiles was greater than that of most natural profiles, although the width was similar to those of the natural profiles under low energy conditions (Table 5.3.1).

Figure 5.3.4 shows the evolution of the upper profile in study area 1 since the artificial replenishment to the end of the study period. Only one month after the artificial replenishment, and under prevailing low energy conditions and total run-up lower than 1.4 m until survey 17 (Figures 5.3.1 and 5.3.2a), the unit volume loss was about 2.6 m^2 in study area 1 and 3.3 m^2 in study area 2. Berms started to appear due to the total run-up attained during this period (Figures 5.3.3 and 5.3.4).

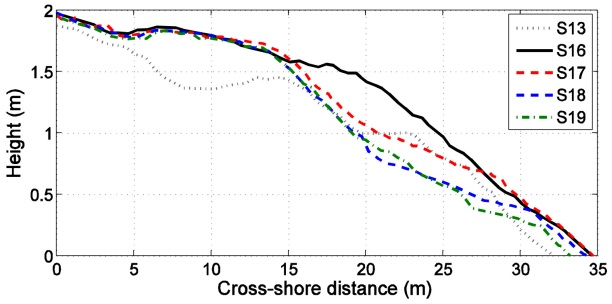

Figure 5.3.4: Pre-nourished upper profile and evolution since the artificial replenishment until the end of the study period in study area 1. Height = 0 indicates the MLWS level. (Source: Bergillos et al. (2016d). Reproduced with permission of Elsevier).

Between surveys 17 and 18, the profile shape also changed significantly in both study areas, but the variation was less between surveys 18 and 19 (Figures 5.3.3 and 5.3.4), most likely due to the smaller magnitude of the forcing agents and the total run-up (Figures 5.3.1 and 5.3.2a). The attenuation of the system response after the discharge of sediments could be another cause of this lower variation. However, not only wave processes, but also the gusts of wind after the nourishment project could contribute to the rapid loss of fine sediments, considering that wind velocities reached maximum values of 14.5 m/s and 13.5 m/s before surveys 17 and 18, respectively (Figure 5.3.1).

Altogether, the beach width in study areas 1 and 2 decreased by approximately 4% and 6% in the months after the nourishment, respectively, whereas the unit volume loss was 6.2 m^3/m in study area 1 and 9.8 m^3/m in study area 2. Furthermore, despite the artificial replenishment, the unit volumes measured in study areas 1 and 2 in September 2014 (39.16 m^2 and 77.8 m^2) were similar to those measured in October 2013 (38.74 m^2 and 73.03 m^2), as shown in Figure 5.3.3. Thus, the long-term benefit of the nourishment was very limited.

5.3.4 Beach sediments

The average grain size distribution (based on all sediment samples) before the artificial replenishment (Figure 5.3.5a) shows that three sediment fractions are predominant in Playa Granada: sand ($D_1 = 0.25 - 0.5$ mm, Figure 5.3.5c), fine gravel ($D_2 = 2 - 8$ mm, Figure 5.3.5d) and coarse gravel ($D_3 = 8 - 32$ mm, Figure 5.3.5e). The foreshore (from the MLWS to the maximum total run-up reached under low energy conditions) showed greater sediment size variability than the backshore in both study areas, as shown in Section 5.3.5. In addition to this cross-shore variability, different levels of gradation at depth were also found. The sand-gravel ratio limits were $30 - 70\%$ and $36 - 64\%$ in study area 1, and $33 - 67\%$ and $23 - 77\%$ in study area 2.

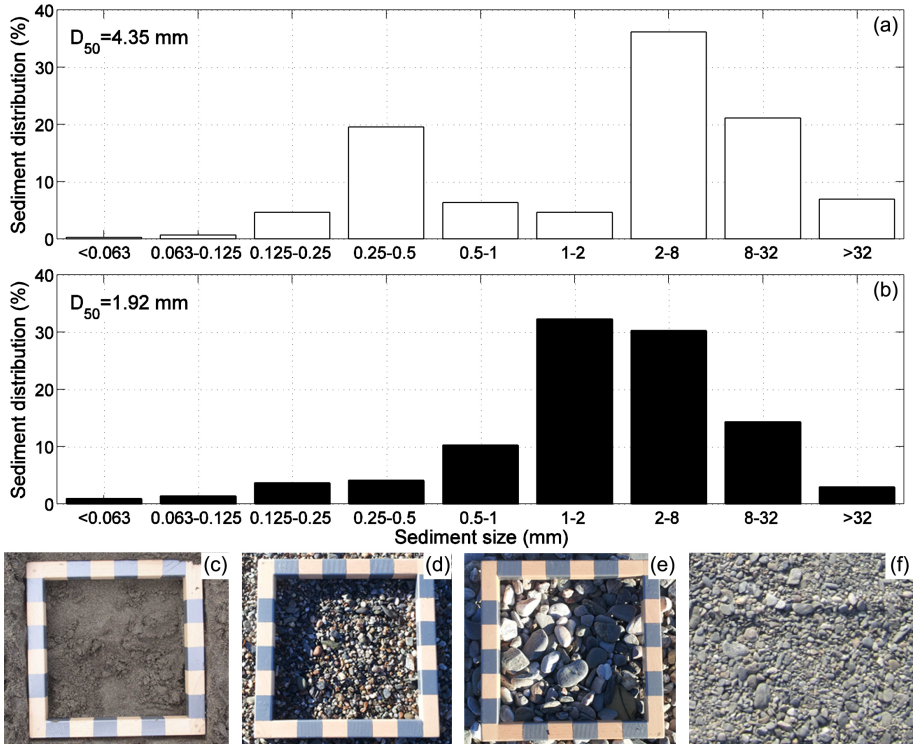

Figure 5.3.5: Grain size histograms of the set of samples in both study areas before the artificial replenishment (a) and of the sediments used for the artificial replenishment (b); sand (c), fine gravel (d) and coarse gravel (e) natural fractions; and sediments supplied in June 2014 (f). The D_{50} of the nourishment was lower than that of the natural sediment. (Source: Bergillos et al. (2016d). Reproduced with permission of Elsevier).

The nourished material (Figure 5.3.6a), shown in Figure 5.3.5b, was significantly finer than the natural sediment ($D_{50} = 1.92$ mm *vs* $D_{50} = 4.35$ mm). Coarse sand ($1 - 2$ mm) and fine gravel ($2 - 8$ mm) dominated (Figure 5.3.5f), with a sand-gravel ratio of about $52.5\% - 47.5\%$. Thus, the sand fraction of the nourished sediment was higher than that of the native sediment. After the nourishment, the sand-gravel ratio progressively reduced from its initial value ($52.5\% - 47.5\%$) to about $46.15\% - 53.35\%$ and $41.65\% - 58.35\%$ in study areas 1 and 2, respectively. Therefore, the reduction in the percentage of sand was higher in study area 2, where the unit volume loss was also higher (Table 5.3.1).

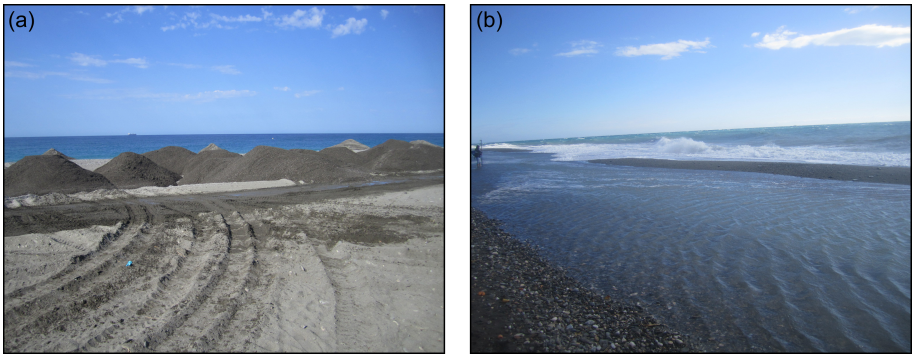

Figure 5.3.6: (a) Artificial replenishment done in June 2014, consisting of an input of sediment with uniform distribution. (b) Upper profile after the storm 1: Gravels on the storm berm and the surface layer of sand on the bar feature are observed. (Source: Bergillos et al. (2016d). Reproduced with permission of Elsevier).

Figure 5.3.7 shows the results of applying the formulation of Sunamura and Takeda (1984) during the study period. Considering the three prevailing sediment fractions in the study site (D_1, D_2 and D_3), the erosion ($S_r > 0$) and accretion ($S_r < 0$) states alternated for the sand fraction (Figure 5.3.7a, upper panel), while for the two gravel fractions only deposition states occurred (Figure 5.3.7a, middle and lower panels). These results are similar to those obtained by Bramato et al. (2012) through application of this formulation and observations based on high-resolution images for an MSG beach near the study site: sand was transported offshore during storms and beach recovery was limited to low-energy sea states, whereas only onshore migration took place for the gravels.

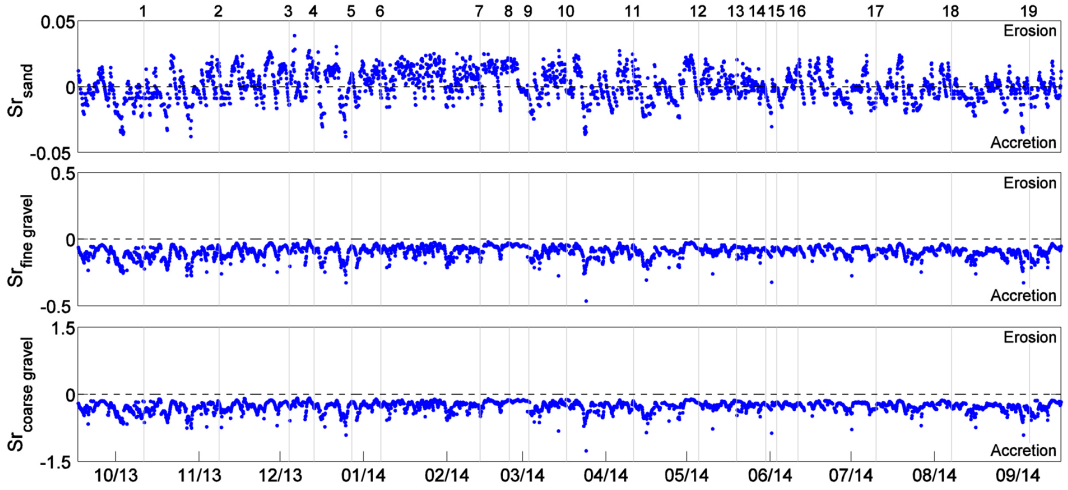

Figure 5.3.7: Difference between the terms of erosion and accretion in the Equation 5.1 (Sunamura and Takeda, 1984) in study area 1. The three prevailing sediment sizes were considered: sand (upper panel), fine gravel (middle panel) and coarse gravel (lower panel). The vertical lines (grey) indicate the date of the field surveys. (Source: Bergillos et al. (2016d). Reproduced with permission of Elsevier).

5.3.5 Morpho-sedimentary beach states

5.3.5.1 Low energy state

Under prevailing low energy conditions, the upper profile in study area 1 has two berms (B1 and B2, Figure 5.3.8a) composed of a surface layer of coarse gravels ($D_1 = 8 - 32$ mm), a subsurface layer of fine gravels ($D_2 = 2 - 8$ mm), and a layer of sand ($D_3 = 0.25 - 0.5$ mm) at the base of the deposit (Figure 5.3.8a). This pattern is repeated at depth, probably reflecting previous berm deposits. The average percentage of sand-gravel along the sampled sediment layer is 35.8% – 64.2%. The backshore (cross-shore distance < 15 m, Figure 5.3.8a) consists mainly of sand (Table 5.3.2), whereas the composition of the sediment in the active swash zone is highly variable (sand-fine gravel) in time and space (Figure 5.3.8a), with average proportions of 31.7% sand and 68.3% gravel. The upper profile in study area 2 is similar to that of the study area 1, but the beach is wider (~ 50 m). The average sand-gravel ratio sampled across the entire upper profile for study area 1 is larger than for study area 2 (Table 5.3.2).

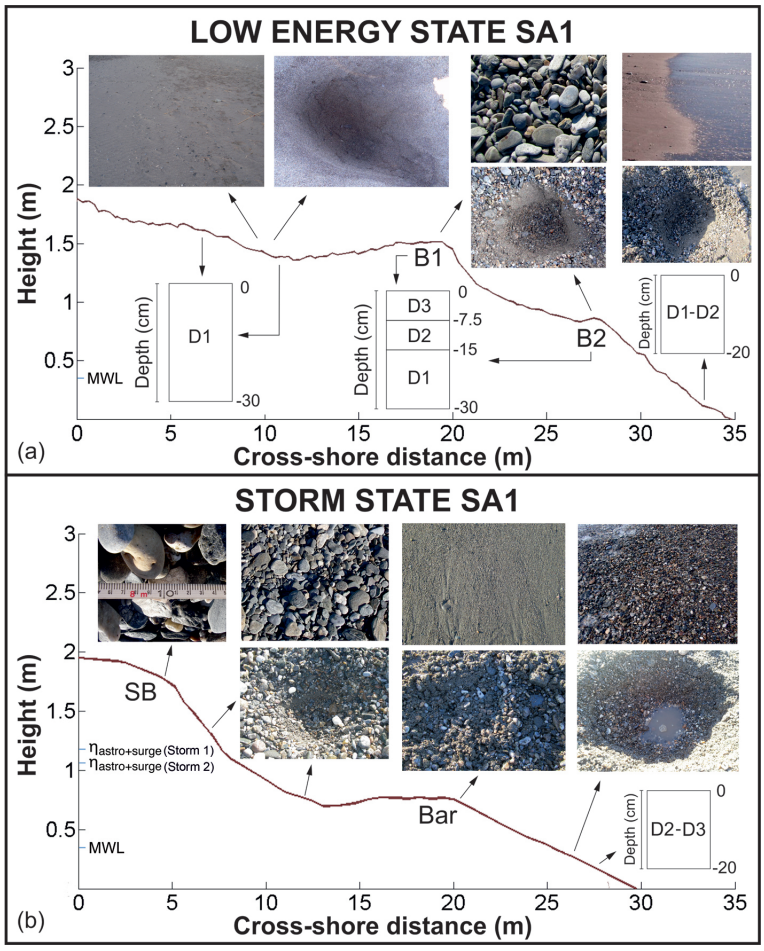

Figure 5.3.8: (a) Low energy state in study area 1: morphology (including the berms B1 and B2), sedimentology and photographs. (b) State after storms in study area 1: morphology (including the storm berm -SB- and the bar feature), sedimentology and photographs. Height = 0 indicates the MLWS level. (Source: Bergillos et al. (2016d). Reproduced with permission of Elsevier).

5.3.5.2 Storm state

The two storms that occurred over the survey period (1 and 2, Figure 5.3.1) induced marked changes to the beach profile. The low energy state berms were eroded and the upper beach profiles assumed a more concave shape (Figure 5.3.8b). The storms also caused a decrease in the beach width of about 5 m and 10 m in study areas 1 and 2, respectively. A storm berm developed on the upper part of the profile and a bar feature was generated in the lower part of the beach with a surface layer of sand over a gravel-dominated substrate (Figures 5.3.6b and 5.3.8b). In both study profiles, higher slopes were generally attained during storm conditions and the percentage of gravel increased by between 6 and 10 percent from the low energy state to the storm state (Table 5.3.2).

Considering the total number of samples taken after the two storms (18) and during the low energy states of the profile (27) in study area 1 and applying the *Student's t-test*, the result also confirm that the percentage of gravel is higher after storms (null hypothesis), with a significance level equal to 0.01. The same conclusion is drawn after applying the test in study area 2. These results are consistent with those obtained in Section 5.3.4: the finer material is selective transported offshore during storms, whereas under calm conditions the sand returns, covering most of the lag gravel (Figure 5.3.8). This is a mechanism that differentiate MSG beaches from sandy and pure gravel beaches (Mason and Coates, 2001; Bramato et al., 2012).

Table 5.3.2: Sand-gravel percentages for the low energy and storm states on the backshore, foreshore and entire beach.

		Low energy state	Storm state
Study area 1	Backshore	81.8% – 18.2%	34.8% – 65.2%
	Foreshore	31.7% – 68.3%	24.8% – 75.2%
	Entire beach	35.8% – 64.2%	29.2% – 70.8%
Study area 2	Backshore	80.8% – 19.2%	31.1% – 68.9%
	Foreshore	30% – 70%	19.7% – 80.3%
	Entire beach	33.1% – 66.9%	23.7% – 76.3%

5.3.5.3 Transitional states

After the passing of storms, berms developed and progressively overlapped under the influence of low energy waves, contributing to the sediment variability both cross-shore and at depth (Figure 5.3.9). The generation of berms represents a recovery trajectory, which is closely related to the total run-up (Figures 5.3.2, 5.3.3 and 5.3.9), but this development of the berms can be interrupted at any one time by another storm. Figure 5.3.3 shows that the erosion/deposition rates were higher in the foreshore, where the measured sediment variability was also higher (Table 5.3.2). This is consistent with the conceptual model presented in Figure 5.3.9, which suggests that the number of berms depends on the state of the profile and varies during the recovery process.

Figure 5.3.10a depicts the contribution of the wave run-up (vertical axis) and the sum of astronomical tide and storm surge (horizontal axis) to the unit volume variation (circles). Before the replenishment, it is observed that when the total run-up elevation was higher than the height of the upper berm ($\sim$ 1.52 m, Figure 5.3.8a), the upper profile lost volume, whereas lower elevations increased the volume of the beach (Figure 5.3.10a). Hence, beach erosion took place not only during both storms, when overwashing of the entire beach occurred; but also before surveys 2, 6 and 11, when the upper berm was overwashed.

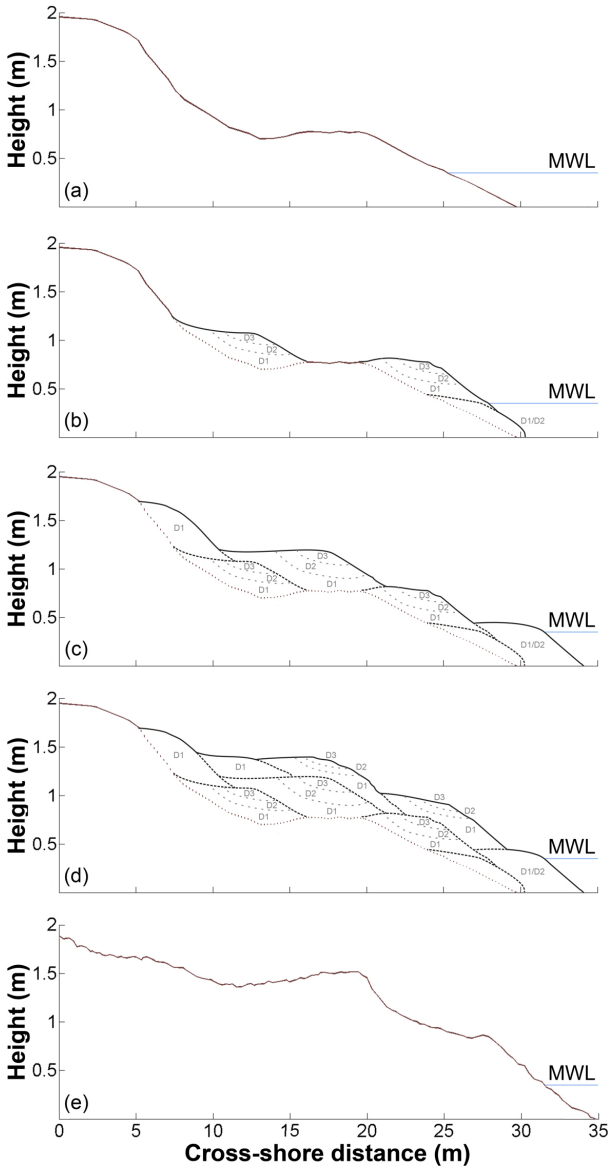

Figure 5.3.9: Conceptual model describing the beach's accretionary response in study area 1. From top to bottom: storm (S), transitional-storm (T-S), transitional (T), transitional-low energy (T-L) and low energy (L) states. The number of berms depends on the state of the beach profile. (Source: Bergillos et al. (2016d). Reproduced with permission of Elsevier).

Although the total run-up was similar in both study areas and the erosion/accretion behaviour of the upper profile was equal (Figure 5.3.3, middle panel), the threshold elevation in study area 2 was ~ 1.58 m (Figure 5.3.10b), coinciding with the height of the upper berm at this profile. These results indicate that the overwash process plays a key role in the beach dynamics, which is in agreement with previous works, such as Matias et al. (2014). Hence, other variables apart from wave height, such as pressure gradient and wind velocity, are essential in the evolution of the profile on micro-tidal beaches and the total run-up is demonstrated to be a more accurate threshold than wave height to differentiate between erosional and depositional conditions.

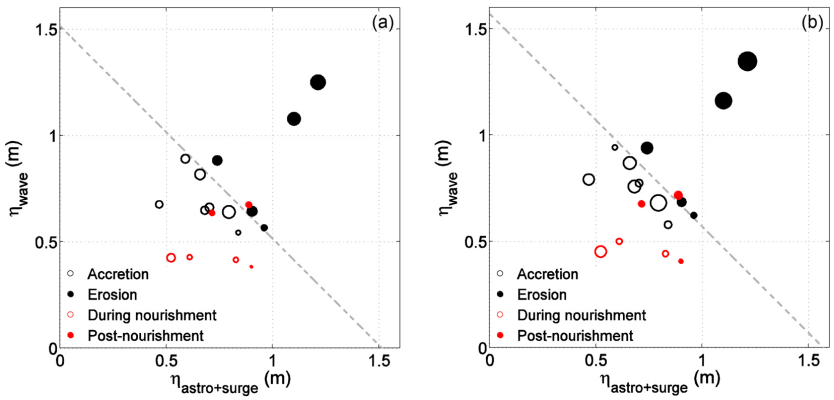

Figure 5.3.10: Relationship between the wave run-up and the water-level elevation in study areas 1 (a) and 2 (b). Black circles indicate accretion (unfilled) and erosion (filled) before the replenishment, whereas red circles indicate the artificial accretion (unfilled) and erosion (filled) afterwards. The size of the circles is proportional to the sediment volume change and the dashed grey line represents a total run-up of 1.52 m (a) and 1.58 (b). (Source: Bergillos et al. (2016d). Reproduced with permission of Elsevier).

5.4 Discussion

Although MSG beaches have received increasing attention in recent years, the number of field observations on these coasts is still limited. This chapter presents a field investigation of the morpho-sedimentary dynamics of a MSG beach under varying wave and water-level conditions.

The observed low energy states are similar to those observed on a sandy beach (Avoca, Australia) and a pure gravel beach (Slapton Sands, UK) by Weir et al. (2006) and Austin and Masselink (2006), respectively. They proposed that berm location(s) is (are) linked to both tide level and wave run-up, and their destruction and construction depends on wave height. The location of the upper berm and the process of berm formation in Playa Granada are also related to the maximum water-level elevation on the beach under low energy conditions and the wave action (Figures 5.3.2a, 5.3.3 and 5.3.8a). The generation and subsequent overlapping of berms is responsible for the different levels of grain size gradation at depth and cross-shore (Figure 5.3.9), i.e., the evolutionary pathway is responsible for the beach stratification, being the morphological evolution partly stored in the stratigraphy. However, the results indicate that not only wave height, but also storm surge is important for the destruction of berms on micro-tidal beaches.

The storm berm and the bar feature observed following the storms resemble the eroded state on other MSG beach of the Mediterranean Spanish coast (Carchuna) described by Bramato et al. (2012). They found that the profile after high energetic events promotes wave breaking over a newly formed storm bar, resulting in less capacity to transport sediments and protecting the beach from further erosion. The steeper shape of the upper profile after storms is also similar to the reflective morphodynamic state detailed by Poate et al. (2013) on the gravel beach of Loe Bar (UK), who measured a depositional feature in the foreshore similar to that of Playa Granada (Figures 5.3.6 and 5.3.8b). This bar feature could be associated with the landward migration and growth of the beach step during storms coincident with the removal and offshore transport of the sand fractions from the swash zone, as observed on Slapton Sands (Masselink et al., 2010).

The evolution of both study areas was similar during the study period (Figures 5.3.3 and 5.3.10), indicating that they are representative of the beach behaviour of that section of the coastline. Differences between erosion/deposition rates and changes between low energy and storm states were higher in study area 2, probably because it experiences more energetic wave conditions (Figure 5.3.1, second panel). The recovery rates at the two study areas seem to be related to the incoming wave directions: when the beach was subjected to westerly waves (surveys 2-3 and 11-12, Figure 5.3.1), the accretion rates of study area 2 were higher than those of study area 1, whereas under prevailing easterly ones (surveys 9-10 and 12-13) the latter recovered faster. This could be due to the different longshore sediment transport gradients depending on the incoming wave direction, detailed by Bergillos et al. (2016b).

The results obtained in Section 5.3.4 for the sand (alternation of erosion and accretion states) are more related with the beach behaviour than those for gravel fractions (only accretion); however, erosion states prevail for the sand fraction (Figure 5.3.7) whereas beach accretion was more frequent before the nourishment (Figure 5.3.10). They suggest that the overall behaviour of MSG beaches cannot simply be determined by a single sediment size. Actually, the recovery periods (rates) in the study site after the third most severe storm since 1958, less than two weeks, were significant lower (higher) than those detailed by Lee et al. (1998), Thom and Hall (1991) and Scott et al. (2015), who measured average recovery rates of about 0.09 m^2/day, 0.11 m^2/day and 0.26 m^2/day on the sandy beaches of Duck (USA), Moruya (Australia) and Perranporth (UK), respectively. This supports the conclusions of Mason et al. (1997) and Ivamy and Kench (2006): MSG beaches may experience more active sediment transport than sandy beaches.

Replenished profiles were eroded even under no storm conditions (Figures 5.3.1, 5.3.3 and 5.3.4) and the unit volumes of the upper profiles 3 months after the nourishment (September 2014) were similar to those measured at the beginning of the study period (October 2013), when no artificial replenishment took place. This may be partly due to the lack of response from the nourished material to waves in the same manner as natural beaches (Horn and Walton, 2007). Dean and Dalrymple (2002) suggested that the fill material should match the native sediment to minimize changes in the beach response. This did not happen in Playa Granada, where neither the sediment sizes nor the morphology of the natural and replenishment profiles were similar (Figures 5.3.4 and 5.3.5). The variations in the sand-gravel ratio after the artificial nourishment agree with the formulation of Sunamura and Takeda (1984), which establishes that the eroded sediment appeared to be selectively transported offshore from the upper profile. However, wind action could also have contributed to the removal of the finer nourished sediment, as has been widely demonstrated in previous works (e.g, Van der Wal (1998), Van der Wal (2000b), Van der Wal (2000a), and Jackson and Nordstrom (2011)).

5.5 Conclusions

This chapter presents a study of the evolution of Playa Granada based on field measurements over a one-year period and its correlation with wave and water-level variations. A total of 20 profiles were periodically surveyed and sediment samples from each profile were sieved. Estimations of the total run-up and sediment mobility were also performed. After the analysis, the following conclusions were drawn:

1. The generation and subsequent overlapping of berms is responsible for the sediment variability cross-shore and at depth on MSG beaches. The cross-shore locations of these berms are related to the total run-up, as berms are modified by swash action. Thus, waves play a main role in the beach recovery.

2. The recovery of MSG beaches has been shown to occur at a faster rate than on sandy beaches. This quicker recovery on MSG coasts acquires importance for the design of strategies to help mitigate or adapt to global coastal erosion problems and the action of sea-level rise.

3. The formation of a storm berm, the more concave shape of the upper profile and the increase in the percentage of gravels after storms all indicate reflective behaviour of MSG beaches during high-energy conditions, and is dominated by the gravel fractions due to the selective removal of the finer material.

4. Total run-up elevations that exceed the height of the upper berm generate erosion, whereas lower elevations increase the unit volume of the upper profile representative of beach accretion. Hence, the total run-up represents a more accurate threshold dictating beach response than wave height.

5. The upper profile was flattened following an artificial input of sediment over June 2014 with different grain size distribution and lower D_{50} than the natural sediment. Three months after the nourishment, and in the absence of significant storms, the upper profile lost between 6 and 10 m^2, probably induced by both wave processes and wind action. The beach volumes in September 2014 were similar to those measured in October 2013, showing the intervention was not effective.

CHAPTER 6

COASTAL RESPONSE FORCED BY ARTIFICIAL NOURISHMENT

This chapter addresses the evolution of Playa Granada forced by an artificial nourishment project through the analysis of field observations and the modelling of hydro- and morphodynamics. The beach profile and coastline were periodically surveyed over a six-month period; a wave propagation model was calibrated by means of hydrodynamic measurements; four longshore sediment transport (LST) equations were tested through comparisons with bathymetric data; and the one-line model was applied between topographic surveys. The results indicate that severe coastline retreat (dry beach area loss > 208 m^2/day) occurred during the 45 days following the intervention. This is mainly attributable to the morphology of the nourished coastline, the different characteristics of the sediment used for replenishment compared to natural sizes, and the occurrence of an intense westerly storm. The dry beach extension increased afterwards influenced by the westward LST due to the dominance of easterly waves. The Van Rijn formulation was found to provide the best fits to the observed volumetric changes, obtaining modelled/measured ratios of 93.1% and 77.4% for the two study beach profiles. The outputs of the one-line model based on the Van Rijn approach were also the best, with root-mean-square errors decreasing during the study period and lower than 4.6 m over the last 3 months. These results show that the joint application of a calibrated wave propagation model, the LST equation proposed by Van Rijn and the one-line model constitutes a management tool for predicting the evolution of these complex coastal settings.

6.1 Objectives

The main objectives of this chapter are to characterize and to model the morphodynamic response of a mixed sand and gravel (MSG) deltaic coast (Playa Granada) forced by an artificial nourishment project. To meet these goals, the evolution of wave, wind and water level conditions is analysed; a wave propagation model is calibrated and applied to address nearshore wave patterns; and morphological changes of the beach profile and the coastline are quantified and related to forcing agents. The propagation model is also used to apply different longshore sediment transport (LST) equations and the one-line model, selecting the formulation that best reproduces coastal evolution patterns through comparison with field observations to develop an integrated tool for the design of nourishments projects.

6.2 Methodology

This chapter mainly discusses (1) bathymetric and topographic measurements of the beach profile and coastline, respectively, following the execution of an artificial replenishment project, (2) their relation to maritime forcing agents and to wave propagation patterns through the application of a calibrated numerical model, and (3) the validity of different LST formulations by means of comparisons with field observations (Figure 6.2.1). Artificial nourishment consisted of the sediment input of 106,676 m^3 with uniform distribution (D_{50} = 2 mm) in the southeast of the river mouth over a beach area equal to 18,108 m^2 (Figure 6.2.2). The project budget was 544,000 euros and it ended on December 22nd, 2014. Field surveys were performed between December 23rd, 2014 and June 21st, 2015 (hereinafter referred to as the study period).

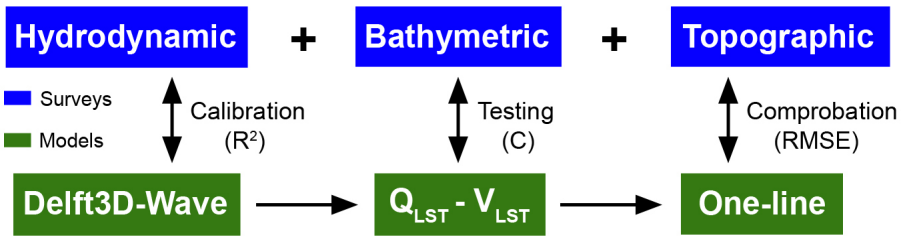

Figure 6.2.1: Diagram of the methodological framework followed in this chapter. (Source: Bergillos et al. (2017a). Reproduced with permission of Elsevier).

6.2.1 Maritime data and total run-up

A series of 4,320 sea states (hourly hindcasted data for the study period), corresponding to SIMAR point number 2041080 (Figure 6.2.3) and provided by *Puertos del Estado*, was used to study the evolution of the following deep-water wave and wind variables: significant wave height (H_0), spectral peak period (T_p), wave direction (θ_0), wind velocity (V_w) and wind direction (θ_w). The quality of the SIMAR network data for the Mediterranean region has been widely assessed in previous works (e.g. Tomas et al. (2008) or Mínguez et al. (2011)). Storms were identified by means of the peaks over threshold method considering H_0 higher than 3.1 m ($H_{99.9\%}$) and storm durations lasting longer than 6 hours according to recommendations presented by Bergillos et al. (2016d) for this site.

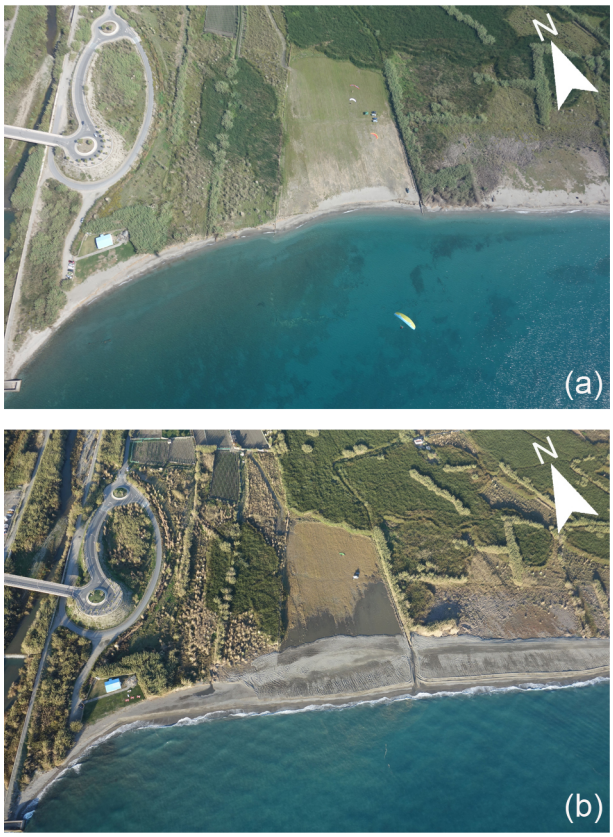

Figure 6.2.2: Aerial images of the nourished section of beach before (a) and after (b) the artificial nourishment project. (Source: Bergillos et al. (2017a). Reproduced with permission of Elsevier).

In addition, the total run-up (η) was obtained as the sum of astronomical tide (measured by a gage located in the Motril Port), storm surge ($\Delta\eta_{\text{wind}} + \Delta\eta_{\text{bar}}$) and wave run-up ($\Delta\eta_{\text{wave}}$). The wind set-up was calculated as $\Delta\eta_{\text{wind}} = \tau_{\text{wind}}/(\rho g h_0)\Delta x$ (Bowden, 1983), where g is the acceleration of gravity, $\rho = 1{,}025$ kg/m^3 is the density of salt water, the depth of the wave base level is calculated as $h_0 = L_0/4$, where L_0 is the wavelength in deep water, Δx is the wave fetch from the centre of the low-pressure system to the coast (estimated through isobar maps) and the tangential wind stress is obtained from $\tau_{\text{wind}} = \rho_a U_*^2$, where ρ_a is the air density and U_* is the friction velocity, estimated by means of the logarithmic wind profile (Stull, 2000). The barometric set-up was obtained from $\Delta\eta_{\text{bar}} = \Delta P_a/\rho g$ (Dean and Dalrymple, 2002), where ΔP_a represents the atmospheric pressure variation relative to the long-term average pressure at Motril Port. Finally, the wave run-up was calculated through the equation $\Delta\eta_{\text{wave}} = 0.36\, g^{0.5} H_{8,0}^{0.5} T_p \tan\beta$ (Nielsen and Hanslow, 1991), where $\tan\beta$ is the beach slope and $H_{8,0}$ is the modelled wave height at 8 m water depth ($H_{8\text{m}}$) de-shoaled to deep water using linear theory and assuming parallel bottom contours. Bergillos et al. (2016d) obtained high correlation (differences less than 9%) between measured and estimated total run-up values (sum of astronomical tide, storm surge and wave run-up) with these formulations, and found that total run-up higher than 1.52 m generates beach erosion due to the overwash process (Matias et al., 2012).

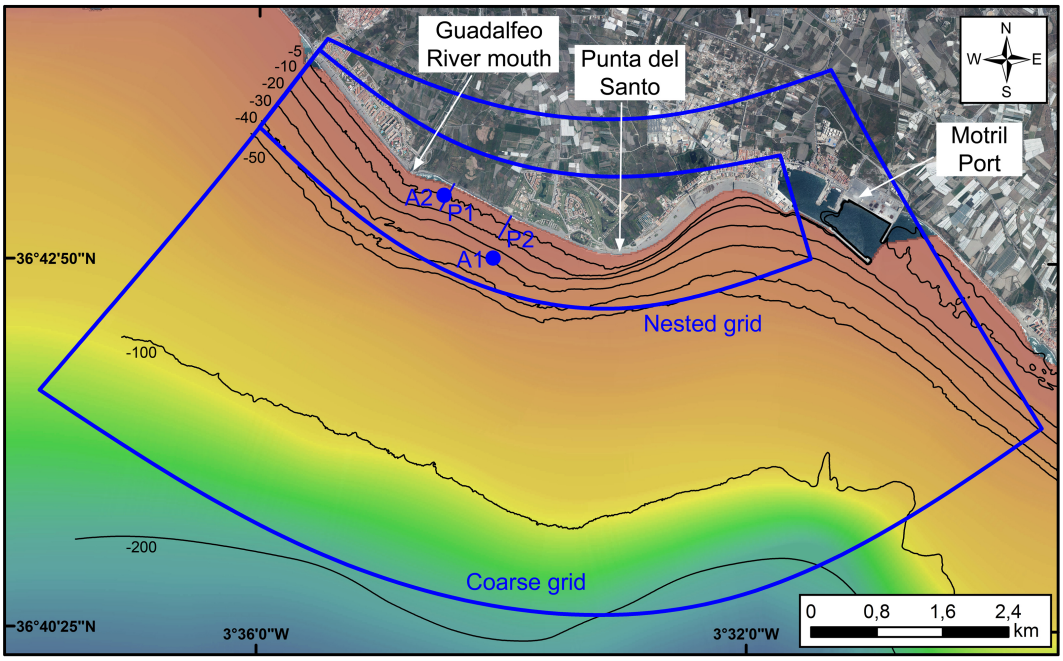

Figure 6.2.3: Bathymetric contours (in meters), positions of the ADCPs (blue circles A1 and A2), location of the surveyed profiles (blue lines P1 and P2) and grids used in the numerical model. (Source: Adapted from Bergillos et al. (2017a). Reproduced with permission of Elsevier).

6.2.2 Field measurements

6.2.2.1 Multibeam bathymetries

A high-resolution multibeam bathymetric survey was performed at the beginning of the study period covering the entire deltaic region. Data were acquired using Differential Global Positioning System (DGPS) navigation in reference to the WGS-84 ellipsoid. Accurate navigation and real-time pitch, roll and heave were corrected. These bathymetric data were used as the bottom boundary conditions for the wave propagation model (Section 6.2.3).

In addition, two specific surveys were carried out in the middle and at the end of the study period in two selected study profiles (Figure 6.2.3): in front of the nourished section (P1) and in the central area of the section river mouth - *Punta del Santo* (P2), which has been proven to be representative of the beach behavior of the studied coastline alignment (Bergillos et al., 2016d). Five shore-normal profiles were measured in each study area (1 every 5 m) through both specific surveys to obtain an alongshore-averaged profile representative of this cell for the proper comparison with the modelled LST results. Thus, the uncertainties associated with measurement errors and alongshore variability were reduced. These specific surveys were used to analyse the evolution of beach profiles after nourishment and to test the LST formulations (Section 6.2.4) through the comparison between modelled and measured volumetric changes at the profile locations.

6.2.2.2 Coastline topographies

Five periodic topographic surveys were carried out during the study period (Table 6.2.1) to measure the positions of the coastline along the nourished stretch of beach (Figure 6.2.2). Each survey was performed under low tide conditions. Topographic measurements were recorded using a highly accurate DGPS (Javad Maxor) with less than 2 cm of horizontal and vertical instrument errors. These measurements were used to address the coastline evolution after the artificial replenishment and to test the LST formulations by means of the one-line model (Section 6.2.4).

Table 6.2.1: Timeline of the bathymetric (B) and topographic (T) surveys performed during the study period.

No. Survey	1	2	3	4	5
Date	23/12	06/02	23/03	07/05	21/06
Type of Survey	B+T	T	B+T	T	B+T

6.2.3 Wave propagation: model description and calibration

SIMAR point sea states for the entire study period were propagated from deep-water areas to the nearshore using the WAVE module of the Delft3D model (Lesser et al., 2004; Lesser, 2009), which is based on the SWAN model (Holthuijsen et al., 1993). These results were used to address inshore wave conditions and to apply the LST formulations.

The model domain consisted of two different grids as shown in Figure 6.2.3. The first is a coarse curvilinear 82x82-cell grid covering the entire deltaic region, with cell sizes that decrease with depth from 170x65 to 80x80 m. The second is a nested grid covering the beach area with 244 and 82 cells in the alongshore and cross-shore directions, respectively, and with cell sizes of approximately 25x15 m. For the spectral resolution of the frequency space, 37 logarithmically distributed frequencies ranging from 0.03 to 1 Hz were used, whereas for the directional space, 72 directions covering 360° in increments of 5° were defined.

The model was calibrated for these particular grids through the comparison with field data collected from December 23rd, 2014 (beginning of the study period) to January 30th, 2015 by means of two ADCPs (Figure 6.2.3). The wave model was forced with SIMAR point data, using the initial bathymetric measurements and considering the following physical processes: wind effects, refraction, white-capping, depth-induced breaking ($\alpha = 1$, $\gamma = 0.73$), non-linear triad interactions ($\alpha = 0.1$, $\beta = 2.2$) and bottom friction (Type *Collins*, coefficient=0.02). The diffraction was also considered (smoothing coefficient=0.6, smoothing steps=600) to account for the effect of the river jetties and Motril Port on wave propagation.

Significant wave heights measured with the instruments were compared with equivalent wave heights propagated by the model for the same locations (Figure 6.2.1), and coefficients of determination (R^2) equal to 0.8616 (A1) and 0.8894 (A2) were obtained (Figure 6.2.4). These values slightly improve those obtained by Bergillos et al. (2016b) with different computational grids, detailed in the Chapter 4 of this thesis.

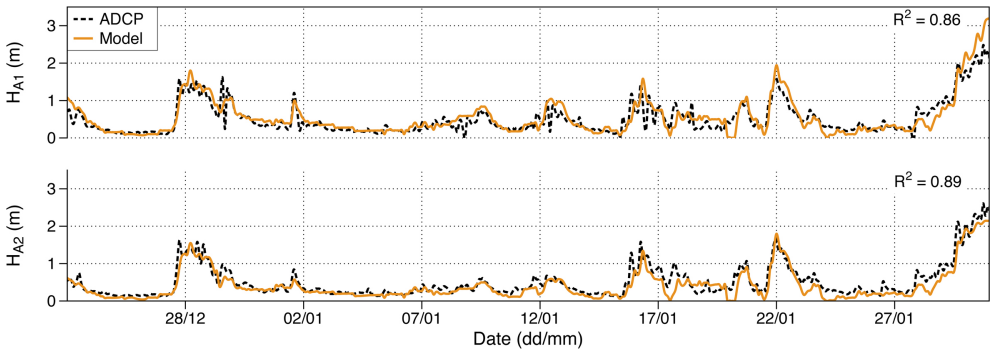

Figure 6.2.4: Comparisons between measured and modelled wave height time series for locations A1 (a) and A2 (b) according to Figure 6.2.3. (Source: Bergillos et al. (2017a). Reproduced with permission of Elsevier).

6.2.4 LST formulations and one-line model

To model the redistribution of nourished sediment and the ensuing changes in the coastline, four LST formulations were tested based on the nourished sediment size (2 mm) and the three prevailing sizes sampled under natural conditions (0.35 mm, 5 mm and 20 mm). They were applied considering alongshore variations in the shoreline, wave variables and/or beach slope. Surf zone parameters were calculated based on the results of the wave propagation model, obtaining breaking conditions for 341 (shore-normal) beach profiles equally distributed (1 every 20 m) along the coastline.

The LST results were evaluated by means of comparisons with the field measurements detailed in Section 6.2.2. Thus, the role of the different sediment fractions in the coastline response was discussed and the best formula for modelling coastal evolution after artificial nourishment projects was selected, representing a tool for the management of these complex coastal settings from morphological and sedimentary points of view. The tested LST equations corresponds to some of the formulations that have gained worldwide acceptance in confidently predicting LST rates; however, this does not imply a disagreement or a lessening of the importance of other formulas not discussed here.

The most widely used formula in coastal engineering practice for the total LST rate is the CERC equation (USACE, 1984). It is based on the principle that the LST volume is proportional to the longshore wave power per unit length of beach, and it can be expressed as follows:

$$Q = \frac{K \rho \sqrt{g}}{16 \sqrt{\gamma} (\rho_s - \rho)(1 - p)} H_b^{2.5} \sin(2\theta_b) \tag{6.1}$$

where Q is the LST rate in volume per unit of time, K is an empirical coefficient, ρ_s is the sediment density, p is the porosity index ($p = 0.4$), H_b is the significant wave height at breaking, γ is the breaker index and θ_b is the wave angle at breaking. The shore protection manual (USACE, 1984) recommends a value of $K = 0.39$ derived from a field study conducted by Komar and Inman (1970). Del Valle et al. (1993) found the following exponential relationship between this coefficient and the sediment size along the Mediterranean coast of southern Spain:

$$K = 1.6 \exp(-2.5 D_{50}) \tag{6.2}$$

The minimum calibrated K, through comparisons with field measurements, was 0.03 (for $D \sim 2$ mm); consequently, this value of K was used for the three gravel fractions tested. Mil-Homens et al. (2013) achieved the best fits with the following polynomial function:

$$K = \left(2232.7 \left(\frac{H_b}{L_0}\right)^{1.45} + 4.505\right)^{-1} \tag{6.3}$$

LST rates were computed with both formulations for K and the results were compared. Inman and Bagnold (1963) proposed a theory whereby wave energy is expended to suspend and support sediment above the bottom, and where any unidirectional current superimposed on the orbital wave motion can in turn produce net transport in the current direction. The LST formula derived based on this theory may be expressed as follows:

$$Q = \frac{\sqrt{2}}{8} \frac{K \rho \sqrt{g}}{(\rho_s - \rho)(1-p)} H_b^{2.5} \sin(2\theta_b) \tag{6.4}$$

Note that this equation is equivalent to the CERC formulation (USACE, 1984) for a breaker index equal to 0.125. The approach of Inman and Bagnold (1963) has been successfully tested for curvilinear coasts by López-Ruiz et al. (2014).

Kamphuis (1991a) developed the following relationship for estimating LST rates:

$$Q_m = 2.27 H_b^2 T_p^{1.5} (\tan\beta)^{0.75} D_{50}^{-0.25} [\sin(2\theta_b)]^{0.6} \tag{6.5}$$

where Q_m is the LST rate of immersed mass per unit of time and $\tan\beta$ is the beach slope. The immersed weight is related to the volumetric rate as $Q_m = (\rho_s - \rho)(1-p)Q$. This formulation, based primarily on physical model experiments and applicable for both field and laboratory measurements (Kamphuis, 2002), is useful for the present study as it includes the effects of both the beach slope and the grain size on the LST. These are key variables for the mobilization and transport of sediment along Spanish Mediterranean coasts, which are commonly characterized by complex morphologies (Lobo et al., 2006; Ortega-Sánchez et al., 2017) and sediment heterogeneity (Bárcenas et al., 2011; Bergillos et al., 2016d).

Due to this sediment variability, the general formula proposed by Van Rijn (2014), which was deduced for sand, gravel and shingle beaches, was also applied. The LST rate of this formulation is given by:

$$Q_m = 0.00018 K_{vr} \rho_s g^{0.5} (\tan\beta)^{0.4} D_{50}^{-0.6} H_b^{3.1} \sin(2\theta_b) \tag{6.6}$$

where K_{vr} is a wave correction factor that accounts for the effect of swell waves on LST, since these waves have been demonstrated to yield much larger LST rates than wind waves of the same wave height. This expression was tested on MSG beaches subjected to a strongly by-modal wave climate along the eastern coast of the UK (French and Burningham, 2015).

The validity of these LST formulations for the four sediment fractions was evaluated based on the coefficient $C = V_{mod}/V_{meas}$ (Figure 6.2.1), where V_{mod} is the cumulative LST volume modelled between bathymetric surveys (obtained as the summation of the LST gradient multiply by the duration of each sea state) and V_{meas} denotes sediment volumetric changes per meter of coastline (until the maximum breaking depth) based on the field measurements detailed in Section 6.2.2.1 (both in m^3/m). The LST gradient was obtained as the ratio between the difference in the LST rates among consecutive shore-normal beach profiles (boundaries) and the distance between them (20 m).

Finally, the one-line model was applied between topographic surveys (Section 6.2.2.2) for each LST formulation and each sediment size. This model is based on the following equation (Pelnard-Considère, 1956):

$$\frac{\partial y_s}{\partial t} = \frac{1}{D}\left(-\frac{\partial Q}{\partial x}\right) \tag{6.7}$$

where y_s is the coastline position and D is the sum of the closure depth and the height of the berm. The model was solved numerically by means of the 341 shore-normal boundaries defined to obtain the LST rates and gradients (resolution equal to 20 m). The goodness of the results was evaluated based on comparisons with the measured coastlines through the root-mean-square error (RMSE, Figure 6.2.1).

6.3 Results

6.3.1 Wave, wind and water level conditions

The deep-water significant wave height and spectral peak period were generally $H_0 < 1$ m (70% of the time) and $T_p < 6$ s (69% of the time), respectively, indicating that the beach was predominantly forced by low energy waves (Figure 6.3.1a-b). The predominant deep-water wave directions were west-southwest (40% of the time) and east-southeast (56% of the time), whereas the wind velocity was generally less than 10 m/s (90% of the time), with incoming directions from the east-southeast and west-southwest that were closely related to the wave directions (Figure 6.3.1c-d).

Two storms occurred with maximum H_0 of 4.9 m and 4.5 m and durations of 22 and 30 hours. The first storm arrived between surveys 1-2 and was associated with westerly waves ($\theta_0 \in [235°, 239°]$); whereas the second, between surveys 3-4, was forced by easterly waves ($\theta_0 \in [105°, 108°]$). The maximum V_w occurring during storms 1 and 2 were 19.9 m/s and 17 m/s with θ_w from the west-southwest and the east-southeast, respectively (Figure 6.3.1). Total run-up exceeded 1.52 m and caused dry beach erosion six times during the study period: two between surveys 1-2, two between 2 and 3, and two between 3 and 4. These erosive events were longer (37 hours) and more severe (maximum η equal to 2.6 m) between surveys 1-2 than those between surveys 2-3 (5 hours and $\eta_{max} = 1.6$ m) and between surveys 3-4 (33 hours and $\eta_{max} = 2$ m).

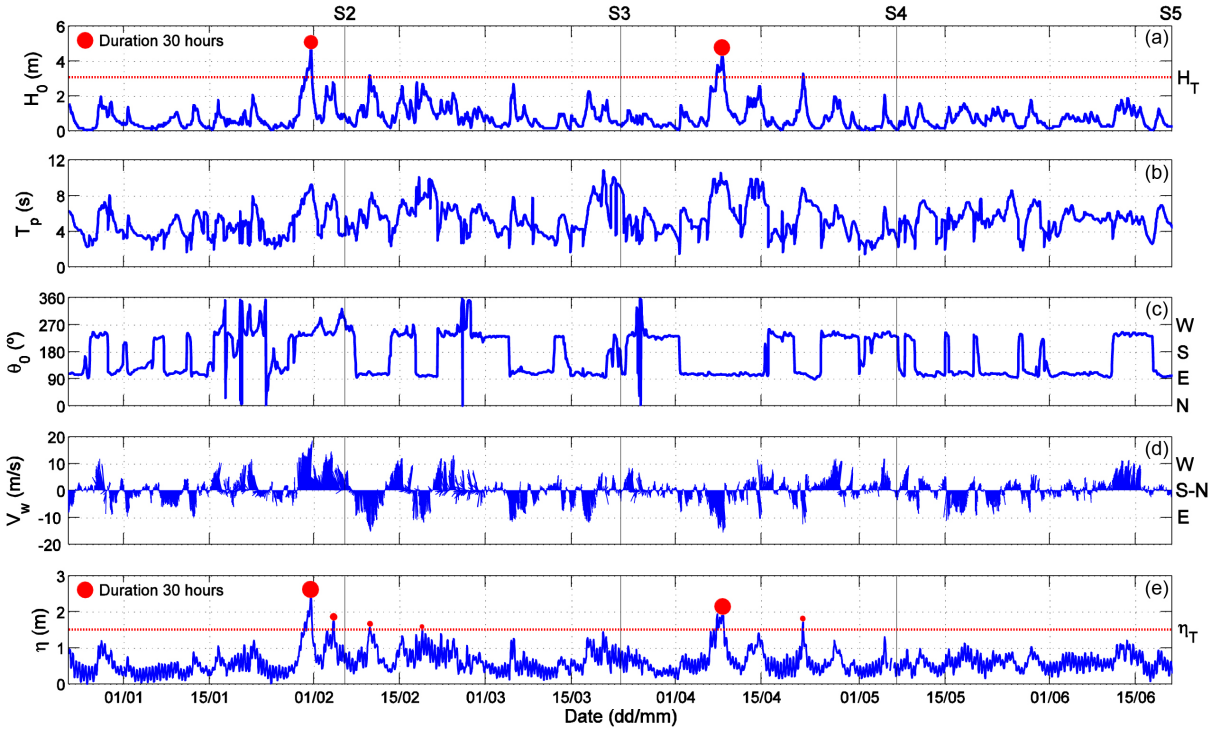

Figure 6.3.1: Evolution of the deep-water significant wave height (a), spectral peak period (b), deep-water wave direction (c), wind velocity and direction (d) and total run-up (e) over the study period. Vertical lines (black) indicate the date of the field surveys and horizontal lines (red) represent thresholds of wave height and total run-up. Storms and erosive events are marked (red circles). (Source: Bergillos et al. (2017a). Reproduced with permission of Elsevier).

6.3.2 Wave propagation patterns in the nearshore zone

Although average values of H_0 and T_p for the first period (0.79 m and 4.67 s) were lower than those during periods 2 (0.97 m and 5.77 s) and 3 (0.85 m and 5.4 s), nearshore wave energy levels in the studied stretch of beach over the first period were significantly higher than those during periods 2, 3 and 4 (Figure 6.3.2). This highlights the importance of the incoming wave direction for nearshore wave propagation patterns, as the highest relative percentage of westerly waves occurred over the first period (Figure 6.3.1c). Nearshore wave energy levels decreased significantly during the last period (Figure 6.3.2d), when both the average wave height (0.71 m) and the percentage of westerly waves (24.5%) were the lowest for the study period.

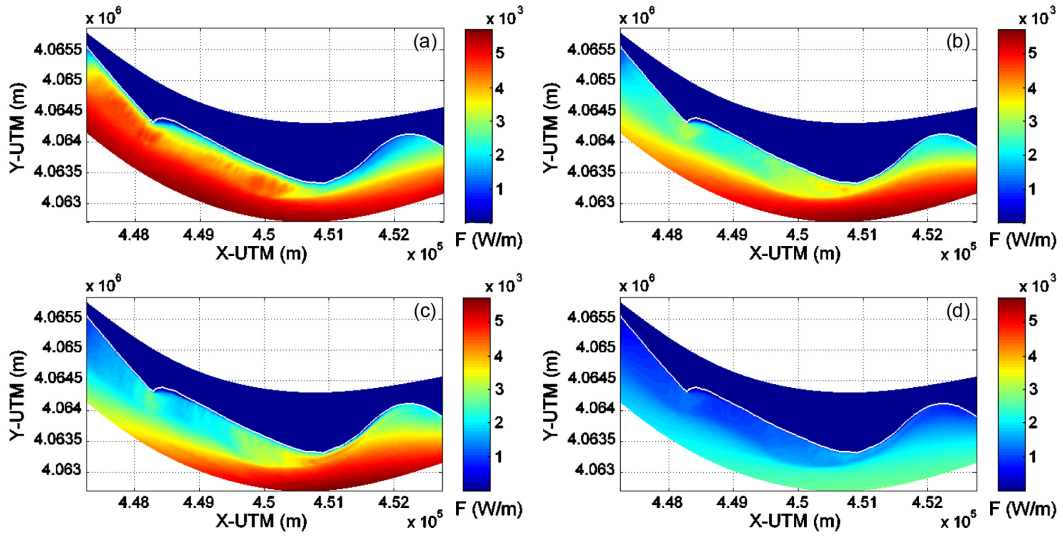

Figure 6.3.2: Time-average of energy flux between field surveys modelled with Delft3D-WAVE: (a) surveys 1-2, (b) surveys 2-3, (c) surveys 3-4 and (d) surveys 4-5. The shorelines are indicated in white. (Source: Bergillos et al. (2017a). Reproduced with permission of Elsevier).

6.3.3 Beach profile changes

The observed evolution of beach profile P1 (Figure 6.3.3b) reveals a loss of sediment volume (per meter of coastline) at shallower depths ($0 - 3.2$ m) equal to 30.95 m^3/m between surveys 1-3, which was mainly induced by erosive events (Figure 6.3.1e) and coastline retreat (Figure 6.3.4b) occurring during this period. In contrast, a positive sediment balance equal to 17.96 m^3/m took place across the whole profile. Hence, it seems that nourished sediment was eroded and partly transported offshore due to the overwash events over this period (Figure 6.3.1e), increasing the unit volume of the beach profile by 48.9 m^3/m at depths of 3.2 to 10 m. Sediment accumulation occurred across profile P2 (Figure 6.3.3c) between surveys 1-3, with a total gain of 38.66 m^3/m, which was more uniformly distributed than in profile P1. Thus, part of the eroded sediment around the mouth was transported towards the east due to medium- to high-energy westerly events during this period (Figures 6.3.1 and 6.3.2) and to the ensuing LST (Section 6.3.5).

Between surveys 3-5, shape variations in profile P1 were lower than those recorded between surveys 1-3. This was most likely due to the prevailing easterly waves (Figure 6.3.1e) and the lower energetic waves in the nourished section during this period (Figure 6.3.2), although the attenuation of the coastal response three months after the nourishment forcing could be another cause of this lower variation. Volume differences were even lower in profile P2 during this period (sediment balance of 13.06 m^3/m in P1 versus 3.65 m^3/m in P2), but sediment volume variations near the coast were higher than those in profile P1 (Figure 6.3.3b-c). Again, these results reveal the role of the LST in the coastal response.

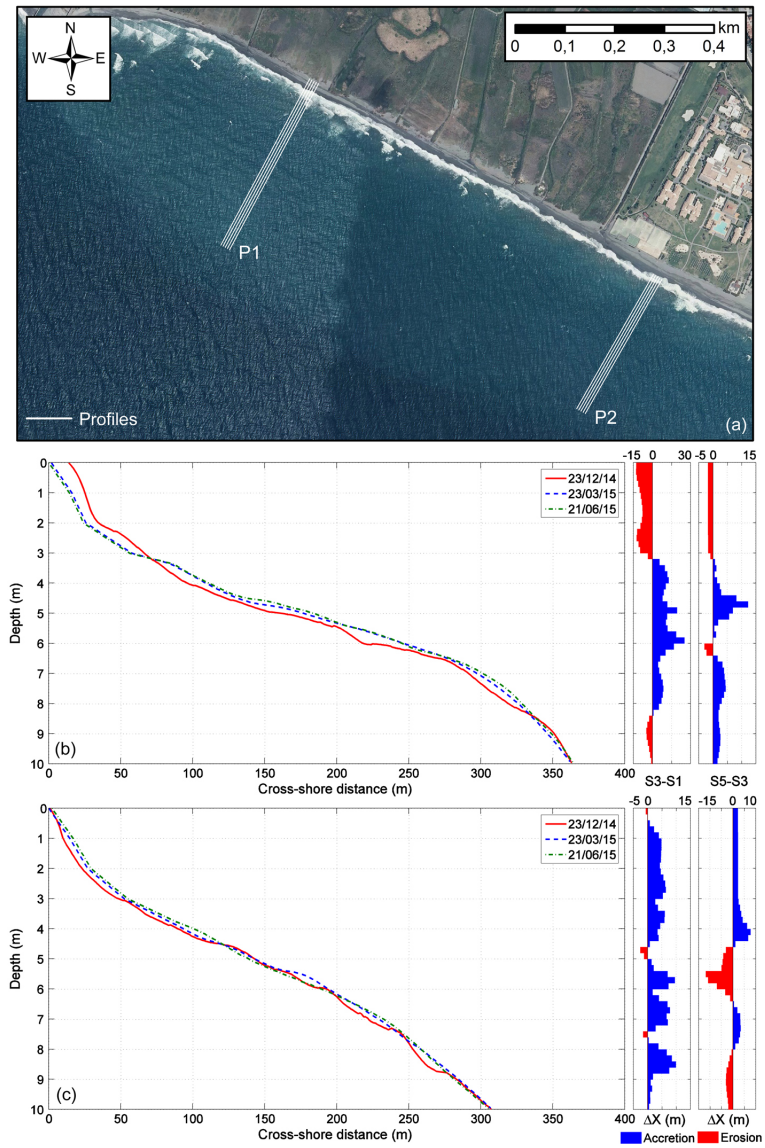

Figure 6.3.3: (a) Location of the study beach profiles. Evolution of profiles P1 (b) and P2 (c) during the study period. Differences in cross-shore distances between profiles (ΔX) are indicated. (Source: Bergillos et al. (2017a). Reproduced with permission of Elsevier).

6.3.4 Coastline evolution

Regarding plan view evolution patterns, Figure 6.3.4 shows that severe coastline retreat took place between surveys 1-2 in the southeast of the river mouth. The total loss of dry beach area in the nourished section was equal to 9367 m^2. This erosion pattern was influenced by the westerly storm that occurred in January 2015 (Figure 6.3.1), although the initial coastline shape after nourishment (Figure 6.3.4a) could also have played a significant role in coastline retreat during this period - the further the morphology of the beach is from the dynamic equilibrium, the faster the coastline evolves towards its natural configuration due to the greater LST gradients.

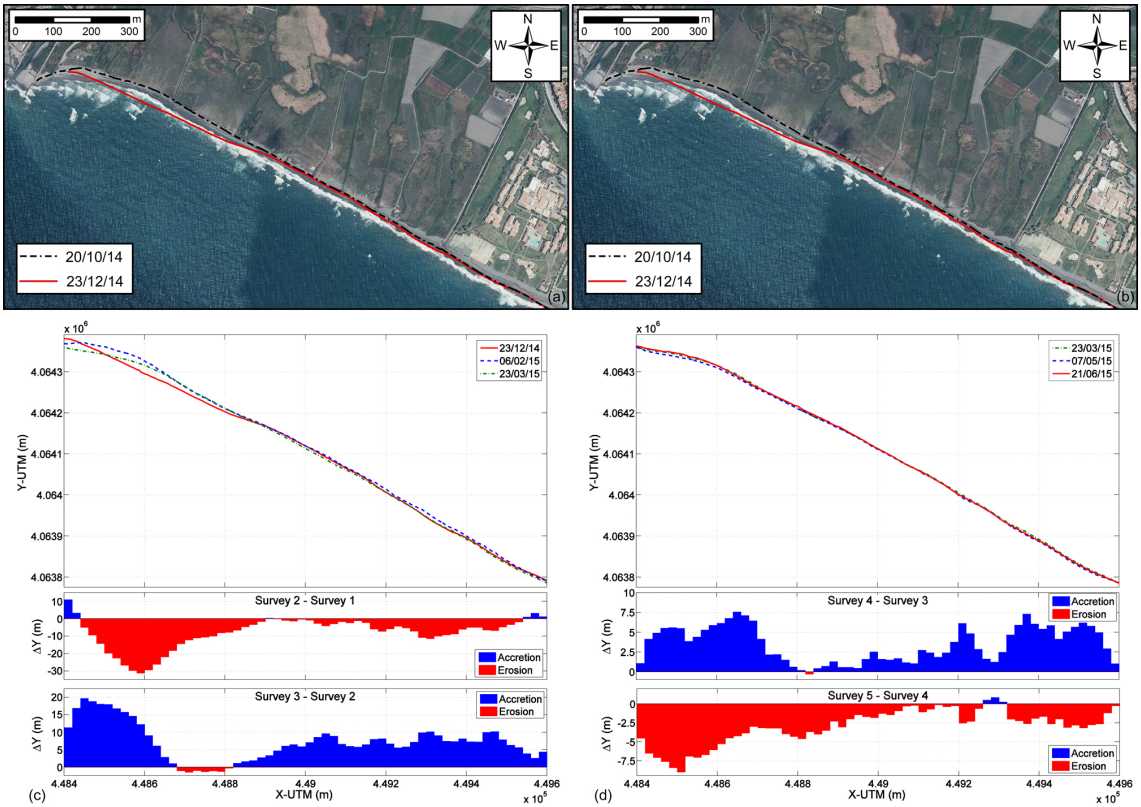

Figure 6.3.4: Coastline position before (black) and after (red) the artificial nourishment project (a-b). Evolution of the coastline position between surveys 1-3 (c), and between surveys 3-5 (d). Differences in vertical distances between coastlines (ΔY) are indicated. (Source: Adapted from Bergillos et al. (2017a). Reproduced with permission of Elsevier).

On the other hand, the dry beach area increased along the nourished stretch of coastline by almost 8,900 m^2 between surveys 2-3 and by more than 4,200 m^2 between surveys 3-4. This seaward advance of the coastline position most likely occurred due to a dominance of easterly waves during these periods (Figure 6.3.1), contributing to the westward LST and to the subsequent sediment accretion along the studied stretch of beach. Although the percentages of easterly waves between surveys 2-3 and between surveys 3-4 were almost equal (54.5% versus 53.5%), and average wave conditions were also similar (Figures 6.3.1 and 6.3.2), the area gain was more than two times greater between surveys 2-3. This could be due to the recovery cycle of the beach after the storm of January 2015, considering the fast recovery of this type of beaches compared to that of sandy coasts (Bergillos et al., 2016d).

Finally, the coastline variation between surveys 4-5 was the lowest, likely due to the lower wave energy level during this period (Figure 6.3.2d). This is in agreement with observations of Bramato et al. (2012) on a nearby MSG beach. They found that a minimum wave energy is required to generate not only coastal erosion but also accretion changes. The attenuation of the beach response after nourishment may also have been important. In fact, the observed coastline evolution along the nourished stretch of beach is clearly related to the profile variations (Figures 6.3.3b and 6.3.4), experiencing an initial significant change and lower variations thereafter.

6.3.5 Modelled LST volumes: comparison and discussion

Figure 6.3.5 depicts the alongshore variation of cumulative LST volumes in the nourished stretch of beach between bathymetric surveys for each sediment size based on the four formulations detailed in Section 6.2.4. The ratios between the modelled and measured volumes in both study profiles are summarized in Table 6.3.1. The four tested formulas overestimate measured volumetric changes when the sand fraction is considered, revealing that this size is not representative of the behaviour of the beach as a whole, which is in agreement with previous works on MSG beaches (e.g., Bramato et al. (2012), Bergillos et al. (2016d)).

Table 6.3.1: Coefficient $C = V_{mod}/V_{meas}$ for each formulation and for each sediment size. The coefficients obtained with the K of Del Valle et al. (1993) and Mil-Homens et al. (2013) are shown on the left and right sides, respectively.

		Profile 1		Profile 2	
		S1-S3	S3-S5	S1-S3	S3-S5
Modelled CERC	D_{50} = 2 mm	0.73 | 1.24	5.47 | 11.4	1.59 | 8.39	0.65 | 3.31
	D_{50} = 0.35 mm	15.09 | 1.24	89.48 | 11.4	32.97 | 8.39	10.7 | 3.31
	D_{50} = 5 mm	0.73 | 1.24	5.47 | 11.4	1.59 | 8.39	0.65 | 3.31
	D_{50} = 20 mm	0.73 | 1.24	5.47 | 11.4	1.59 | 8.39	0.65 | 3.31
Modelled Inman	D_{50} = 2 mm	1.84 | 3.14	10.93 | 28.83	4.03 | 21.22	1.78 | 8.38
	D_{50} = 0.35 mm	38.18 | 3.14	226.36 | 28.83	83.4 | 21.22	27.06 | 8.38
	D_{50} = 5 mm	1.84 | 3.14	10.93 | 28.83	4.03 | 21.22	1.78 | 8.38
	D_{50} = 20 mm	1.84 | 3.14	10.93 | 28.83	4.03 | 21.22	1.78 | 8.38
Modelled Kamphuis	D_{50} = 2 mm	2.29	32.06	9.2	7.56
	D_{50} = 0.35 mm	3.6	14.49	50.5	11.91
	D_{50} = 5 mm	1.82	25.5	7.32	6.01
	D_{50} = 20 mm	1.29	8.03	5.17	4.25
Modelled Van Rijn	D_{50} = 2 mm	2.37	10.77	3.89	1.15
	D_{50} = 0.35 mm	7.06	69.4	11.57	3.39
	D_{50} = 5 mm	1.37	6.12	2.24	0.66
	D_{50} = 20 mm	**1.01**	**2.66**	**0.98**	**0.39**

Results obtained from the formulations proposed by USACE (1984) and Inman and Bagnold (1963) with the equation of Del Valle et al. (1993) are equal for the three gravel fractions, as the K factor is considered to be equal for these gravel sizes. With the equation of K proposed by Mil-Homens et al. (2013), results are the same for all the fractions, since it does not account for sediment size. Table 6.3.1 shows that the fits obtained through the K factor of Del Valle et al. (1993) are generally better (lower values of C) than those computed with the formula of Mil-Homens et al. (2013). The LST volumes modelled with the CERC equation (USACE, 1984) and the K factor of Del Valle et al. (1993) range from 0.65 to almost 5.5 with respect to field measurements, whereas the approaches of Inman and Bagnold (1963) and Kamphuis (1991a) over-predict observed changes in P1 and P2 during the two periods. This in agreement with previous works, which found that these expressions, deduced for sandy beaches, overestimate LST rates in gravel coastal settings (e.g., Van Wellen et al. (2000), Reeve et al. (2012), Van Rijn (2014)).

The LST volumes calculated with the equation of Van Rijn (2014) for the coarse gravel fraction provide the best fit to the measured volumetric changes in both profiles. The rate $|1-C|_{S1-S3}+|1-C|_{S3-S5}$ obtained from this formulation is more than 2.8 times lower (better) than those calculated through the other formulations in P1 and more than 1.4 times better in P2. In addition, ratios between modelled and measured volumetric changes for the full study period based on the formula of Van Rijn (2014) exceed 93% and 77% in P1 and P2, respectively.

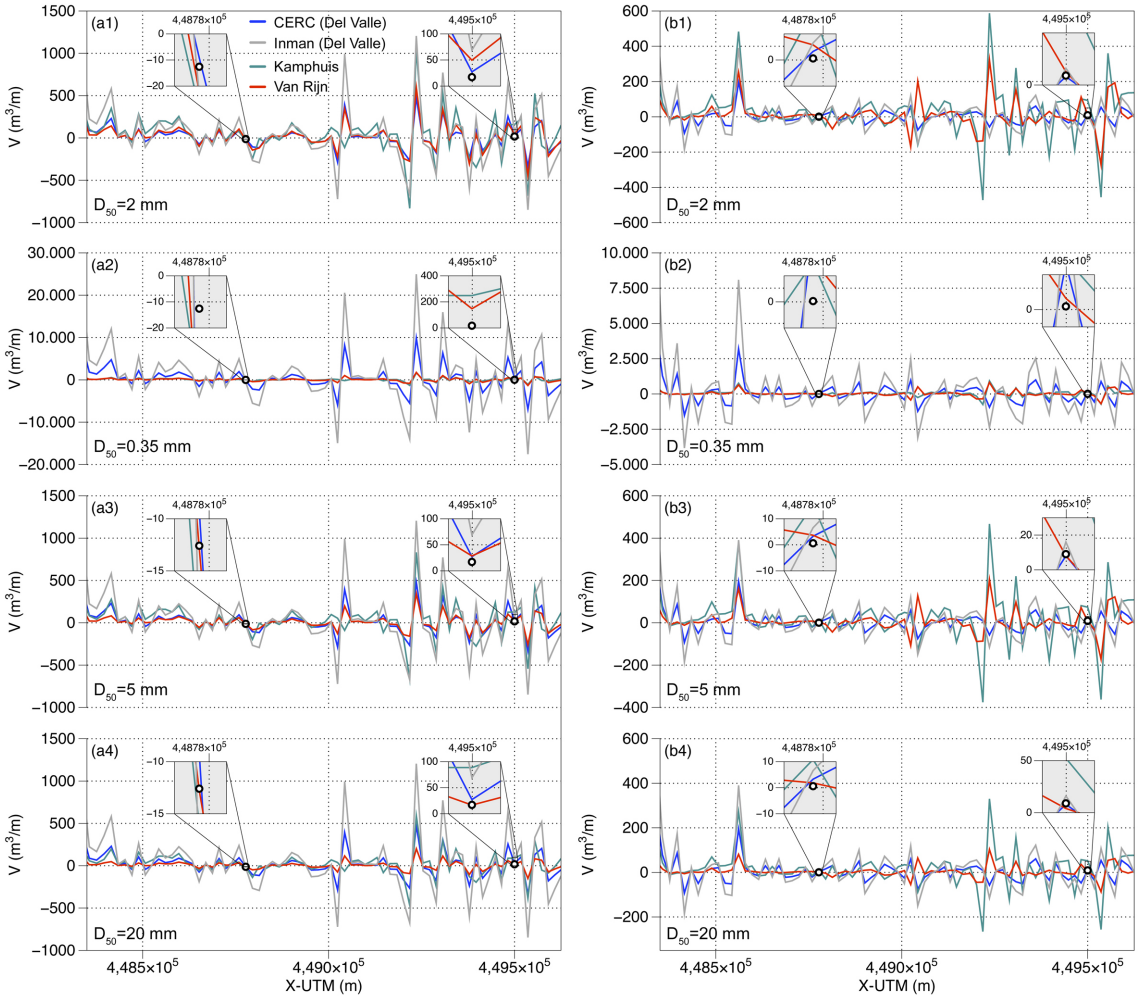

Figure 6.3.5: Alongshore variation of the modelled LST volume gradients between surveys 1-3 (a) and between surveys 3-5 (b) for the nourished sediment size (1) and the three prevailing natural sizes (2-4). Observations of measured volumetric changes (per meter of shoreline) in study profiles P1 and P2 are indicated (black circles). (Source: Bergillos et al. (2017a). Reproduced with permission of Elsevier).

These findings are consistent with observations in the study site detailed in Bergillos et al. (2016d), who proposed that the morphodynamic response of the beach is dominated by the coarse gravel fraction due to the selective removal of the finer material and is similar to those found in gravel beaches, such as Slapton Sands (Masselink et al., 2010) and Loe Bar (Poate et al., 2013) in the UK. This is in agreement with results obtained by Bergillos et al. (2016c) through the model XBeach-G (McCall et al., 2014; McCall et al., 2015) by assuming that the beach is made up of coarse gravel. These results are also consistent with those detailed by French and Burningham (2015) for the eastern coast of the UK, which presents similar wave and sediment conditions to those of Playa Granada.

6.3.6 Modelling of coastline responses: comparison and discussion

LST formulations were used to apply the one-line model and the results were compared to topographic measurements of the coastline (Figure 6.2.1). The RMSEs for the four formulations and each sediment size are shown in Table 6.3.2. Again, the K factor of Del Valle et al. (1993) provides better fits (lower RMSEs) than those obtained with the K proposed by Mil-Homens et al. (2013) for the equations of CERC (USACE, 1984) and Inman and Bagnold (1963). However, as expected, the best fits for all periods between surveys are those obtained from the equation of Van Rijn (2014) for the coarse gravel size.

Table 6.3.2: RMSE (in m) for each formulation and for each sediment size. The sums of the RMSEs are indicated in the last column. The RMSEs for the K of Del Valle et al. (1993) and Mil-Homens et al. (2013) are shown on the left and right sides, respectively.

		S1-S2	S2-S3	S3-S4	S4-S5	Sum
Modeled CERC	D_{50} = 2 mm	19.07 | 29.34	14.38 | 45.57	9.74 | 23.17	5 | 13.16	48.19 | 107.24
	D_{50} = 0.35 mm	166.83 | 29.34	245.39 | 45.57	145.51| 23.17	57.82 | 13.16	615.55 | 107.24
	D_{50} = 5 mm	19.07 | 29.34	14.38 | 45.57	9.74 |23.17	5 | 13.16	48.19 | 107.24
	D_{50} = 20 mm	19.07 | 29.34	14.38 | 45.57	9.74 | 23.17	5 | 13.16	48.19 | 107.24
Modeled Inman	D_{50} = 2 mm	26.32 | 61.79	31.15 | 81.9	18.27 | 57.28	7.93 | 26.33	83.66 | 227.3
	D_{50} = 0.35 mm	421.36 | 61.79	620.23 | 81.9	367.79 | 57.28	145.91 | 26.33	1555.29 | 227.3
	D_{50} = 5 mm	26.32 | 61.79	31.15 | 81.9	18.27 | 57.28	7.93 | 26.33	83.66 | 227.3
	D_{50} = 20 mm	26.32 | 61.79	31.15 | 81.9	18.27 | 57.28	7.93 | 26.33	83.66 | 227.3
Modeled Kamphuis	D_{50} = 2 mm	20.15	24.46	14.62	6.33	65.57
	D_{50} = 0.35 mm	24.57	36.74	22.4	9.31	93.01
	D_{50} = 5 mm	19	20.22	11.91	5.37	56.51
	D_{50} = 20 mm	18.06	15.6	8.9	4.42	46.98
Modeled Van Rijn	D_{50} = 2 mm	18.96	18.87	8.91	4.14	50.88
	D_{50} = 0.35 mm	29.9	49.83	20.54	7.1	107.37
	D_{50} = 5 mm	17.93	12.94	6.38	3.71	40.96
	D_{50} = 20 mm	**17.65**	**10.12**	**4.57**	**3.5**	**35.84**

Errors are higher for the first period and decrease progressively for the remaining periods between surveys. This could be due to the different coastal responses occurring immediately after the artificial replenishment and to the higher cross-shore sediment transport due to the overwash process under the westerly storm during this period. In fact, the greatest discrepancies between modelled and measured coastline responses over the first and second periods for all model predictions (Figure 6.3.6a-b) are found in the stretch of beach where both the plan view variations induced by artificial nourishment (Figure 6.3.4) and the observed cross-shore transport (Figure 6.3.3b) were higher. The uncertainties associated with both measurements and modelling (Brad Murray et al., 2016) should also be considered.

However, the RMSEs obtained (especially for the last two periods) provide confidence in the results obtained through the formulation of Van Rijn (2014) for the coarse gravel fraction, confirming that the joint application of this equation and the one-line model is capable of reproducing the plan view response of this type of coasts.

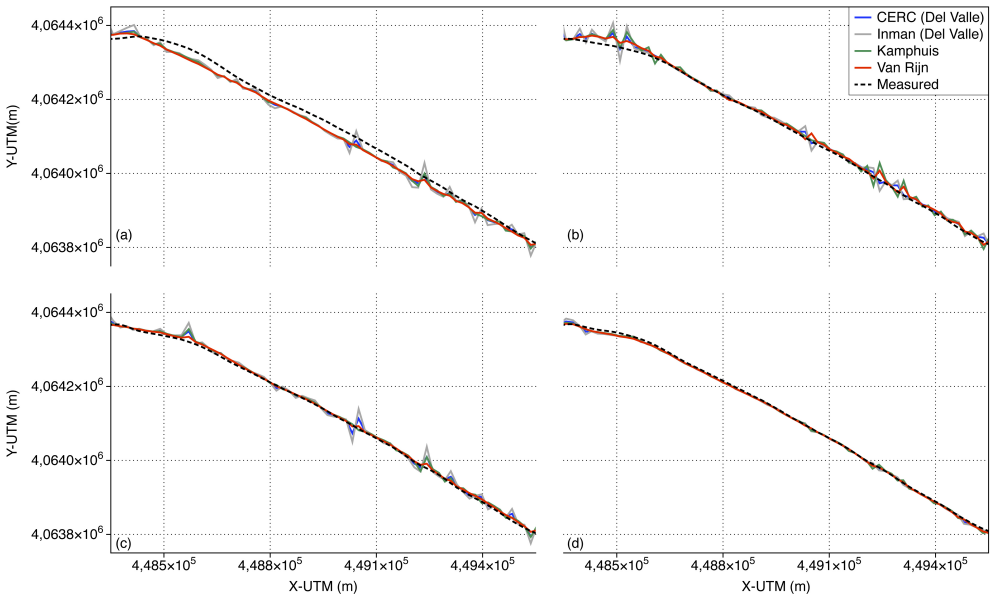

Figure 6.3.6: Results of the one-line model between surveys based on the sediment size that provided the best fit to the measured morphological changes: (a) surveys 1-2, (b) surveys 2-3, (c) surveys 3-4 and (d) surveys 4-5. Measured coastlines are marked as black dashed lines. (Source: Bergillos et al. (2017a). Reproduced with permission of Elsevier).

6.4 Conclusions

Although MSG deltaic coasts have received increasing attention over recent years, the number of morphological field observations and numerical models used to reproduce their responses are still limited. This chapter presents a study on the evolution of Playa Granada after an artificial nourishment project based on measurements and modelling during a six-month period. Continuous hydrodynamic data were collected over 39 days to calibrate a wave propagation model, and 30 beach profiles and 5 coastlines were surveyed to analyse coastal dynamics and to test different LST formulations. Based on this analysis, the following conclusions were drawn.

Coastline evolution patterns reveal a severe retreat in the short-term, with a loss of dry beach area equal to 9367 m^2 (more than 50% of the nourished area) after 45 days, representing an average erosion higher than 200 m^2/day. This is mainly attributable to the morphology of the nourished coastline, which was significantly different from the natural configuration, generating greater LST gradients and, consequently, more significant changes in the coastline position. However, the occurrence of a high-energetic westerly storm 40 days after the intervention should also be taken into account to further understand the coastline erosion. In addition, the wind action (Van der Wal, 1998; Van der Wal, 2000b; Van der Wal, 2000a; Jackson and Nordstrom, 2011) and the porosity decrease after nourishment (Román-Sierra et al., 2014) could also contribute to the sediment removal. Finally, the different characteristics of the nourished sediment (uniform distribution of D_{50} = 2 mm) with respect to natural sediment (heterogeneous distribution of three prevailing sizes: 0.35 mm, 5 mm and 20 mm) played a major role in the relatively rapid erosion of the nourished beach area due to the lack of response from the artificial material to waves in the same manner as natural sediments (Dean and Dalrymple, 2002; Horn and Walton, 2007).

For this reason, four LST formulations were tested for the nourished sediment size and the three natural fractions. The Delft3D-WAVE model allowed obtaining the breaking wave variables required to apply LST equations. The comparison of modelled cumulative LST volumes with bathymetric observations highlights that the equation of Van Rijn (2014) for the coarse gravel fraction clearly provides the best fits to the measured volumetric changes (per meter of coastline) for both study profiles. Ratios between modelled and measured volumes over the study period were equal to 93.1% and 77.4% in study profiles P1 and P2, respectively.

LST rates were also used to apply the one-line model between topographic surveys. The results also indicate that the approach of Van Rijn (2014) considering that the beach is made up of coarse gravel provides the lowest root-mean-square errors (Table 6.3.2 and Figure 6.3.6), which is in agreement with previous experimental (Bergillos et al., 2016d) and numerical (Bergillos et al., 2016c) works carried out in the study site. Error levels decreased over the study period (induced by the highly altered shape of the coastline immediately after nourishment) and almost vanished over the last three months (RMSE < 4.6 m). Hence, this chapter shows that the combination of a calibrated wave propagation model (such as Delft3D-WAVE), the LST equation proposed by Van Rijn (2014) and the one-line model represents an integrated tool to predict the morphodynamic response of these complex coastal systems, particularly for long-term predictions, with direct management applications.

CHAPTER 7

STORM RESPONSE OF THE BEACH UNDER VARYING WAVE DIRECTIONS

This chapter investigates the profile response of Playa Granada forced by storm waves from varying directions. Beach morphology was monitored over a 36-day period with variable wave conditions, and profile response was compared to model predictions using the XBeach-G model and a longshore sediment transport (LST) formulation. XBeach-G was applied over 2-day periods of low energy, south-westerly (SW) storm and south-easterly (SE) storm conditions, and was coupled to LST using a parametric approach which distributes the LST across the swash, surf and nearshore zones. A calibrated wave propagation model (Delft3D) was used to obtain the inshore conditions required to drive the XBeach-G model and the LST formulation. The storm response is clearly influenced by the free-board (difference between the height of the berm and the total run-up) and is also strongly dependent on storm-wave direction, with the SW storm eroding the surveyed area, while the SE storm induced beach accretion. Model results indicate that XBeach-G on its own is capable of adequately reproducing the response of the beach under SW storm conditions (BSS > 0.95), but not under SE storms due to the higher LST gradients at the study location. The combination of XBeach-G and LST fits the measured profiles reasonably well under both SW (BSS > 0.96) and SE (BSS > 0.88) storms, inspiring confidence in the coupled model to predict the storm response under varying wave conditions. The combined XBeach-G/LST model was applied to the entire 6.8-km deltaic coastline to investigate the impact of an extreme SW and SE storm event, and the model results reiterate the importance of cross-shore and longshore sediment transport in driving coastal storm response at this location. The approach proposed in this chapter can be extended to other worldwide coasts highly influenced by both cross-shore and longshore sediment transport, such as beaches with different coastline orientations and/or forced by varying wave directions.

7.1 Objectives

The main objectives of this chapter are to characterize and to model the storm response of Playa Granada under varying wave directions. Thirteen field surveys were performed and a numerical model (Delft3D) calibrated for the study site was used to relate the wave propagation patterns with the coastal dynamics. Delft3D results were also used to apply and test the XBeach-G model forced by low energy (LE) conditions, and south-westerly (SW) and south-easterly (SE) storms. In addition, XBeach-G was combined with the longshore sediment transport (LST) equation of Van Rijn (2014) by means of a parametric formulation to consider different cross-shore distributions of LST. Finally, the approach that best fitted the observed response was used to model extreme SE and SW storms along the entire deltaic coastline, highlighting the potential of the proposed coupled model to extend XBeach-G towards larger longshore scales.

7.2 Methodology

7.2.1 Maritime data and total run-up

A 36-day time series of 864 sea states (hourly hindcasted data for the study period), corresponding to SIMAR point number 2041080 (Figure 7.2.1) and provided by *Puertos del Estado*, was used to study the evolution of the following deep-water wave and wind variables: significant wave height (H_0), spectral peak period (T_p), wave direction (θ_0), wind velocity (V_w) and wind direction (θ_w). They were also used as boundary conditions to apply the wave propagation model.

In addition, the total run-up (η) was estimated as the sum of astronomical tide (measured by a gauge located in the Motril Port), wind set-up ($\Delta\eta_{\text{wind}}$), barometric set-up ($\Delta\eta_{\text{bar}}$) and wave run-up ($\Delta\eta_{\text{wave}}$). The wind set-up was calculated as $\Delta\eta_{\text{wind}} = \tau_{\text{wind}}/(\rho g h_0)\Delta x$ (Bowden, 1983), where g is the acceleration of gravity, $\rho = 1,025$ kg/m^3 is the density of salt water, Δx is the wave fetch from the centre of the low-pressure system to the coast (estimated through isobar maps), the depth of the wave base level is represented by $h_0 = L_0/4$, where L_0 is the wavelength in deep water, and the tangential wind stress is obtained from $\tau_{\text{wind}} = \rho_a U_*^2$, where ρ_a is the air density and U_* is the friction velocity. The barometric set-up was calculated as $\Delta\eta_{\text{bar}} = \Delta P_a/(\rho g)$ (Dean and Dalrymple, 2002), where ΔP_a represents the atmospheric pressure variation relative to the long-term average pressure at Motril Port. The wave run-up was estimated as $\Delta\eta_{\text{wave}} = 0.36 g^{0.5} H_{8,0}^{0.5} T_p \tan\beta$ (Nielsen and Hanslow, 1991), where $\tan\beta$ is the intertidal slope and $H_{8,0}$ is the modelled wave height at 8 m water depth de-shoaled to deep water using linear theory and assuming parallel bottom contours. Bergillos et al. (2016d) obtained high correlation (differences less than 9%) between measured and estimated total run-up values with these formulations.

7.2.2 Field measurements

Thirteen topographic surveys were performed during the 36-day study period (Table 7.2.1) to measure the morphology of the beach profile in the central area of the stretch river mouth - *Punta del Santo* (Figure 7.2.1). This coastal section is considered representative of the beach behaviour of that section of the coastline (Bergillos et al., 2016d). Each survey was performed under low tide conditions and the observations were referenced to the mean low water spring (MLWS) level.

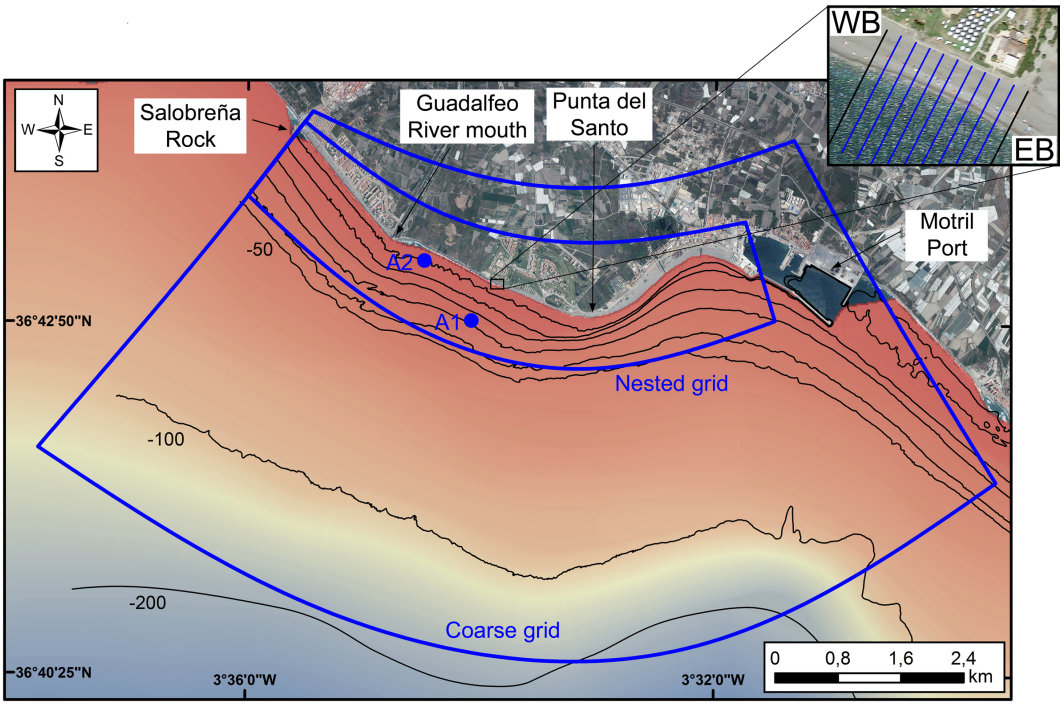

Figure 7.2.1: Bathymetric contours, grids used in the wave propagation model and positioning of the ADCPs (A1 and A2). Upper right panel: west (WB) and east (EB) boundaries of the surveyed area and measured beach profiles. (Source: Adapted from Bergillos et al. (2017b). Reproduced with permission of Elsevier).

Table 7.2.1: Timeline of the profile surveys carried out during the study period.

Survey	S1	S2	S3	S4	S5	S6	S7	S8	S9	S10	S11	S12	S13
Date	15/1	16/1	18/1	20/1	22/1	23/1	27/1	30/1	2/2	6/2	9/2	13/2	20/2

Topographic measurements were carried out using a highly accurate DGPS (Javad Maxor) with less than 0.02 m of instrument error. Eleven equally-spaced (10 m) shore-normal profiles were measured (Figure 7.2.1) and combined to obtain an alongshore-averaged profile representative of the surveyed area. This alongshore-averaged beach profile was used to address the evolution of the beach under varying wave conditions, as well as for comparison with model predictions.

A high-resolution multibeam bathymetric survey was performed at the beginning of the study period covering the entire deltaic region. Data were acquired using Differential Global Positioning System (DGPS) navigation in reference to the WGS-84 ellipsoid. Accurate navigation and real-time pitch, roll and heave were corrected. A topographic survey along the entire deltaic beach was carried out simultaneously to complement the multibeam bathymetry. These morphological data were used as the bottom boundary conditions for the wave propagation model. To calibrate this model, wave data were continuously collected from December 20th, 2014 to January 30th, 2015 by means of two ADCPs (Figure 7.2.1).

7.2.3 Numerical modelling

7.2.3.1 Wave propagation model: Delft3D

SIMAR point data for the entire study period (Section 7.2.1) were propagated from deep-water areas to the nearshore using the WAVE module of the Delft3D model (Lesser et al., 2004; Lesser, 2009), which is based on the SWAN model (Holthuijsen et al., 1993). These results were used to address inshore wave conditions and to provide the boundary conditions for the XBeach-G model and the LST formulation.

The model domain consisted of two different grids, shown in Figure 7.2.1. The first is a coarse curvilinear 82x82-cell grid covering the entire deltaic region, with cell sizes that decrease with depth from 170x65 to 80x80 m. The second is a nested grid covering the beach area with 244 and 82 cells in the alongshore and cross-shore directions, respectively, and with cell sizes of approximately 25x15 m. This model was calibrated for these particular grids by Bergillos et al. (2017a) through comparison with field data, obtaining coefficients of determination equal to 0.86 and 0.89 for the ADCPs A1 and A2 (Figure 7.2.1), respectively.

7.2.3.2 Morphodynamic model of the beach profile: XBeach-G

The 1D process-based model XBeach-G is an extension of the XBeach model that incorporates: (1) a non-hydrostatic pressure correction term that allows solving waves explicitly in model; (2) a groundwater model that allows infiltration and exfiltration; and (3) the computation of bedload transport, including the effects of groundwater ventilation and flow acceleration forces, for estimating bed level changes (McCall et al., 2014; McCall et al., 2015; Masselink et al., 2014).

Bergillos et al. (2016c) has shown that the model is capable of reproducing the morphodynamic response of the beach at the study site under SW storms for a grain size of 20 mm; however, it has not been tested under SE waves. For this reason, XBeach-G was applied to model the profile response of the surveyed area during three 2-day wave windows, depicted in Figure 7.3.1, which are representative of LE, SW storm and SE storm conditions. Values of sediment friction factor and Nielsen's boundary layer phase lag used for the simulations were 0.03 and 20°, respectively, which were found to be optimum during the calibration of the model (Bergillos et al., 2016c). These values are slightly different to those found on pure gravel beaches (0.01 and 25°, respectively) by Masselink et al. (2014) and McCall (2015).

Measured topographic data during surveys 6, 7 and 11 were used as initial condition of the upper profile (beach profile above the MLWS level) for the LE, SW and SE cases, respectively. Measured bathymetric data were used as initial lower profile (beach profile below the MLWS level) for the LE and SW cases since morphological changes between surveys 1 and 7 were comparatively insignificant, whereas the final lower profile for the SW case was used as initial condition for the SE storm. The input wave boundary conditions were obtained from the Delft3D-WAVE model at a depth of 10 m. This water depth offshore boundary fulfils all requirements detailed in the manual of the XBeach-G model (Deltares, 2014), and is deeper than the closure depth in the study site (Bergillos et al., 2016a; Bergillos et al., 2017a). The infrastructure associated with the hotel complex located landward of the surveyed area (Figure 7.2.1) was included in the cross-shore profile as a non-erodible object.

7.2.3.3 Longshore sediment transport: formulation and cross-shore distribution

To model LST and the ensuing changes in the upper profile, the LST expression proposed by Van Rijn (2014), which was deduced for sand, gravel and shingle beaches, was applied:

$$Q_m = 0.00018 K_{vr} \rho_s g^{0.5} (\tan\beta)^{0.4} D_{50}^{-0.6} H_b^{3.1} \sin(2\theta_b) \tag{7.1}$$

where Q_m is the LST rate (dry mass, in kg/s), K_{vr} is a wave correction factor that accounts for the effect of the wave period on the LST rate, $\rho_s = 2650$ kg/m^3 is the sediment density, $\tan\beta$ is the beach slope, D_{50} is the sediment size, H_b is the significant wave height at breaking and θ_b is the wave angle from shore-normal at breaking.

The expression was applied considering alongshore variations in the shoreline, wave variables and beach slope. Surf zone parameters were calculated based on the results of the wave propagation model, obtaining breaking conditions for 69 (shore-normal) beach profiles equally distributed (1 every 100 m) along the coastline between Salobreña Rock and Motril Port. The application of this formulation for the coarse gravel fraction ($D_{50} = 20$ mm) was found to provide the best fit to measured morphological changes of the shoreline in the study site (Bergillos et al., 2017a). LST gradients were obtained as the ratio between the differences in LST rates among consecutive beach profiles (boundaries) and the distance between them (100 m).

For the cross-shore distribution of the modelled LST volume gradients per meter of shoreline, the following equation was proposed:

$$q = a \frac{x}{x_b} \exp\left(-k \frac{x}{x_b}\right) \tag{7.2}$$

where q (in m) is the cross-shore distribution of the LST volume gradient (V, in m^3/m), x is the length across the beach profile ($x = 0$ represents the position of the total run-up), $x_b = s_R + s_b$, where s_R is the length (across the profile) between the total run-up limit and the shoreline, and s_b is the length (across the profile) between the shoreline and the breaking line. The constant k determines where the peak of the cross-shore distribution is located ($k\,x/x_b = 1$), whereas the parameter a (in m) is obtained numerically as a function of V and x_b through the following equation:

$$V = \frac{\partial Q}{\partial l} \Delta t = \int_0^{x_b} q(x)\,dx = \int_0^{x_b} a \frac{x}{x_b} \exp\left(-k \frac{x}{x_b}\right) dx \tag{7.3}$$

Through modification of k, this approach can reproduce relatively symmetrical cross-shore distributions of LST reported for sandy beaches (e.g, Bayram et al. (2001)), as well as the asymmetrical distributions on mixed sand-gravel (MSG) and gravel beaches, whose peaks are expected to be located landward of the peaks on sandy beaches due to the importance of swash processes in gravel environments (Buscombe and Masselink, 2006). In this chapter, the profiles resulting from the three values of k were tested, compared and optimised against the observed profile changes ($k_1 = 2$, $k_2 = 5$, $k_3 = 10$).

7.2.3.4 Coupling XBeach-G and longshore sediment transport

The three 2-day windows of varying wave conditions selected to apply the XBeach-G model (indicated in Figure 7.3.1) were also simulated through the combination of XBeach-G and LST. For that, the shape of the final beach profile modelled with XBeach-G was modified after each sea-state considering the LST volume gradients and the three cross-shore distributions of LST detailed in Section 7.2.3.3.

The goodness of fit for each approach was evaluated through the root-mean-square error (RMSE, in m), the relative bias normalised by the absolute mean of the observations (bias), the correlation coefficient (ρ) and the Brier Skill Score (BSS). All statistics were computed using data interpolated to a regularly-spaced grid and including only points where the measured or modelled bed level changes were greater than the maximum between the estimated instrument error and $3D_{50}$, according to McCall et al. (2015). Following the criteria proposed by Van Rijn et al. (2003), the fits were qualified from *bad* to *excellent* based on the BSS values.

Finally, the impact of extreme SW and SE storms ($H_{99.9\%}$) was modelled using both XBeach-G and the coupled model for the entire 6.8-km deltaic coastline to further determine the importance of cross-shore and longshore sediment transport in driving storm response under varying wave directions. The modelled wave variables were $H_0 = 3.1$ m, $T_p = 8.4$ s (the most frequent period under storm conditions), $\theta_{0,\mathrm{SW}} = 238^\circ$ and $\theta_{0,\mathrm{SE}} = 107^\circ$ (the most frequent directions under SW and SE storms, respectively). These sea states, summarized in Table 7.2.2, were simulated considering a storm surge (η_{ss}) of 0.5 m for two different durations: 6 hours around high tide and 12 hours representing a full tidal cycle.

Table 7.2.2: Sea-states modelled with XBeach-G and XBeach-G/LST to study storm response under varying wave directions along the entire deltaic coastline.

	SW storm	SE storm
H_0 (m)	3.1	3.1
T_p (s)	8.4	8.4
θ_0 (°)	238	107
η_{ss}	0.5	0.5

7.3 Results

7.3.1 Wave, wind and water level conditions

The deep-water significant wave height and the spectral peak period were lower than 1 m and 6 s during the 56.3% and 62% of the study period, respectively (Figure 7.3.1a-b). These values are significantly lower than average percentages from January 1958 till the end of the study period (84.6% and 83.8%, respectively, based on the SIMAR 2041080 data), indicating that the beach was forced by relatively high energy waves during this 36-day period. The predominant deep-water wave directions were $180^\circ < \theta_0 < 270^\circ$ (SW sector, 50.9% of the time) and $90^\circ < \theta_0 < 180^\circ$ (SE sector, 36% of the time). This period was, thus, more westerly-dominated than the average (41.6% and 55.7%, respectively), in agreement with the trend in wave direction over last six years (Bergillos et al., 2016b). The average wind velocity was 7.4 m/s, with prevailing values less than 10 m/s (73.3% of the time) and incoming directions from the W-SW and E-SE (Figure 7.3.1d).

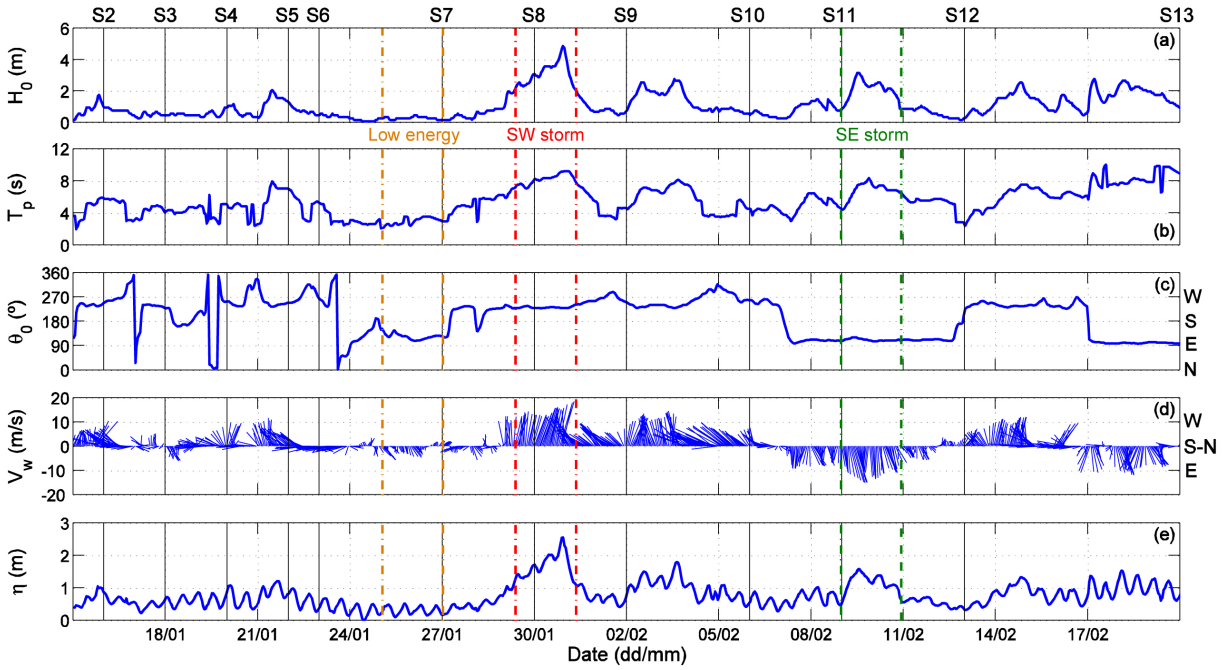

Figure 7.3.1: Evolution of the deep-water significant wave height (a), spectral peak period (b), wave direction (c), wind velocity and direction (d), and total run-up (e) over the study period. The vertical black lines indicate the date of the field surveys and the vertical coloured lines delimit the windows selected to model the profile response. (Source: Bergillos et al. (2017b). Reproduced with permission of Elsevier).

Two extreme storms ($H_0 > H_{99.9\%}$) occurred with maximum H_0 of 4.9 m and 3.2 m, and maximum T_p equal to 9.2 s and 8.4 s, respectively. The first storm, which occurred between surveys 7 and 9 (S7-S9), was associated with westerly waves ($\theta_0 \in [235°, 239°]$); whereas the second storm, during period S11-S12, was forced by easterly waves ($\theta_0 \in [104°, 117°]$). The maximum V_w during storms 1 and 2 were 19.9 m/s and 16.5 m/s with θ_w from the W-SW (extra-tropical Atlantic cyclone) and the E-SE (Mediterranean storm), respectively. The SW storm was the second most severe since 1958. The maximum total run-up (sum of the astronomical tide, storm surge and wave run-up) during this storm was 2.6 m (Figure 7.3.1e), generating overwash along the entire beach profile (Section 7.3.3).

7.3.2 Wave propagation patterns in the nearshore zone

Figure 7.3.2 depicts the spatial distribution of the time-averaged energy flux between surveys 1-7, 7-10 and 10-13 according to Delft3D-WAVE modelling. Nearshore wave energy levels were comparatively insignificant during S1-S7 (Figure 7.3.2a), when the average wave height ($H_0 = 0.62$ m), mean period ($T_z = 2.95$ s) and peak period ($T_p = 4.19$ s) were the lowest, and the percentages of SW-SE waves were the most balanced (46.9%-30.5%). Between S7 and S10, the highest values of nearshore wave energy were concentrated in the studied section of coastline due to the prevailing SW waves during this period (Figure 7.3.1c).

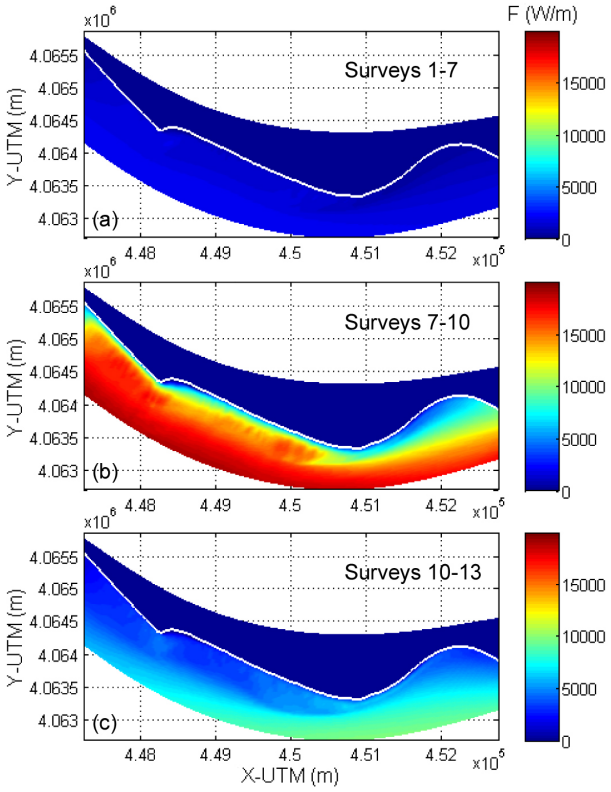

Figure 7.3.2: Spatial distribution of the time-averaged energy flux: (a) surveys 1-7 (LE conditions), (b) surveys 7-10 (SW storm), and (c) surveys 10-13 (SE storm). The shorelines are highlighted in white. (Source: Bergillos et al. (2017b). Reproduced with permission of Elsevier).

Nearshore wave energy levels between S10 and S13 were significantly lower than those over the period S7-S10 (Figure 7.3.2b-c). Considering that the average values of mean and peak wave periods were similar (T_z = 4.13 s and T_p = 6.01 s during S7-S10 *vs* T_z = 4.15 s and T_p = 6.26 during S10-S13), the lower energy levels over S10-S13 are attributable to both the less average wave height (H_0 = 1.54 m *vs* H_0 = 1.34 m) and the more balanced percentages of SW-SE waves (75.8%-4.6% *vs* 36.7%-63.1%). The dominance of SE waves during S10-S13 generated higher energy levels along the section *Punta del Santo* - Motril Port compared to those in Playa Granada (Figure 7.3.2c). This highlights the importance of the incoming wave directions in the nearshore wave propagation patterns, with direct implications in the profile response.

7.3.3 Observed morphological response of the upper profile

Three different profile responses were observed during the study period (Figure 7.3.3). The morphological changes were relatively insignificant between S1 and S7 due to the lower total run-up and energy level over this period (Figures 7.3.1e and 7.3.2a), but the profile strongly eroded during S7-S9 induced by the extreme SW storm. The profile could not be completely measured during S8 since it coincided with the beginning of the overwash (Figure 7.3.4a); therefore, the morphology of this profile at elevations below 1.5 m should be taken with caution (Figure 7.3.3b). Beach recovery occurred between S10 and S13 influenced by the medium energy content during

this period (Figures 7.3.2c and 7.3.3c). This is in agreement with observations of Bramato et al. (2012) on a nearby MSG beach, who found that a minimum wave energy is required not only to erode the beach, but also to recover it. It is suggested, and demonstrated in Section 7.3.5, that the SE storm between S11 and S12 contributed to this recovery due to LST.

Figure 7.3.5 depicts the maximum total run-up, the minimum free-board (difference between the height of the berm and the maximum total run-up) and the volumetric changes above the MLWS level (in m^3 per unit m of shoreline, or m^2) between surveys. It is observed how between S1 and S7, dominated by swash regime, accretion rates were lower than 0.36 m^2/day; whereas between S7 and S9, when overwash occurred, the average erosion rate was 2.56 m^2/day. Beach recovery up to 1.1 m^2/day took place between S9 and S13, with positive values of the free-board over this whole period. The destruction of the berms between S7 and S9 and the subsequent generation of new berm deposits are also observed in the lower panel of Figure 7.3.5, which shows the cross-shore distribution of the bed level changes between surveys. These patterns confirm the importance of the overwash process (Matias et al., 2014) and the total run-up (Bergillos et al., 2016d) dictating beach response.

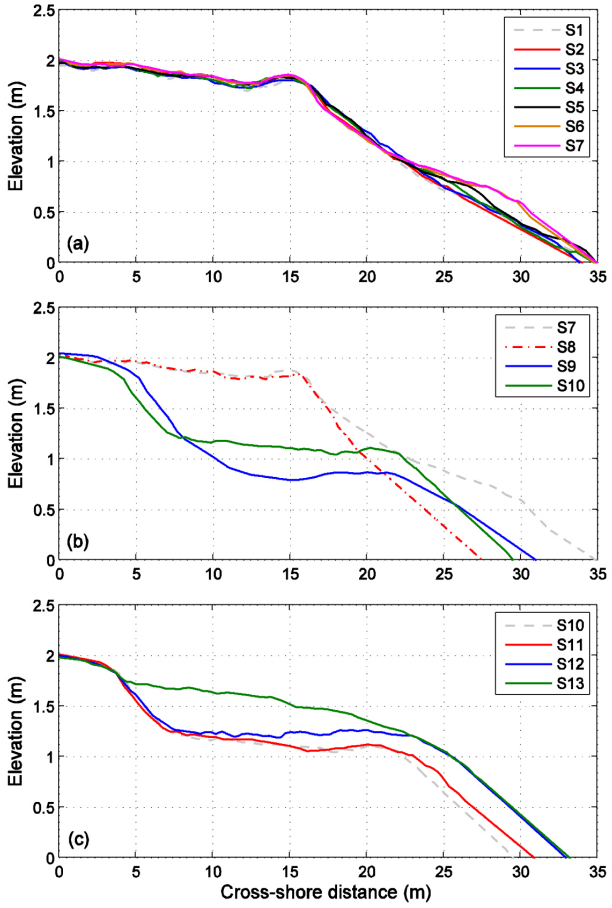

Figure 7.3.3: Evolution of the upper profile during the study period: (a) surveys 1-7 (low energy conditions), (b) surveys 7-10 (south-westerly storm), and (c) surveys 10-13 (south-easterly storm). Elevation = 0 indicates the MLWS level. (Source: Bergillos et al. (2017b). Reproduced with permission of Elsevier).

Figure 7.3.4: (a) Beginning of the overwash during the SW storm (survey 8). (b) Beginning of the SE storm (survey 11). (Source: Bergillos et al. (2017b). Reproduced with permission of Elsevier).

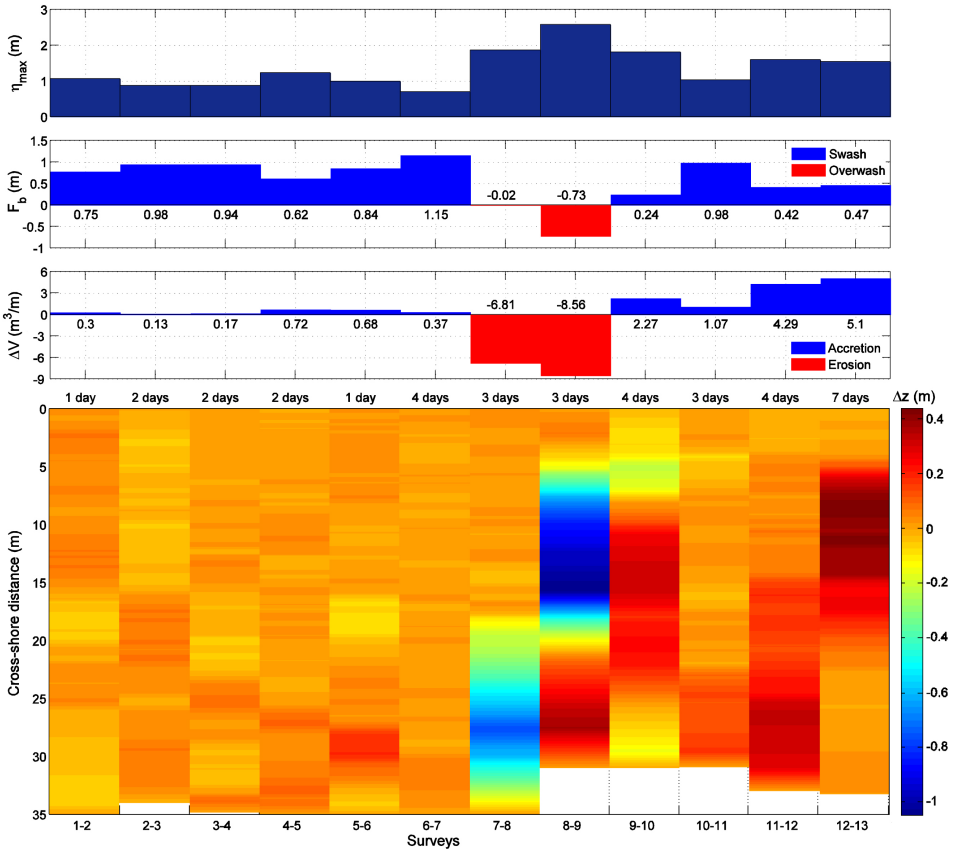

Figure 7.3.5: From top to bottom: maximum total run-up before each survey, minimum free-board before each survey, unit volume differences between surveys, and bed level changes between surveys. The number of days between surveys is indicated in the lower panel. (Source: Bergillos et al. (2017b). Reproduced with permission of Elsevier).

7.3.4 Modelling profile response with XBeach-G

Figure 7.3.6 shows the initial, final measured and final modelled profiles with XBeach-G, along with the differences in the cross-shore distance measured (ΔX_{Meas}) and predicted (ΔX_{Mod}) for the three temporal windows indicated in Figure 7.3.1. As expected, the XBeach-G model does not reproduce the relatively small ($\Delta X_{\text{Meas}} < 0.5$ m) accretional changes observed under LE conditions; however, the fit between modelled and measured bed level variations forced by the SW storm is *excellent* (BSS = 0.96), with RMSE < 0.14 m and bias < 0.13 (Table 7.3.1). This indicates that the model is capable of reproducing the response of the studied coastline section under SW storm conditions, which is in agreement with previous results of the model for two less energetic SW storms in December 2013 and March 2014 (Bergillos et al., 2016c).

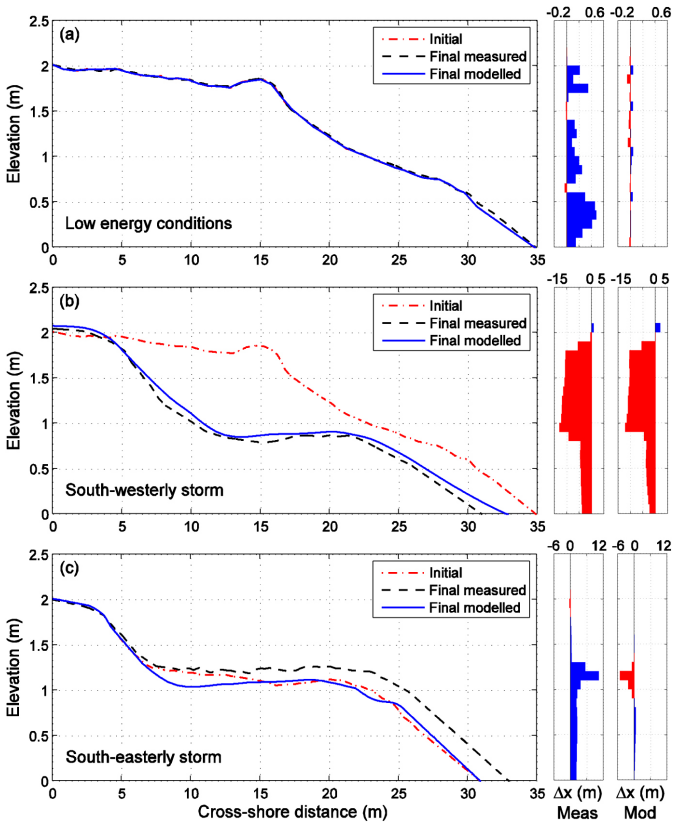

Figure 7.3.6: Initial, final measured and final modelled profiles with XBeach-G: (a) LE conditions window, (b) SW storm, and (c) SE storm. Elevation = 0 indicates the MLWS level. Differences in measured (Meas) and modelled (Mod) cross-shore distances between profiles (Δx) are indicated in the right panels. (Source: Bergillos et al. (2017b). Reproduced with permission of Elsevier).

The comparison of pre- and post-storm measured profiles under SE waves reveals that accretion took place across the upper profile. This deposition was mainly concentrated at an elevation of 1.2 – 1.3 m, coinciding with the total run-up during this window (Figure 7.3.1e) and contrasting with the erosion predicted by the model at this location (Figure 7.3.6c). This behaviour is influenced by the higher LST gradients for SE storms with respect to those for SW conditions (Section 7.3.5), and highlights the need to combine the XBeach-G results with LST gradients to provide more confident predictions of the morphological response under SE storms.

Table 7.3.1: Root-mean-square error (RMSE, in m), relative bias (bias), correlation coefficient (ρ) and Brier Skill Score (BSS) of the modelled changes relative to the measurements of the upper profile.

	Low energy conditions				South-westerly storm				South-easterly storm			
	RMSE	bias	ρ	BSS	RMSE	bias	ρ	BSS	RMSE	bias	ρ	BSS
XBeach-G	0.02	-0.73	0.117	0.007	0.134	0.125	0.966	0.956	0.175	-1.122	0.564	0.137
LST (k=2)	0.015	-0.076	0.519	0.453	0.103	0.091	0.967	0.962	0.082	-0.503	0.91	0.768
LST (k=5)	0.014	-0.068	0.523	0.457	0.09	0.072	0.966	0.964	0.057	-0.269	0.938	0.887
LST (k=10)	0.015	0.074	0.521	0.455	0.092	-0.11	0.961	0.963	0.099	0.516	0.929	0.662

7.3.5 Modelling profile response with XBeach-G and longshore sediment transport

To couple XBeach-G and longshore processes, LST rates along the entire deltaic coastline were computed for the three 2-day windows on the basis of the formulation of Van Rijn (2014), detailed in Section 7.2.3.3. The results indicate that the time-averaged LST rates during the SW storm were greater in the section *Punta del Santo* - Motril Port (up to 0.038 m^3/s) than in the studied section (up to 0.02 m^3/s).

However, the opposite occurred over the SE storm, except in the vicinity of Motril Port, where the shoreline alignment is NW-SE, inducing higher breaking angles from shore-normal (Figure 7.3.7). The maximum and time-averaged LST rates (in absolute value) along the section Guadalfeo River mouth - *Punta del Santo* during the SE storm were up to 0.025 m^3/s (90 m^3/h) and 0.013 m^3/s (46.8 m^3/h), respectively. These values were similar to those under the SW storm (0.022 m^3/s and 0.02 m^3/s, respectively), which was a significantly more energetic window ($H_{max,SW}$ = 4.9 m and $H_{mean,SW}$ = 3.2 m *vs* $H_{max,SE}$ = 3.2 m and $H_{mean,SE}$ = 2.1 m), revealing the importance of LST in this coastal section forced by SE conditions. The average LST rates over the LE window were two orders of magnitude lower than those obtained for both storms (Figure 7.3.7).

Figure 7.3.8 details the LST rates during the entire study period for the surveyed area, whose boundaries are indicated in Figures 7.2.1 and 7.3.7. It is observed that the difference in breaking angles and LST rates between the two boundaries was greater under SE wave conditions, inducing higher gradients in the LST rates and volumes. In addition, the breaking depths and cross-shore distances were significantly lower over the SE storm window than those during the SW window, i.e., LST was concentrated in a smaller width across the nearshore zone, resulting in higher bed level changes across the upper beach profile for the SE storm. To model this cross-shore distribution of LST volume, three different options were tested based on the parametric approach reported in Section 7.2.3.3.

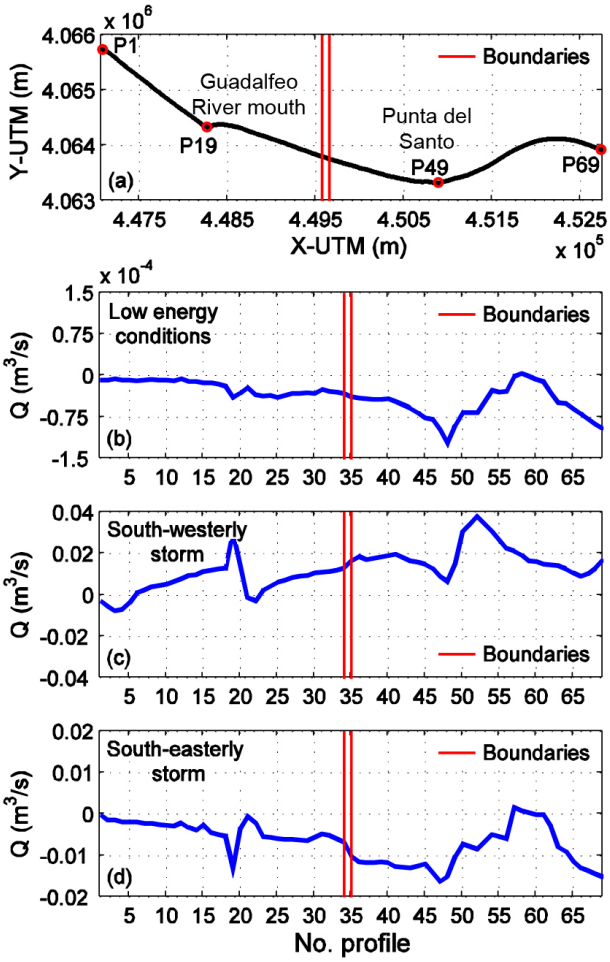

Figure 7.3.7: Alongshore evolution of the time-averaged LST rates: (b) LE conditions window, (c) SW storm, and (d) SE storm. The shoreline and four profile locations are shown in panel a. (Source: Bergillos et al. (2017b). Reproduced with permission of Elsevier).

The cross-shore distributions for each sea state of the three modelled windows are shown in Figure 7.3.9. The LST distribution for $k = 2$ is the most uniform with the maximum located in the middle between the total run-up limit and the breaking line (at $x/x_b = 0.5$). This distribution is similar to that previously observed on sandy beaches (Berek and Dean, 1982; Bayram et al., 2001). The LST distribution for $k = 10$ is the most asymmetrical with the maximum located at $x/x_b = 0.1$, concentrating most of the LST in the inner nearshore region (Figure 7.3.9a3-d3). This behaviour is considered more typical of gravel beaches, where the surf zone does not exist and most of the sediment transport occurs in the swash zone (Buscombe and Masselink, 2006). The LST distribution for $k = 5$ is intermediate between the previous two, with the maximum located at $x/x_b = 0.2$, which is suggested to be expected for MSG beaches. These three cross-shore distributions were used to combine XBeach-G and LST, updating the morphology of the beach profile after each sea state by means of the computed total run-up locations, breaking lengths across the profile and LST volume gradients (Figure 7.3.8).

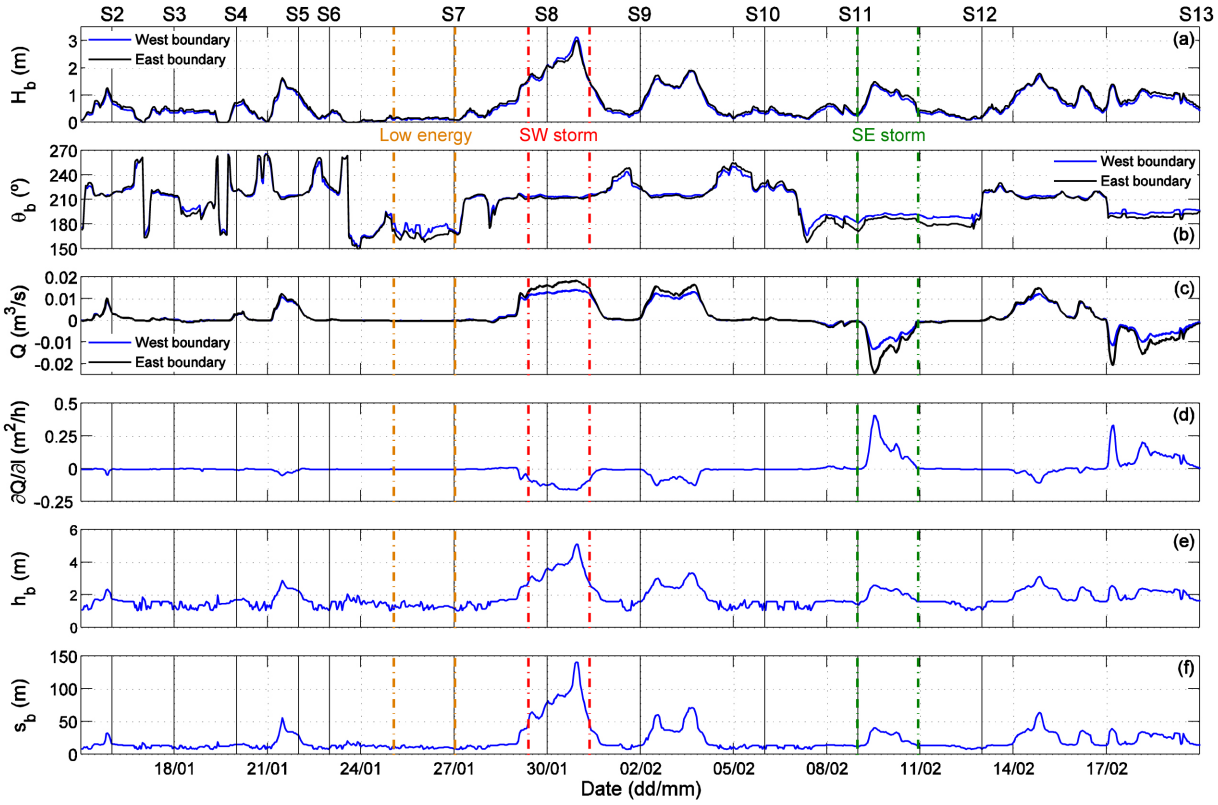

Figure 7.3.8: Evolution of the breaking wave height (a), breaking wave direction (b), LST rate (c), LST gradient (d), breaking depth (e), and breaking cross-shore distance (f) during the study period. The vertical black lines indicate the date of the field surveys and the vertical coloured lines delimit the windows selected to model the profile response. (Source: Bergillos et al. (2017b). Reproduced with permission of Elsevier).

The results of the coupling for the three simulated windows and the three tested cross-shore distributions are shown in Figure 7.3.10. The goodness-of-fit parameters obtained for the different model approaches are summarized in Table 7.3.1. The best model performance (lower RMSE-bias and higher ρ-BSS) is obtained for the combination of XBeach-G and LST considering the intermediate cross-shore distribution of LST ($k = 5$, Figure 7.3.9a2-d2), with the only exception of the slightly higher ρ with $k = 2$ for the SW storm (Table 7.3.1). The intermediate approach improves the XBeach-G results for LE easterly conditions, although the fit for this case is only *fair* (BSS = 0.46). However, the obtained fits for both SW and SE storms are *excellent* (BSS = 0.96 and BSS = 0.89, respectively), inspiring confidence in the proposed approach to model the storm response under varying wave conditions. The improvements with respect to the XBeach-G results are primarily relevant under SE storms ($|\Delta RMSE| > 0.11$ m, $|\Delta bias| > 0.85$, $\Delta\rho > 0.37$ and $\Delta BSS > 0.7$). These results reveal the importance of LST on the coastal response of the surveyed area under SE wave conditions.

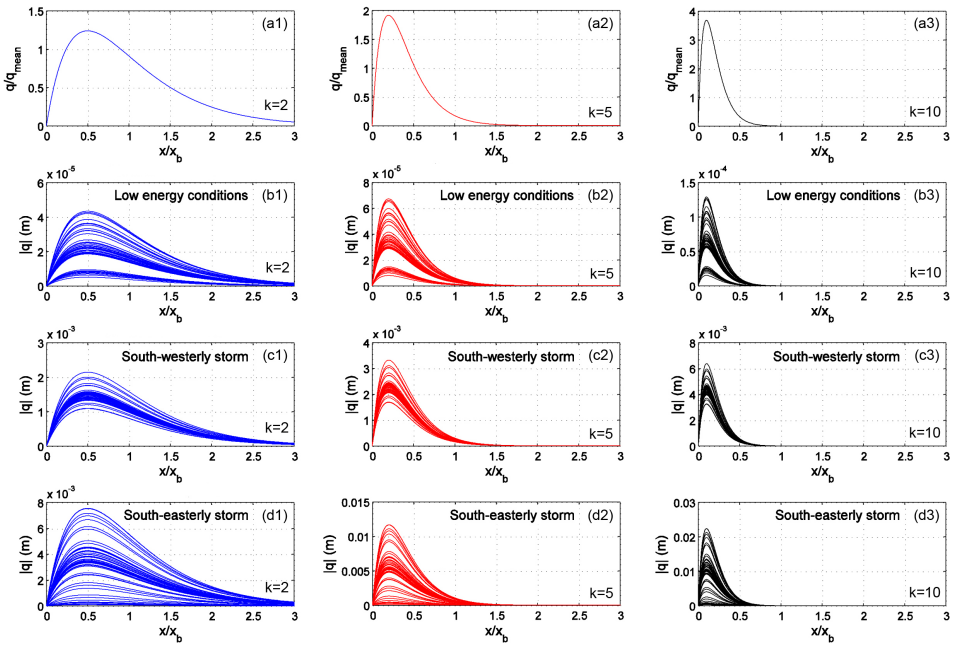

Figure 7.3.9: (a) Normalized cross-shore distribution of LST for $k = 2$, $k = 5$ and $k = 10$. Cross-shore distribution during the LE window (b), the SW storm (c), and the SE storm (d) for k=2 (1), k=5 (2) and k=10 (3). (Source: Bergillos et al. (2017b). Reproduced with permission of Elsevier).

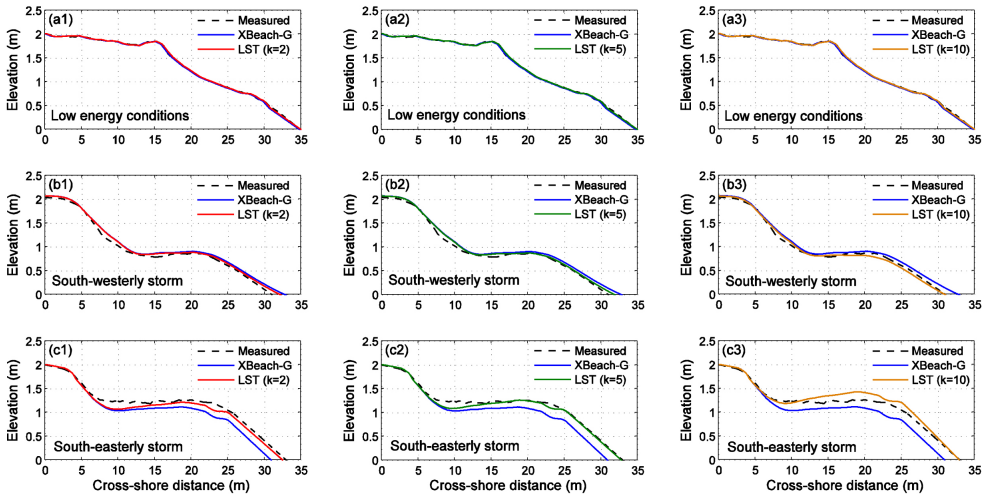

Figure 7.3.10: Measured and modelled profiles with XBeach-G and XB-G+LST: (a) LE window, (b) SW storm and (c) SE storm for $k = 2$ (1), $k = 5$ (2) and $k = 10$ (3). Elevation = 0 indicates the MLWS level. (Source: Bergillos et al. (2017b). Reproduced with permission of Elsevier).

7.3.6 Storm response along the coastline under varying wave directions

Figure 7.3.11 depicts the volumetric changes of the upper profile along the entire 6.8-km deltaic coastline modelled with XBeach-G and through the combination of XBeach-G and LST for $k = 5$. It is observed how XBeach-G predicts beach erosion along most of the coastline, with only some relatively low depositional changes in the stretch Salobreña Rock - *Punta del Santo* (western section) and *Punta del Santo* - Motril Port (eastern section) for SE and SW storms, respectively. As expected, volumetric changes on the basis of the XBeach-G results are significantly higher along the western (eastern) section under SW (SE) storms (Figure 7.3.11b1-b2).

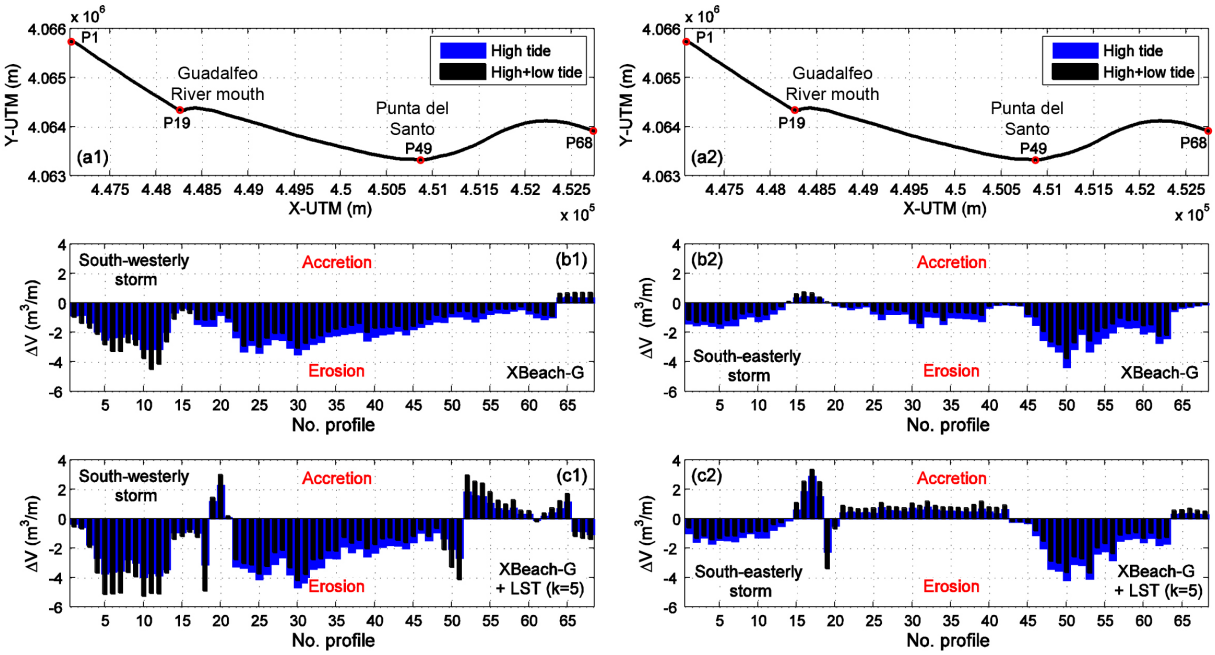

Figure 7.3.11: Alongshore evolution of the modelled volumetric changes on the beach (above the MLWS level) with XBeach-G (b) and coupling XBeach and LST (c) for south-westerly (1) and south-easterly (2) storm conditions. The shoreline and four profile locations are shown in panels a1 and a2. (Source: Bergillos et al. (2017b). Reproduced with permission of Elsevier).

Results with the coupled model for SW storm conditions show more erosion than those obtained with XBeach-G along most of the western section, and also show accretion rather than erosion along most of the eastern section (Figure 7.3.11b1-c1). Under SE storms, the combined approach reverts XBeach-G results along the section Guadalfeo River mouth - *Punta del Santo* (Figure 7.3.11b2-c2), predicting depositional rather than erosional changes, and in agreement with the observations reported in Section 7.3.3. Results along the eastern section reveal larger erosion than XBeach-G predictions in the vicinity of *Punta del Santo* and accretion instead of erosion near Motril Port, influenced by the LST patterns at these locations under SE storms. The variations between both models for such conditions are significantly lower in the stretch Salobreña Rock - Guadalfeo River mouth due to the less LST gradients along this section under SE waves (Figure 7.3.7).

The comparison between the two simulated periods indicates that most of the morphological changes are induced by cross-shore and LST during high tide. During low tide conditions, beach recovery takes place at some locations of the western (eastern) section under SW (SE) storms (Figure 7.3.11), highlighting the importance of the total run-up and overwash process dictating beach response. The results of this section show the potential of the proposed coupled approach to provide more confident predictions of the storm response on coasts dominated by both cross-shore and longshore sediment transport.

7.4 Conclusions

Although gravel and MSG coasts have received increasing attention during recent years, relatively few numerical models have been applied to and compared with field data for these coastal settings. This chapter studies and models the storm response of Playa Granada under varying wave directions by means of field measurements, the application of the XBeach-G model and the proposal of a parametric approach to couple XBeach-G and LST. Based on the observations and results, the following conclusions were drawn:

1. The morphological storm response is clearly related to the difference between the height of the berm and the total run-up (i.e., the free-board). Wave propagation patterns are influenced by the incoming wave directions, generating varying values of total run-up and resulting in different beach responses, with the SW and SE storms eroding and building up the surveyed area, respectively.

2. The XBeach-G model is capable of reproducing the storm response of the beach under SW waves, with BSS > 0.95 and a relative bias < 0.13. However, the accretionary response of the upper profile under SE storms contrasts with the erosion predicted by the model (BSS < 0.14 and |bias| > 1.12). This is influenced by the higher LST gradients under SE storms at the study location compared to those under SW conditions, revealing the necessity to combine XBeach-G with LST.

3. The coupling of XBeach-G and the LST equation of Van Rijn (2014), through consideration of different cross-shore distributions of LST, improved the model predictions, especially under SE storm conditions. The best fits (BSS > 0.96 and BSS > 0.88 for the SW and SE storms, respectively) were obtained with a distribution where the peak of the LST volume is located at a distance from the total run-up limit equal to 20% of the length across the profile between this limit and the breaking line, providing insights into the cross-shore distribution of LST on MSG beaches.

4. The approach that best fitted the beach response was applied to model extreme SW and SE storms along a 6.8-km section of deltaic coastline. Erosional changes were obtained along most of the western section for the SW storm, and in the eastern section and to the west of the river mouth for the SE storm. Erosion occurred in particular under high tide conditions. In contrast, the coupled model predicted accretion along most of the eastern section and in the stretch river mouth - *Punta del Santo* under SW and SE storms, respectively. These depositional responses were not predicted by the XBeach-G model on its own. Thus, the approach proposed in this chapter represents an extension of XBeach-G to make it more suitable for coasts highly influenced by both cross-shore and longshore sediment transport.

CHAPTER 8

CONCLUSIONS AND FUTURE RESEARCH LINES

8.1 Conclusions

This thesis analyses and models the dynamics of mixed sand and gravel (MSG) deltaic coasts based on a multi-scale research carried out in a study site in southern Spain (Guadalfeo delta). For this purpose, five specific objectives were proposed: (1) quantification of the influence of river regulation on the coast, (2) assessment of the implications of delta retreat on coastal process, (3) characterization of the morpho-sedimentary dynamics of the beach profile, (4) study of the coastal response forced by artificial nourishment and (5) investigation of the storm response of the beach under varying wave directions. Based on the observations and results associated with each objective, the following conclusions were drawn:

- The analysis of fluvial and coastal measurements reported in Chapter 3 shows that the dynamics of the Guadalfeo deltaic system is governed by the sediment supplies of the river during intense events. The deltaic coast has lost almost 0.3 hm^3 of sediments since the entry into operation of the dam, whereas the differences between managed and unmanaged scenarios is greater than 0.75 hm^3. Therefore, Rules Reservoir has prevented the advance of a delta that was prograding before the construction of the dam. Based on the results, three new management scenarios were proposed, consisting of the constant or seasonal flow that should be drained by the dam, in combination with the required sediment bypass from the reservoir upstream, to reduce coastal erosion during drought periods.
- The results detailed in Chapter 4 indicate that coastline retreat (up to 40 m/year) and significant erosion in the submerged morphology around the river mouth (up to $190 \cdot 10^3$ m^3/m/year) have occurred since the river damming. The erosion in the delta wedge has been lower since 2008 but the sediment deficit is being propagated towards the east side of the mouth, influenced by the dominance of westerly waves and the presence of river jetties. The erosion in the delta wedge induced lower refraction and greater wave energy around the mouth: the breaking wave height under storm conditions increased up to 10%

(21%) at the eastern (western) flank of the mouth for incoming westerly (easterly) waves. Finally, longshore sediment transport (LST) was significantly modified by the combined effect of changes in the nearshore morphology (partly induced by river regulation) and wave conditions (mainly wave directionality).

- The study of field observations described in Chapter 5 highlights that the generation and subsequent overlapping of berms across the upper profile is responsible for the sediment variability cross-shore and at depth on MSG beaches. The cross-shore locations of these berms are related to the total run-up, as berms are modified by swash action. The beach response was dominated by the coarse gravel fraction due to the selective removal of the finer material and the observed reflective shape of the profile after storms was also similar to those found on pure gravel beaches. On the other hand, the beach recovery was shown to occur at a faster rate than on sandy beaches. Finally, the results of this chapter indicate that total run-up (including water-level) reached during an event represents a more accurate threshold than wave height for differentiating between erosional and depositional conditions.

- According to the results presented in Chapter 6, severe coastline retreat (dry beach area loss > 208 m^2/day) occurred during the 45 days following the artificial nourishment ended in December 2014. This was attributable to the morphology of the nourished coastline, the different characteristics of the sediment used for replenishment compared to natural sizes, and the occurrence of an intense westerly storm. The dry beach extension increased afterwards influenced by the westward longshore sediment transport due to the dominance of easterly waves. The formulation of Van Rijn (2014) was demonstrated to provide the best fits to the observed volumetric changes, obtaining modelled/measured ratios of 93.1% and 77.4% for the two study beach profiles. Finally, the outputs of the one-line model based on the Van Rijn approach were also the best, with root-mean-square errors decreasing during the study period and lower than 4.6 m over the last 3 months. These results show that the joint application of a calibrated wave propagation model, the LST equation proposed by Van Rijn (2014) and the one-line model constitutes a management tool to predict the plan view response of MSG coasts.

- Finally, the investigation carried out in Chapter 7 reveals that wave propagation patterns are influenced by the incoming wave directions, generating varying values of total run-up and resulting in different beach responses, with the south-westerly (SW) and south-easterly (SE) storms eroding and building up the beach, respectively. The XBeach-G model was capable of reproducing the storm response of the beach under SW waves, with Brier Skill Scores (BSS) higher than 0.95. However, the accretionary response of the beach observed under SE storms contrasted with the erosion predicted by the model (BSS<0.14). For this reason, the model was coupled to the LST equation of Van Rijn (2014) through a parametric formulation to consider different cross-shore distributions of LST. The results of the coupling improved the model predictions, especially under SE storms. The best fits (BSS>0.88) were obtained with a distribution where the peak of the LST is located at a distance from the total run-up limit equal to 20% of the length across the profile between this limit and the breaking line. These results provide insights into the cross-shore distribution of LST on MSG beaches and represent an extension of XBeach-G to make it more suitable for coasts highly influenced by both cross-shore and longshore sediment transport.

8.2 Future research lines

The results obtained in this thesis and the conclusions derives from them allow suggesting the following future research lines in order to complement the main experimental findings, improve the potential of the developed tools and apply the proposed methodologies for management purposes:

- To perform large-scale laboratory experiments of MSG beach profiles to complement both the field observations analysed in this thesis and previous large-scale laboratory studies of sandy beaches (Wang and Kraus, 2005; Guannel et al., 2007; Baldock et al., 2011; Masselink et al., 2016a) and gravel barriers (Williams et al., 2012a).
- To compare the profile responses of MSG coasts with those previously addressed on sandy beaches (e.g., Medina et al. (1993), Muñoz-Perez et al. (1999), Muñoz-Perez and Medina (2006) or Muñoz-Perez and Medina (2010), among others). This comparison would focus on: (1) assessment of erosion/accretion rates as a function of wave and water-level, (2) analysis of empirical orthogonal functions, and (3) testing and analysis of different hydrodynamic and morphological parameters (e.g., the Dean Number). The final purpose would be finding dimensionless parameters that allow a proper comparison between both types of beaches.
- To use both the field data and laboratory measurements in order to develop and validate a morphodynamic model for the prediction of the beach profile response under non-storm conditions. This would allow extending the coupled approach proposed in Chapter 7 from the profile response to single storms to the long-term beach dynamics.
- To combine the methodologies proposed in Chapters 6 and 7 with maritime climate simulation methods (including the effects of global warming), statistical downscaling approaches and Monte Carlo techniques in order to forecast the coastline evolution and the storm response of MSG beaches, respectively, including the quantification of the predictions uncertainty. This coupling could be extensible to the recovery model proposed in the previous research line.
- To investigate the efficiency of different management strategies for mitigating and/or adapting to global erosional problems and the future consequences of sea-level rise, such as: (1) sediment bypass from the reservoirs upstream (testing different volumes and sediment sizes), artificial nourishment and mega-nourishment (testing different coastline geometries, nourished volumes and sediment sizes), or (3) maritime structures (testing different number of structures, orientations and dimensions). This is particularly relevant in deltaic areas, which are experiencing severe erosion due to human interventions and are especially vulnerable to the effects of global warming.

Bibliography

Abam, T. (1999). “Impact of dams on the hydrology of the Niger Delta”. In: *Bulletin of Engineering Geology and the Environment* 57.3, pp. 239–251.

Aguilar, C (2008). “Efectos de escala en procesos hidrológicos. Aplicación a la cuenca del río Guadalfeo (Granada)”. PhD thesis. University of Córdoba.

Aguilar, C, Herrero, J, and Polo, M. (2010). “Topographic effects on solar radiation distribution in mountainous watersheds and their influence on reference evapotranspiration estimates at watershed scale”. In: *Hydrology and Earth System Sciences* 14.12, pp. 2479–2494.

Aguilar, C., Herrero, J., Millares, A., Losada, M. A., and Polo, M. J. (2014). “Meteomap: Generation Of Meteorological Variables For Distributed Physically-Based Hydrological Modeling”. In: *Proceedings of the 11th International Conference on Hydroinformatics*.

Almar, R. et al. (2015). “Response of the Bight of Benin (Gulf of Guinea, West Africa) coastline to anthropogenic and natural forcing, Part1: Wave climate variability and impacts on the longshore sediment transport”. In: *Continental Shelf Research* 110, pp. 48–59.

Almeida, L. P., Masselink, G., McCall, R., and Russell, P. (2017). “Storm overwash of a gravel barrier: Field measurements and XBeach-G modelling”. In: *Coastal Engineering* 120, pp. 22–35.

Amblas, D., Canals, M., Lastras, G., Berné, S., and Loubrieu, B. (2004). “Imaging the Seascapes of the Mediterranean”. In: *Oceanography* 17, pp. 144–55.

Anthony, E., Almar, R, and Aagaard, T (2016). “Recent shoreline changes in the Volta River delta, West Africa: the roles of natural processes and human impacts”. In: *African Journal of Aquatic Science* 41.1, pp. 81–87.

Anthony, E. J. (2015). “Wave influence in the construction, shaping and destruction of river deltas: A review”. In: *Marine Geology* 361, pp. 53–78.

Anthony, E. J., Marriner, N., and Morhange, C. (2014). “Human influence and the changing geomorphology of Mediterranean deltas and coasts over the last 6000 years: From progradation to destruction phase?” In: *Earth-Science Reviews* 139, pp. 336–361.

Arnaud-Fassetta, G. (2003). “River channel changes in the Rhône Delta (France) since the end of the Little Ice Age: geomorphological adjustment to hydroclimatic change and natural resource management”. In: *Catena* 51.2, pp. 141–172.

Austin, M. J. and Masselink, G (2006). “Observations of morphological change and sediment transport on a steep gravel beach”. In: *Marine Geology* 229.1, pp. 59–77.

Ávila, A (2007). “Procesos de múltiple escala en la evolución de la línea de costa”. PhD thesis. University of Granada.

Baldock, T., Alsina, J., Caceres, I, Vicinanza, D, Contestabile, P, Power, H, and Sanchez-Arcilla, A (2011). “Large-scale experiments on beach profile evolution and surf and swash zone sediment transport induced by long waves, wave groups and random waves”. In: *Coastal Engineering* 58.2, pp. 214–227.

Baquerizo, A. and Losada, M. A. (2008). “Human interaction with large scale coastal morphological evolution. An assessment of the uncertainty”. In: *Coastal Engineering* 55.7, pp. 569–580.

Bárcenas, P, Lobo, F. J., Macías, J, Fernández-Salas, L., and Río, V. D. del (2011). “Spatial variability of surficial sediments on the northern shelf of the Alboran Sea: the effects of hydrodynamic forcing and supply of sediment by rivers”. In: *Journal of Iberian Geology* 37.2, pp. 195–214.

Bayram, A., Larson, M., Miller, H. C., and Kraus, N. C. (2001). “Cross-shore distribution of longshore sediment transport: comparison between predictive formulas and field measurements”. In: *Coastal Engineering* 44.2, pp. 79–99.

Berek, E. P. and Dean, R. G. (1982). “Field investigation of longshore transport distribution”. In: *Coastal Engineering Proceedings*. Vol. 1. 18.

Bergillos, R. J. and Ortega-Sánchez, M. (2017). “Assessing and mitigating the landscape effects of river damming on the Guadalfeo River delta, southern Spain”. In: *Landscape and Urban Planning* 165, pp. 117–129.

Bergillos, R. J., Rodríguez-Delgado, C, López-Ruiz, A, Millares, A, Ortega-Sánchez, M, and Losada, M. A. (2015a). “Recent human-induced coastal changes in the Guadalfeo river deltaic system (southern Spain)”. In: *Proceedings of the 36th IAHR-International Association for Hydro-Environment Engineering and Research World Congress*.

Bergillos, R. J., Ortega-Sánchez, M, Masselink, G, and Losada, M. A. (2015b). “Urban planning analysis of Mediterranean deltas - Guadalfeo case study”. In: *12th International Conference on the Mediterranean Coastal Environment*. Vol. 1, pp. 143–154.

Bergillos, R. J., Rodríguez-Delgado, C, Millares, A, Ortega-Sánchez, M, and Losada, M. A. (2016a). “Impact of river regulation on a Mediterranean delta: assessment of managed versus unmanaged scenarios”. In: *Water Resources Research* 52, pp. 5132–5148.

Bergillos, R. J., López-Ruiz, A, Ortega-Sánchez, M, Masselink, G, and Losada, M. A. (2016b). “Implications of delta retreat on wave propagation and longshore sediment transport - Guadalfeo case study (southern Spain)”. In: *Marine Geology* 382, pp. 1–16.

Bergillos, R. J., Masselink, G, McCall, R. T., and Ortega-Sánchez, M (2016c). “Modelling overwash vulnerability along mixed sand-gravel coastlines with XBeach-G: Case study of Playa Granada, southern Spain”. In: *Coastal Engineering Proceedings*. Vol. 1. 35.

Bergillos, R. J., Ortega-Sánchez, M, Masselink, G, and Losada, M. A. (2016d). “Morpho-sedimentary dynamics of a micro-tidal mixed sand and gravel beach, Playa Granada, southern Spain”. In: *Marine Geology* 379, pp. 28–38.

Bergillos, R. J., Rodríguez-Delgado, C, and Ortega-Sánchez, M (2017a). “Advances in management tools for modeling artificial nourishments in mixed beaches”. In: *Journal of Marine Systems* 172, pp. 1–13.

Bergillos, R. J., Masselink, G, and Ortega-Sánchez, M (2017b). “Coupling cross-shore and longshore sediment transport to model storm response along a mixed sand-gravel coast under varying wave directions”. In: *Coastal Engineering* 129C, pp. 93–104.

Bernabeu Tello, A., Muñoz Pérez, J., and Medina Santamaría, R (2002). “Influence of a rocky platform in the profile morphology: Victoria Beach, Cádiz (Spain)”. In: *Ciencias Marinas* 28.2, pp. 181–192.

Booij, N, Ris, R. C., and Holthuijsen, L. H. (1999). “A third-generation wave model for coastal regions: 1. Model description and validation”. In: *Journal of Geophysical Research: Oceans* 104.C4, pp. 7649–7666.

Bowden, K. F. (1983). *Physical oceanography of coastal waters*. Ellis Horwood Ltd., Chichester England.

Brad Murray, A, Gasparini, N. M., Goldstein, E. B., and Wegen, M. van der (2016). "Uncertainty quantification in modeling earth surface processes: more applicable for some types of models than for others". In: *Computers & Geosciences* 90, pp. 6–16.

Bramato, S., Ortega-Sánchez, M., Mans, C., and Losada, M. A. (2012). "Natural recovery of a mixed sand and gravel beach after a sequence of a short duration storm and moderate sea states". In: *Journal of Coastal Research* 28.1, pp. 89–101.

Buscombe, D. and Masselink, G. (2006). "Concepts in gravel beach dynamics". In: *Earth-Science Reviews* 79.1, pp. 33–52.

Camus, P., Mendez, F. J., and Medina, R. (2011). "A hybrid efficient method to downscale wave climate to coastal areas". In: *Coastal Engineering* 58.9, pp. 851–862.

Camus, P. et al. (2014). "A weather-type statistical downscaling framework for ocean wave climate". In: *Journal of Geophysical Research: Oceans* 119.11, pp. 7389–7405.

Capel-Molina, J. (1974). "Génesis de las inundaciones de Octubre de 1973 en el Sureste de la Península Ibérica". In: *Cuadernos geográficos de la Universidad de Granada* 4, pp. 149–166.

Carter, R. W. G. and Orford, J. D. (1984). "Coarse clastic barrier beaches: a discussion of the distinctive dynamic and morphosedimentary characteristics". In: *Developments in Sedimentology* 39, pp. 377–389.

— (1991). "The sedimentary organisation and behaviour of drift-aligned gravel barriers". In: *Proceedings of the 3rd Coastal Sediments*, pp. 934–948.

Cats, G. and Wolters, L. (1996). "The Hirlam project [meteorology]". In: *Computational Science & Engineering* 3.4, pp. 4–7.

Cavazza, W. and Wezel, F. C. (2003). "The Mediterranean region - A geological primer". In: *Episodes* 26.3, pp. 160–168.

Chen, L. and Stone, M. C. (2008). "Influence of bed material size heterogeneity on bedload transport uncertainty". In: *Water Resources Research* 44.1, W01405.

Clemmensen, L. B. and Nielsen, L. (2010). "Internal architecture of a raised beach ridge system (Anholt, Denmark) resolved by ground-penetrating radar investigations". In: *Sedimentary Geology* 223.3, pp. 281–290.

Clemmensen, L. B., Glad, A. C., and Kroon, A. (2016). "Storm flood impacts along the shores of micro-tidal inland seas: A morphological and sedimentological study of the Vesterlyng beach, the Belt Sea, Denmark". In: *Geomorphology* 253, pp. 251–261.

Coleman, J. M. and Wright, L. (1975). "Modern river deltas: variability of processes and sand bodies". In: *Houston Geological Society*.

Comas, M. C., Platt, J. P., Soto, J. I., and Watts, A. B. (1999). "The origin and Tectonic History of the Alboran Basin: Insights from Leg 161 Results". In: *Ocean Drilling Program*. Ed. by R. Zahn, M. C. Comas, and A. Klaus. Scientific Results, 161: Proceedings of the Ocean Drilling Program, pp. 555–580.

Dashtgard, S. E., Gingras, M. K., and Butler, K. E. (2006). "Sedimentology and stratigraphy of a transgressive, muddy gravel beach: Waterside Beach, Bay of Fundy, Canada". In: *Sedimentology* 53.2, pp. 279–296.

De Alegría-Arzaburu, A. R. and Masselink, G. (2010). "Storm response and beach rotation on a gravel beach, Slapton Sands, UK". In: *Marine Geology* 278.1, pp. 77–99.

De Vriend, H. J., Capobianco, M, Chesher, T, De Swart, H. E. d., Latteux, B, and Stive, M. J. F. (1993). "Approaches to long-term modelling of coastal morphology: a review". In: *Coastal Engineering* 21.1-3, pp. 225–269.

Dean, R. G. and Dalrymple, R. A. (2002). *Coastal processes with engineering applications*. Cambridge University Press, New York.

Del Valle, R., Medina, R., and Losada, M. A. (1993). "Dependence of coefficient K on grain size". In: *Journal of Waterway, Port, Coastal, and Ocean Engineering* 119.5, pp. 568–574.

Deltares (2014). *XBeach-G GUI 1.0. User Manual*. Delft, The Netherlands.

Díez, J., Uriarte, A., Cánovas, V., and Medina, R. (2017). "A parametric model for dry beach equilibrium profiles". In: *Coastal Engineering* 127, pp. 134–144.

Duque, C., Calvache, M. L., Pedrera, A., Martín-Rosales, W., and López-Chicano, M. (2008). "Combined time domain electromagnetic soundings and gravimetry to determine marine intrusion in a detrital coastal aquifer (Southern Spain)". In: *Journal of Hydrology* 349.3, pp. 536–547.

Duque, C., Calvache, M. L., and Engesgaard, P. (2010). "Investigating river–aquifer relations using water temperature in an anthropized environment (Motril-Salobreña aquifer)". In: *Journal of Hydrology* 381.1, pp. 121–133.

Egüen, M, Aguilar, C, Polo, M., Moreno, I, Herrero, J, Millares, A, and Losada, M. (2009). "WiMMed, a distributed physically-based watershed model (II): application examples". In: *Environmental Hydraulics: Theoretical, Experimental & Computational Solutions, López-Jiménez el al.(eds.), Taylor&Francis, London*, pp. 229–231.

Eikaas, H. S. and Hemmingsen, M. A. (2006). "A GIS approach to model sediment reduction susceptibility of mixed sand and gravel beaches". In: *Environmental Management* 37.6, pp. 816–825.

El Banna, M. M. and Frihy, O. E. (2009). "Human-induced changes in the geomorphology of the northeastern coast of the Nile delta, Egypt". In: *Geomorphology* 107.1, pp. 72–78.

Elshinnawy, A. I., Medina, R., and González, M. (2017). "On the relation between the direction of the wave energy flux and the orientation of equilibrium beaches". In: *Coastal Engineering* 127, pp. 20–36.

Engels, S. and Roberts, M. C. (2005). "The architecture of prograding sandy-gravel beach ridges formed during the last Holocene highstand: Southwestern British Columbia, Canada". In: *Journal of Sedimentary Research* 75.6, pp. 1052–1064.

Fan, H., Huang, H., and Zeng, T. (2006). "Impacts of anthropogenic activity on the recent evolution of the Huanghe (Yellow) River Delta". In: *Journal of Coastal Research* 22.4, pp. 919–929.

Félix, A, Baquerizo, A, Santiago, J. M., and Losada, M. A. (2012). "Coastal zone management with stochastic multi-criteria analysis". In: *Journal of Environmental Management* 112, pp. 252–266.

Fernández-Salas, L. M., Lobo, F. J., Sanz, J. L., Río, V Díaz-del, García, M. C., and Moreno, I (2007). "Morphometric analysis and genetic implications of pro-deltaic sea-floor undulations in the northern Alboran Sea margin, western Mediterranean Basin". In: *Marine Geology* 243.1, pp. 31–56.

Folk, R. L. (1980). *Petrology of sedimentary rocks*. Hemphill Publishing Company.

Forbes, D. L., Orford, J. D., Carter, R. W. G., Shaw, J, and Jennings, S. C. (1995). "Morphodynamic evolution, self-organisation, and instability of coarse-clastic barriers on paraglacial coasts". In: *Marine Geology* 126.1, pp. 63–85.

French, J. and Burningham, H. (2015). "Wave-driven sediment pathways on a gravel-dominated coast subject to a strongly bi-modal wave climate, Suffolk, eastern UK". In: *Proceedings of the 8th Coastal Sediments*.

Frihy, O. and Komar, P. (1993). "Long-term shoreline changes and the concentration of heavy minerals in beach sands of the Nile Delta, Egypt". In: *Marine Geology* 115.3-4, pp. 253–261.

Frihy, O. E., Fanos, A. M., Khafagy, A. A., and Komar, P. D. (1991). "Patterns of nearshore sediment transport along the Nile Delta, Egypt". In: *Coastal Engineering* 15.5-6, pp. 409–429.

Frihy, O. E., Debes, E. A., and El Sayed, W. R. (2003). "Processes reshaping the Nile delta promontories of Egypt: pre-and post-protection". In: *Geomorphology* 53.3, pp. 263–279.

Garel, E, Sousa, C, Ferreira, Ó, and Morales, J. (2014). "Decadal morphological response of an ebb-tidal delta and down-drift beach to artificial breaching and inlet stabilisation". In: *Geomorphology* 216, pp. 13–25.

Garel, E, Sousa, C, and Ferreira, Ó (2015). "Sand bypass and updrift beach evolution after jetty construction at an ebb-tidal delta". In: *Estuarine, Coastal and Shelf Science* 167, pp. 4–13.

Goda, Y. (2010). *Random seas and design of maritime structures*. World Scientific.

Gómez-Beas, R, Monino, A, and Polo, M. (2012). "Development of a management tool for reservoirs in Mediterranean environments based on uncertainty analysis". In: *Natural Hazards and Earth System Science* 12.5, pp. 1789–1797.

González, M., Medina, R., and Losada, M. (2010). "On the design of beach nourishment projects using static equilibrium concepts: Application to the Spanish coast". In: *Coastal Engineering* 57.2, pp. 227–240.

Guannel, G., Özkan-Haller, H. T., Haller, M. C., and Kirby, J. T. (2007). "Influence of velocity moments on sand bar movement during CROSSTEX". In: *Proceedings of the 6th Coastal Sediments*, pp. 28–41.

Herrero, J (2007). "Modelo físico de acumulación y fusión de la nieve: aplicación en Sierra Nevada (España)". PhD thesis. University of Granada.

Herrero, J, Polo, M., Moñino, A, and Losada, M. (2009). "An energy balance snowmelt model in a Mediterranean site". In: *Journal of Hydrology* 371.1, pp. 98–107.

Herrero, J., Millares, A., Aguilar, C., Egüen, M., Losada, M. A., and Polo, M. J. (2014). "Coupling Spatial And Time Scales In The Hydrological Modelling Of Mediterranean Regions: WiMMed". In: *Proceedings of the 11th International Conference on Hydroinformatics*.

Hoffmann, G. (1987). "Holozänstratigraphie und Küstenlinienverlagerung an der andalusischen Mittelmeerküste". PhD thesis. Universität Bremen.

Holthuijsen, L., Booij, N, and Ris, R. (1993). "A spectral wave model for the coastal zone". In: *Ocean Wave Measurement and Analysis*. ASCE, pp. 630–641.

Hood, W. G. (2010). "Delta distributary dynamics in the Skagit River Delta (Washington, USA): extending, testing, and applying avulsion theory in a tidal system". In: *Geomorphology* 123.1, pp. 154–164.

Hooke, J. M. (2006). "Human Impacts on Fluvial Systems in the Mediterranean Region". In: *Geomorphology* 79.3-4, pp. 311–35.

Horn, D. P. and Walton, S. M. (2007). "Spatial and temporal variations of sediment size on a mixed sand and gravel beach". In: *Sedimentary Geology* 202.3, pp. 509–528.

Ibáñez, C., Day, J. W., and Reyes, E. (2014). "The Response of Deltas to Sea-Level Rise: Natural Mechanisms and Management Options to Adapt to High-End Scenarios". In: *Ecological Engineering* 65, pp. 122–130.

Inman, D. L. and Bagnold, R. A. (1963). "Littoral processes". In: *The Sea* 3, pp. 529–553.

Inman, D. L. and Jenkins, S. A. (1984). "The Nile littoral cell and man's impact on the coastal zone of the southeastern Mediterranean". In: *Coastal Engineering Proceedings* 1.19.

Ivamy, M. C. and Kench, P. S. (2006). "Hydrodynamics and morphological adjustment of a mixed sand and gravel beach, Torere, Bay of Plenty, New Zealand". In: *Marine Geology* 228.1, pp. 137–152.

Jabaloy-Sánchez, A., Lobo, F. J., Azor, A., Bárcenas, P., Fernández-Salas, L. M., Del Río, V. D., and Pérez-Peña, J. V. (2010). "Human-driven coastline changes in the Adra River deltaic system, southeast Spain". In: *Geomorphology* 119.1, pp. 9–22.

Jabaloy-Sánchez, A. et al. (2014). "Six thousand years of coastline evolution in the Guadalfeo deltaic system (southern Iberian Peninsula)". In: *Geomorphology* 206, pp. 374–391.

Jackson, D. W. T., Cooper, J. A. G., and Del Rio, L (2005). "Geological control of beach morphodynamic state". In: *Marine Geology* 216.4, pp. 297–314.

Jackson, N. L. and Nordstrom, K. F. (2011). "Aeolian sediment transport and landforms in managed coastal systems: a review". In: *Aeolian Research* 3.2, pp. 181–196.

Jamal, M. H., Simmonds, D. J., and Magar, V (2014). "Modelling gravel beach dynamics with XBeach". In: *Coastal Engineering* 89, pp. 20–29.

Jamal, M. H., Simmonds, D. J., Magar, V., and Pan, S. (2011). "Modelling infiltration on gravel beaches with an XBeach variant". In: *Coastal Engineering Proceedings*. Vol. 1. 32.

Jeftic, L., Keckes, S., and Pernetta, J. C. (1996). *Climate change and the Mediterranean: environmental and societal impacts of climatic change and sea level rise in the Mediterranean region. Volume 2.* Edward Arnold, Hodder Headline, PLC.

Jennings, R and Shulmeister, J (2002). "A field based classification scheme for gravel beaches". In: *Marine Geology* 186.3, pp. 211–228.

Jiménez, J. A. and Sánchez-Arcilla, A. (1993). "Medium-term coastal response at the Ebro delta, Spain". In: *Marine Geology* 114.1, pp. 105–118.

Jiménez, J., Sánchez-Arcilla, A., Valdemoro, H. I., Gracia, V., and Nieto, F. (1997). "Processes reshaping the Ebro delta". In: *Marine Geology* 144.1, pp. 59–79.

Kamphuis, J. W. (1991a). "Alongshore sediment transport rate". In: *Journal of Waterway, Port, Coastal, and Ocean Engineering* 117.6, pp. 624–640.

— (2002). "Alongshore transport rate of sand". In: *Coastal Engineering Proceedings*. Vol. 2. American Society of Civil Engineers, pp. 2478–2490.

Kamphuis, J. (1991b). "Alongshore sediment transport rate distribution". In: *Proceedings of the 3rd Coastal Sediments*, pp. 170–183.

Komar, P. D. and Inman, D. L. (1970). "Longshore sand transport on beaches". In: *Journal of Geophysical Research* 75.30, pp. 5914–5927.

Komar, P. D. (1983). "Nearshore currents and sand transport on beaches". In: *Elsevier oceanography series* 35, pp. 67–109.

Kondolf, G., Rubin, Z., and Minear, J. (2014). "Dams on the Mekong: cumulative sediment starvation". In: *Water Resources Research* 50.6, pp. 5158–5169.

Le, T. V. H., Nguyen, H. N., Wolanski, E., Tran, T. C., and Haruyama, S. (2007). "The combined impact on the flooding in Vietnam's Mekong River delta of local man-made structures, sea level rise, and dams upstream in the river catchment". In: *Estuarine, Coastal and Shelf Science* 71.1, pp. 110–116.

Lee, G.-h., Nicholls, R. J., and Birkemeier, W. A. (1998). "Storm-driven variability of the beach-nearshore profile at Duck, North Carolina, USA, 1981–1991". In: *Marine Geology* 148.3, pp. 163–177.

Lesser, G. R. (2009). "An approach to medium-term coastal morphological modeling". PhD thesis. Delft University of Technology, Delft, The Netherlands.

Lesser, G. R., Roelvink, J. A., Van Kester, J. A.T. M., and Stelling, G. S. (2004). "Development and validation of a three-dimensional morphological model". In: *Coastal Engineering* 51.8, pp. 883–915.

Li, F., Dyt, C., and Griffiths, C. (2006). "Multigrain sedimentation/erosion model based on cross-shore equilibrium sediment distribution: application to nourishment design". In: *Estuarine, Coastal and Shelf Science* 67.4, pp. 664–672.

Liquete, C., Canals, M., Arnau, P., Urgeles, R., and Madron, X. D. de (2004). "The impact of humans on strata formation along Mediterranean margins". In: *Oceanography* 17, pp. 70–79.

Liquete, C, Arnau, P, Canals, M, and Colas, S (2005). "Mediterranean river systems of Andalusia, southern Spain, and associated deltas: a source to sink approach". In: *Marine Geology* 222, pp. 471–495.

Lobo, F. J., Fernández-Salas, L. M., Moreno, I, Sanz, J. L., and Maldonado, A. (2006). "The sea-floor morphology of a Mediterranean shelf fed by small rivers, northern Alboran Sea margin". In: *Continental Shelf Research* 26.20, pp. 2607–2628.

Lobo, F., Goff, J., Mendes, I, Bárcenas, P, Fernández-Salas, L., Martín-Rosales, W, Macías, J, and Río, V. D. del (2015). "Spatial variability of prodeltaic undulations on the Guadalfeo River prodelta: support to the genetic interpretation as hyperpycnal flow deposits". In: *Marine Geophysical Research* 36.4, pp. 309–333.

López-Ruiz, A., Ortega-Sánchez, M., Baquerizo, A., Navidad, D., and Losada, M. A. (2012a). "Nonuniform alongshore sediment transport induced by coastline curvature". In: *Coastal Engineering Proceedings*. Vol. 1. 33, pp. 3046–3052.

López-Ruiz, A., Ortega-Sánchez, M., Baquerizo, A., and Losada, M. A. (2012b). "Short and medium-term evolution of shoreline undulations on curvilinear coasts". In: *Geomorphology* 159, pp. 189–200.

— (2014). "A note on alongshore sediment transport on weakly curvilinear coasts and its implications". In: *Coastal Engineering* 88, pp. 143–153.

López de San Román-Blanco, B (2004). "Dynamics of gravel and mixed sand and gravel beaches". PhD thesis. Imperial College, London, UK.

López de San Román-Blanco, B et al. (2006). "Large scale experiments on gravel and mixed beaches: Experimental procedure, data documentation and initial results". In: *Coastal Engineering* 53.4, pp. 349–362.

López, M., López, I., and Iglesias, G. (2012). "Hindcasting Long Waves in a Port: An ANN Approach". In: *Coastal Engineering Journal* 57.4, p. 1550019.

Losada, M. A., Baquerizo, A, Ortega-Sánchez, M, and Ávila, A (2011). "Coastal evolution, sea level, and assessment of intrinsic uncertainty". In: *Journal of Coastal Research* 59, pp. 218–228.

Maetens, W., Vanmaercke, M., Poesen, J., Jankauskas, B., Jankauskiene, G., and Ionita, I. (2012). "Effects of Land Use on Annual Runoff and Soil Loss in Europe and the Mediterranean: a Meta-Analysis of Plot Data". In: *Progress in Physical Geography* 36.5, pp. 599–653.

Maldonado, A. and Comas, M. C. (1992). "Geology and geophysics of the Alboran Sea: An introduction". In: *Geo-Marine Letters* 12.2-3, pp. 61–65.

Marriner, N. and Morhange, C. (2007). "Geoscience of Ancient Mediterranean Harbours". In: *Earth-Science Reviews* 80.3-4, pp. 137–94.

Mason, T and Coates, T. T. (2001). "Sediment transport processes on mixed beaches: a review for shoreline management". In: *Journal of Coastal Research* 17, pp. 645–657.

Mason, T, Voulgaris, G, Simmonds, D. J., and Collins, M. B. (1997). "Hydrodynamics and sediment transport on composite (Mixed Sand/Shingle) and sand beaches: a comparison". In: *Proceedings of the 3rd Coastal Dynamics*. ASCE, pp. 48–57.

Masselink, G., McCall, R. T., Poate, T., and Van Geer, P. (2014). "Modelling storm response on gravel beaches using XBeach-G". In: *Proceedings of the Institution of Civil Engineers-Maritime Engineering*. Vol. 167. 4. Thomas Telford Ltd, pp. 173–191.

Masselink, G. et al. (2016a). “Large-scale Barrier Dynamics Experiment II (BARDEX II): Experimental design, instrumentation, test program, and data set”. In: *Coastal Engineering* 113, pp. 3–18.

Masselink, G., Scott, T., Poate, T., Russell, P., Davidson, M., and Conley, D. (2016b). “The extreme 2013/2014 winter storms: hydrodynamic forcing and coastal response along the southwest coast of England”. In: *Earth Surface Processes and Landforms* 41.3, pp. 378–391.

Masselink, G., Russell, P., Blenkinsopp, C., and Turner, I. L. (2010). “Swash zone sediment transport, step dynamics and morphological response on a gravel beach”. In: *Marine Geology* 274.1, pp. 50–68.

Mateo, Z. R. P. and Siringan, F. P. (2007). “Tectonic control of high-frequency Holocene delta switching and fluvial migration in Lingayen Gulf bayhead, northwestern Philippines”. In: *Journal of Coastal Research* 23, pp. 182–194.

Matias, A., Williams, J. J., Masselink, G., and Ferreira, Ó. (2012). “Overwash threshold for gravel barriers”. In: *Coastal Engineering* 63, pp. 48–61.

Matias, A., Masselink, G., Kroon, A., Blenkinsopp, C. E., and Turner, I. L. (2013). “Overwash experiment on a sandy barrier”. In: *Journal of Coastal Research* 65.1, pp. 778–783.

Matias, A., Blenkinsopp, C. E., and Masselink, G. (2014). “Detailed investigation of overwash on a gravel barrier”. In: *Marine Geology* 350, pp. 27–38.

Matias, A., Masselink, G., Castelle, B., Blenkinsopp, C. E., and Kroon, A. (2016). “Measurements of morphodynamic and hydrodynamic overwash processes in a large-scale wave flume”. In: *Coastal Engineering* 113, pp. 33–46.

McCall, R. T. (2015). “Process-based modelling of storm impacts on gravel coasts”. PhD thesis. Plymouth University, UK.

McCall, R. T., Masselink, G, Poate, T. G., Roelvink, J. A., Almeida, L. P., Davidson, M, and Russell, P. E. (2014). “Modelling storm hydrodynamics on gravel beaches with XBeach-G”. In: *Coastal Engineering* 91, pp. 231–250.

McCall, R. T., Masselink, G, Poate, T. G., Roelvink, J. A., and Almeida, L. P. (2015). “Modelling the morphodynamics of gravel beaches during storms with XBeach-G”. In: *Coastal Engineering* 103, pp. 52–66.

McCall, R. T., Masselink, G., Poate, T., Bradbury, A., Russell, P., and Davidson, M. (2013). “Predicting overwash on gravel barriers”. In: *Journal of Coastal Research* 65.2, pp. 1473–1478.

McCall, R. T., Masselink, G., Roelvink, D., Russell, P., Davidson, M., and Poate, T. (2012). “Modelling overwash and infiltration on gravel barriers”. In: *Coastal Engineering Proceedings*. Vol. 1. 33.

McManus, J. (2002). “Deltaic Responses to Changes in River Regimes”. In: *Marine Chemistry* 79.3, pp. 155–70.

Medina, R., Vidal, C., Losada, M. A., and Roldan, A. J. (1993). “Three-Mode Principal Component Analysis of Bathymetric Data, applied to Playa de Castilla (Huelva, Spain)”. In: *Coastal Engineering Proceedings*, pp. 2265–2278.

Meyer-Peter, E. and Müller, R (1948). “Formulas for bed-load transport”. In: *Proceedings of the 2nd Meeting of the International Association for Hydraulic Structures Research*. International Association of Hydraulic Research Delft, pp. 39–64.

Mil-Homens, J., Ranasinghe, R., Vries, J. S.M.v. T. de, and Stive, M. J. F. (2013). “Re-evaluation and improvement of three commonly used bulk longshore sediment transport formulas”. In: *Coastal Engineering* 75, pp. 29–39.

Millares, A (2008). “Integración del caudal base en un modelo distribuido de cuenca. Estudio de las aportaciones subterráneas en ríos de montaña”. PhD thesis. University of Granada.

Millares, A, Polo, M., and Losada, M. (2009). "The hydrological response of baseflow in fractured mountain areas". In: *Hydrology and Earth System Sciences* 13.7, pp. 1261–1271.

Millares, A, Gulliver, Z, and Polo, M. J. (2012). "Scale effects on the estimation of erosion thresholds through a distributed and physically-based hydrological model". In: *Geomorphology* 153, pp. 115–126.

Millares, A, Polo, M. J., Moñino, A, Herrero, J, and Losada, M. A. (2014a). "Bedload dynamics and associated snowmelt influence in mountainous and semiarid alluvial rivers". In: *Geomorphology* 206, pp. 330–342.

— (2014b). "Reservoir sedimentation and erosion processes in a snow-influenced basin, in Southern Spain". In: *Reservoir Sedimentation - Special Session on Reservoir Sedimentation of the 7th International Conference on Fluvial Hydraulics, RIVER FLOW 2014*, pp. 91–98.

Mínguez, R, Espejo, A, Tomás, A, Méndez, F., and Losada, I. (2011). "Directional calibration of wave reanalysis databases using instrumental data". In: *Journal of Atmospheric and Oceanic Technology* 28.11, pp. 1466–1485.

Mizuyama, T (1981). "An intermediate phenomenon between debris flow and bed load transport". In: *Symposium on Erosion and Sediment Transport in Pacific Rim Steeplands* 132, pp. 212–224.

Moñino, A., Millares, A., Herrero, J., Polo, M. J., and Losada, M. A. (2011). "Measurement of infilling rate in a small reservoir in a Mediterranean semi-arid area". In: *Geophysical Research Abstracts, EGU General Assembly*. Vol. 13. 10756.

Moses, C. A. and Williams, R. B. G. (2008). "Artificial beach recharge: the South East England experience". In: *Zeitschrift für Geomorphologie, Supplementary Issues* 52.3, pp. 107–124.

Muñoz-Perez, J. and Medina, R (2010). "Comparison of long-, medium-and short-term variations of beach profiles with and without submerged geological control". In: *Coastal Engineering* 57.3, pp. 241–251.

Muñoz-Perez, J., Tejedor, L, and Medina, R (1999). "Equilibrium beach profile model for reef-protected beaches". In: *Journal of Coastal Research* 15.4, pp. 950–957.

Muñoz-Perez, J. J. and Medina, R. (2006). "Short term variability of reef protected beach profiles: an analysis using EOF". In: *Proceedings of the 5th Coastal Dynamics*, pp. 1–11.

Muñoz-Pérez, J. J., Caballero, I., Tejedor, B., and Gomez-Pina, G. (2010). "Reversal in longshore sediment transport without variations in wave power direction". In: *Journal of Coastal Research* 26.4, pp. 780–786.

Nicholls, R. J. and Hoozemans, F. M. J. (1996). "The Mediterranean: vulnerability to coastal implications of climate change". In: *Ocean & Coastal Management* 31.2, pp. 105–132.

Nielsen, P and Hanslow, D. J. (1991). "Wave runup distributions on natural beaches". In: *Journal of Coastal Research* 7, pp. 1139–1152.

Orford, J. D. and Carter, R. W. G. (1995). "Examination of mesoscale forcing of a swash-aligned, gravel barrier from Nova Scotia". In: *Marine Geology* 126.1, pp. 201–211.

Orford, J. D., Carter, R. W. G., McKenna, J, and Jennings, S. C. (1995). "The relationship between the rate of mesoscale sea-level rise and the rate of retreat of swash-aligned gravel-dominated barriers". In: *Marine Geology* 124.1, pp. 177–186.

Orford, J. D. and Anthony, E. J. (2011). "Extreme events and the morphodynamics of gravel-dominated coastal barriers: Strengthening uncertain ground". In: *Marine Geology* 290.1, pp. 41–45.

Orford, J. D., Carter, R. W. G., and Jennings, S. C. (1991). "Coarse clastic barrier environments: evolution and implications for Quaternary sea level interpretation". In: *Quaternary International* 9, pp. 87–104.

Orford, J. D., Forbes, D. L., and Jennings, S. C. (2002). “Organisational controls, typologies and time scales of paraglacial gravel-dominated coastal systems”. In: *Geomorphology* 48.1, pp. 51–85.

Ortega-Sánchez, M, Losada, M. A., and Baquerizo, A (2003). “On the development of large-scale cuspate features on a semi-reflective beach: Carchuna beach, Southern Spain”. In: *Marine Geology* 198.3, pp. 209–223.

Ortega-Sánchez, M, Bramato, S, Quevedo, E, Mans, C, and Losada, M. A. (2008). “Atmospheric-hydrodynamic coupling in the nearshore”. In: *Geophysical Research Letters* 35.23.

Ortega-Sánchez, M, Lobo, F. J., López-Ruiz, A, Losada, M. A., and Fernández-Salas, L. M. (2014). “The influence of shelf-indenting canyons and infralittoral prograding wedges on coastal morphology: The Carchuna system in Southern Spain”. In: *Marine Geology* 347, pp. 107–122.

Ortega-Sánchez, M., Bergillos, R. J., López-Ruiz, A., and Losada, M. A. (2017). *Morphodynamics of Mediterranean Mixed Sand and Gravel Coasts*. Springer.

Orton, G. J. and Reading, H. G. (1993). “Variability of deltaic processes in terms of sediment supply, with particular emphasis on grain size”. In: *Sedimentology* 40.3, pp. 475–512.

Overeem, I. (2005). “Three-dimensional numerical modeling of deltas”. In: *Special Publications of SEPM*.

Palanqués, A. and Guillén, J. (1998). “Coastal changes in the Ebro delta: natural and human factors”. In: *Journal of Coastal Conservation* 4, pp. 17–26.

Payo, A. et al. (2016). “Projected changes in area of the Sundarban mangrove forest in Bangladesh due to SLR by 2100”. In: *Climatic Change* 139.2, pp. 279–291.

Pedrozo-Acuña, A (2005). “Concerning swash on steep beaches”. PhD thesis. University of Plymouth, UK.

Pedrozo-Acuña, A, Simmonds, D. J., Chadwick, A. J., and Silva, R (2007). “A numerical–empirical approach for evaluating morphodynamic processes on gravel and mixed sand–gravel beaches”. In: *Marine Geology* 241.1, pp. 1–18.

Pedrozo-Acuna, A., Simmonds, D. J., Otta, A. K., and Chadwick, A. J. (2006). “On the cross-shore profile change of gravel beaches”. In: *Coastal Engineering* 53.4, pp. 335–347.

Pelnard-Considère, R (1956). “Essai de theorie de levolution des forms de rivages en plage de sable et de galets”. In: *4th Journees de lHydraulique, les Energies de la Mer, Question III* 1, pp. 289–298.

Petropoulos, G. P., Kalivas, D. P., Griffiths, H. M., and Dimou, P. P. (2015). “Remote sensing and GIS analysis for mapping spatio-temporal changes of erosion and deposition of two Mediterranean river deltas: The case of the Axios and Aliakmonas rivers, Greece”. In: *International Journal of Applied Earth Observation and Geoinformation* 35, pp. 217–228.

Poate, T. G., McCall, R. T., and Masselink, G. (2016). “A new parameterisation for runup on gravel beaches”. In: *Coastal Engineering* 117, pp. 176–190.

Poate, T., Masselink, G., Davidson, M., McCall, R. T., Russell, P., and Turner, I. (2013). “High frequency in-situ field measurements of morphological response on a fine gravel beach during energetic wave conditions”. In: *Marine Geology* 342, pp. 1–13.

Polo, M. J., Herrero, J, Aguilar, C, Millares, A, Moñino, A, Nieto, S, and Losada, M. A. (2009). “WiMMed, a distributed physically-based watershed model (I): Description and validation”. In: *Proceedings of the International Workshop on Environmental Hydraulics*, pp. 225–228.

Pont, D, Simonnet, J.-P., and Walter, A. (2002). “Medium-term changes in suspended sediment delivery to the ocean: consequences of catchment heterogeneity and river management (Rhône River, France)”. In: *Estuarine, Coastal and Shelf Science* 54.1, pp. 1–18.

Pontee, N. I., Pye, K, and Blott, S. J. (2004). "Morphodynamic behaviour and sedimentary variation of mixed sand and gravel beaches, Suffolk, UK". In: *Journal of Coastal Research* 20, pp. 256–276.

Poulos, S. E. and Collins, M. B. (2002). "Fluviatile sediment fluxes to the Mediterranean Sea: a quantitative approach and the influence of dams". In: *Geological Society, London, Special Publications* 191, pp. 227–245.

Powell, D. M., Reid, I., and Laronne, J. B. (2001). "Evolution of bed load grain size distribution with increasing flow strength and the effect of flow duration on the caliber of bed load sediment yield in ephemeral gravel bed rivers". In: *Water Resources Research* 37.5, pp. 1463–1474.

Pranzini, E. (1994). "The erosion of the Ombrone river delta (Italy)". In: *Littoral 94*, pp. 26–29.

— (2001). "Updrift river mouth migration on cuspate deltas: two examples from the coast of Tuscany (Italy)". In: *Geomorphology* 38.1, pp. 125–132.

Reeve, D, Chadwick, A, and Fleming, C (2012). *Coastal Engineering: processes, theory and design practice (Second edition)*. Spon Press.

Rickenmann, D (1990). "Bedload capacity of slurry flows at steep slopes". PhD thesis. ETH Zurich.

Rickenmann, D. (2001). "Comparison of bed load transport in torrents and gravel bed streams". In: *Water Resources Research* 37.12, pp. 3295–3305.

Rodero, J, Polo, M. J., and Losada, M. A. (2005). *Estudio Piloto para la Gestión Integrada de la Cuenca Hidrográfica del Río Guadalfeo. University of Granada.*

Rodríguez, J. A., Rodríguez, A. J., Sotelo, A, Monge, G, and De La Rosa, D (2008). "Sistema de Inferencia Espacial de Propiedades Físico-Químicas e Hidráulicas de los Suelos de Andalucía". In: *Herramienta de Apoyo a la Simulación de Procesos Agro-Hidrológicos a Escala Regional. Informe Final. Empresa Pública Desarrollo Agrario y Pesquero, Consejería de Agricultura y Pesca, Sevilla*.

Rohling, E., Abu-Zied, R., Casford, J., Hayes, A., and Hoogakker, B. (2009). "The marine environment: present and past". In: *The Physical Geography of the Mediterranean*. Ed. by J. C. Woodward. Oxford University Press, pp. 33–68.

Román-Sierra, J., Muñoz-Perez, J. J., and Navarro-Pons, M. (2014). "Beach nourishment effects on sand porosity variability". In: *Coastal Engineering* 83, pp. 221–232.

Rovira, A. and Ibáñez, C. (2007). "Sediment management options for the lower Ebro River and its delta". In: *Journal of Soils and Sediments* 7.5, pp. 285–295.

Sabatier, F. and Suanez, S. (2003). "Evolution of the Rhône delta coast since the end of the 19th century". In: *Géomorphologie: relief, processus, environnement* 9.4, pp. 283–300.

Sabatier, F., Maillet, G., Provansal, M., Fleury, T.-J., Suanez, S., and Vella, C. (2006). "Sediment budget of the Rhône delta shoreface since the middle of the 19th century". In: *Marine Geology* 234.1, pp. 143–157.

Sabatier, F., Samat, O., Ullmann, A., and Suanez, S. (2009). "Connecting large-scale coastal behaviour with coastal management of the Rhône delta". In: *Geomorphology* 107.1, pp. 79–89.

Sánchez-Arcilla, A. and Jiménez, J. A. (1997). "Physical impacts of climatic change on deltaic coastal systems (I): an approach". In: *Climatic Change* 35.1, pp. 71–93.

Schoklitsch, A (1962). *Handbuch des Wasserbaus*. Springer.

Scott, T, Masselink, G, O'Hare, T. A., Davidson, M, and Russell, P (2015). "Multi-annual sand and gravel beach response to storms in the southwest of England". In: *Proceedings of the 8th Coastal Sediments*.

Semeoshenkova, V. and Newton, A. (2015). "Overview of Erosion and Beach Quality Issues in Three Southern European Countries: Portugal, Spain and Italy". In: *Ocean & Coastal Management* 118, pp. 12–21.

Shaw, J, Taylor, R. B., and Forbes, D. L. (1990). “Coarse clastic barriers in eastern Canada: patterns of glaciogenic sediment dispersal with rising sea levels”. In: *Journal of Coastal Research* 9, pp. 160–200.

Shulmeister, J and Kirk, R. M. (1993). “Evolution of a mixed sand and gravel barrier system in North Canterbury, New Zealand, during Holocene sea-level rise and still-stand”. In: *Sedimentary Geology* 87.3-4, pp. 215–235.

Simeoni, U. and Corbau, C. (2009). “A review of the Delta Po evolution (Italy) related to climatic changes and human impacts”. In: *Geomorphology* 107.1, pp. 64–71.

Simeoni, U., Fontolan, G., Tessari, U., and Corbau, C. (2007). “Domains of spit evolution in the Goro area, Po Delta, Italy”. In: *Geomorphology* 86.3, pp. 332–348.

Smart, G. M. (1984). “Sediment transport formula for steep channels”. In: *Journal of Hydraulic Engineering* 110.3, pp. 267–276.

Soons, J. M., Shulmeister, J, and Holt, S (1997). “The Holocene evolution of a well nourished gravelly barrier and lagoon complex, Kaitorete Spit, Canterbury, New Zealand”. In: *Marine Geology* 138.1, pp. 69–90.

Spencer, T. et al. (2016). “Global coastal wetland change under sea-level rise and related stresses: the DIVA Wetland Change Model”. In: *Global and Planetary Change* 139, pp. 15–30.

Stanley, D. J. and Warne, A. G. (1993). “Nile Delta: recent geological evolution and human impact”. In: *Science* 260, pp. 628–634.

Stewart, I. S. and Morhange, C. (2009). “Coastal geomorphology and sea-level change”. In: *The Physical Geography of the Mediterranean*. Ed. by J. C. Woodward. Oxford University Press, pp. 385–413.

Stull, R. (2000). *Meteorology for scientists and engineers. Second Edition*. University of British Columbia.

Sunamura, T and Takeda, I (1984). “Landward migration of inner bars”. In: *Developments in Sedimentology* 39, pp. 63–78.

Syvitski, J. P. M. and Saito, Y. (2007). “Morphodynamics of deltas under the influence of humans”. In: *Global and Planetary Change* 57.3, pp. 261–282.

Syvitski, J. P. M., Vörösmarty, C. J., Kettner, A. J., and Green, P. (2005). “Impact of humans on the flux of terrestrial sediment to the global coastal ocean”. In: *Science* 308, pp. 376–380.

Syvitski, J. P. M. et al. (2009). “Sinking deltas due to human activities”. In: *Nature Geoscience* 2.10, pp. 681–686.

Tatui, F., Vespremeanu-Stroe, A., and Preoteasa, L. a. (2014). “Alongshore variations in beach-dune system response to major storm events on the Danube Delta coast”. In: *Journal of Coastal Research* 70, pp. 693–699.

Thom, B. G. and Hall, W (1991). “Behaviour of beach profiles during accretion and erosion dominated periods”. In: *Earth Surface Processes and Landforms* 16.2, pp. 113–127.

Tomas, A., Mendez, F. J., and Losada, I. J. (2008). “A method for spatial calibration of wave hindcast data bases”. In: *Continental Shelf Research* 28.3, pp. 391–398.

Torres, R., Millares, A., Aguilar, C., Moñino, A., Losada, M. Á., and Polo, M. J. (2013). “Zonal characterization of hillslope erosion processes in a semi-arid high mountain catchment”. In: *Geophysical Research Abstracts, EGU General Assembly*. Vol. 15. 13894.

Trincardi, F., Cattaneo, A., and Correggiari, A. (2004). “Mediterranean prodelta systems”. In: *Oceanography* 17.4, pp. 34–45.

Trincardi, F. and Syvitski, J. P. (2005). “Advances on our understanding of delta/prodelta environments: a focus on southern European margins”. In: *Marine Geology* 222, pp. 1–5.

UNEP/MAP (2012). *State of the Mediterranean Marine and Coastal Environment*. Athens: UNEP/MAP - Barcelona Convention.

USACE (1984). "Shore Protection Manual". In: *Coastal Engineering Research Center, Government Printing Office, Washington DC*.

Van Rijn, L. C. and Sutherland, J. R. (2011). "Erosion of gravel barriers and beaches". In: *Proceedings of the 7th Coastal Sediments*.

Van Rijn, L., Walstra, D., Grasmeijer, B, Sutherland, J, Pan, S., and Sierra, J. (2003). "The predictability of cross-shore bed evolution of sandy beaches at the time scale of storms and seasons using process-based profile models". In: *Coastal Engineering* 47.3, pp. 295–327.

Van Rijn, L. C. (2014). "A simple general expression for longshore transport of sand, gravel and shingle". In: *Coastal Engineering* 90, pp. 23–39.

Van Wellen, E, Shadwick, A. J., Lee, M, Baily, B, and Morfett, J (1998). "Evaluation of longshore sediment transport models on coarse grained beaches using field data: A preliminary investigation". In: *Coastal Engineering Proceedings*. Vol. 1. 26.

Van Wellen, E, Chadwick, A. J., and Mason, T (2000). "A review and assessment of longshore sediment transport equations for coarse-grained beaches". In: *Coastal Engineering* 40.3, pp. 243–275.

Van der Wal, D (1998). "Effects of fetch and surface texture on aeolian sand transport on two nourished beaches". In: *Journal of Arid Environments* 39.3, pp. 533–547.

— (2000a). "Modelling aeolian sand transport and morphological development in two beach nourishment areas". In: *Earth Surface Processes and Landforms* 25.1, pp. 77–92.

Van der Wal, D. (2000b). "Grain-size-selective aeolian sand transport on a nourished beach". In: *Journal of Coastal Research* 16, pp. 896–908.

Vanmaercke, M., Poesen, J., Verstraeten, G., Vente, J. de, and Ocakoglu, F. (2011). "Sediment Yield in Europe: Spatial Patterns and Scale Dependency". In: *Geomorphology* 130.3-4, pp. 142–61.

Vespremeanu-Stroe, A, Constantinescu, S, Tatui, F, and Giosan, L (2007). "Multi-decadal evolution and North Atlantic Oscillation influences on the dynamics of the Danube Delta shoreline". In: *Journal of Coastal Research* 50, pp. 157–162.

Walling, D. and Fang, D (2003). "Recent trends in the suspended sediment loads of the world's rivers". In: *Global and Planetary Change* 39.1, pp. 111–126.

Wang, P. and Kraus, N. C. (2005). "Beach profile equilibrium and patterns of wave decay and energy dissipation across the surf zone elucidated in a large-scale laboratory experiment". In: *Journal of Coastal Research* 21, pp. 522–534.

Weir, F. M., Hughes, M. G., and Baldock, T. E. (2006). "Beach face and berm morphodynamics fronting a coastal lagoon". In: *Geomorphology* 82.3, pp. 331–346.

Wentworth, C. K. (1922). "A scale of grade and class terms for clastic sediments". In: *The Journal of Geology* 30.5, pp. 377–392.

Wilcock, P. R. and Crowe, J. C. (2003). "Surface-based transport model for mixed-size sediment". In: *Journal of Hydraulic Engineering* 129.2, pp. 120–128.

Williams, J. J., Buscombe, D, Masselink, G, Turner, I. L., and Swinkels, C (2012a). "Barrier Dynamics Experiment (BARDEX): aims, design and procedures". In: *Coastal Engineering* 63, pp. 3–12.

Williams, J. J., Alegría-Arzaburu, A. R. de, McCall, R. T., and Van Dongeren, A. (2012b). "Modelling gravel barrier profile response to combined waves and tides using XBeach: Laboratory and field results". In: *Coastal Engineering* 63, pp. 62–80.

Wong, M. and Parker, G. (2006). “Reanalysis and correction of bed-load relation of Meyer-Peter and Müller using their own database”. In: *Journal of Hydraulic Engineering* 132, pp. 1159–1168.

Yang, S., Milliman, J., Li, P, and Xu, K (2011). “50,000 dams later: erosion of the Yangtze River and its delta”. In: *Global and Planetary Change* 75.1, pp. 14–20.

Yang, Z.-S., Wang, H.-J., Saito, Y, Milliman, J., Xu, K, Qiao, S, and Shi, G (2006). “Dam impacts on the Changjiang (Yangtze) River sediment discharge to the sea: The past 55 years and after the Three Gorges Dam”. In: *Water Resources Research* 42.W04407.